Universidade de Aveiro Departamento de Química
2009

Cláudia Maria Batista Lopes

Remoção de mercúrio (II) de soluções aquosas utilizando materiais microporosos

Mercury (II) removal from aqueous solutions by microporous materials

Universidade de Aveiro Departamento de Química
2009

Claudia Maria Batista Lopes

Remoção de mercúrio (II) de soluções aquosas utilizando materiais microporosos

Mercury (II) removal from aqueous solutions by microporous materials

dissertação apresentada à Universidade de Aveiro para cumprimento dos requisitos necessários à obtenção do grau de Doutor em Química, realizada sob a orientação científica da Professora Doutora Maria Eduarda Pereira, Professora auxiliar do Departamento de Química da Universidade de Aveiro e do Professor Doutor João Rocha, Professor catedrático do Departamento de Química da Universidade de Aveiro

Apoio financeiro da FCT e do FSE no âmbito do III Quadro Comunitário de Apoio pela Bolsa de Doutoramento Ref.ª SFRH/BD/19098/2004.

Aos meus pais, Beatriz e Horácio e ao Carlos

o júri

presidente

Professor Doutor Luís António Ferreira Martins Dias Carlos
Professor catedrático da Universidade de Aveiro

Professor Doutor Armando da Costa Duarte
Professor catedrático da Universidade de Aveiro

Professor Doutor João Carlos Matias Celestino Gomes da Rocha
Professor catedrático da Universidade de Aveiro

Professor Doutor João Paulo Gil Lourenço
Professor auxiliar da Faculdade de Ciências e Tecnologia da Universidade do Algarve

Professora Doutora Maria Eduarda da Cunha Pereira
Professora auxiliar da Universidade de Aveiro

Professor Doutor Rui Alfredo da Rocha Boaventura
Investigador principal da Faculdade de Engenharia da Universidade do Porto

Doutora Marta Otero Cabero
Investigadora auxiliar do CESAM da Universidade de Aveiro

agradecimentos

Ao longo dos últimos quatro anos e meio tive a oportunidade de planear e de desenvolver um trabalho, que na minha opinião, poderá contribuir de algum modo para uma melhoria na qualidade ambiental. Trabalho este, que me motivou e entusiasmou diariamente, que me permitiu crescer a nível científico e pessoal mas, que não teria sido possível sem a ajuda e dedicação de algumas pessoas a quem eu gostaria de expressar o meu reconhecimento e os meus sinceros agradecimentos.

Aos meus orientadores, Professora Doutora Eduarda Pereira e Professor Doutor João Rocha, agradeço a oportunidade concedida na realização deste trabalho, a orientação científica do mesmo e a disponibilidade e apoio que sempre me dispensaram ao longo da realização do trabalho.

Ao Investigador do CICECO, Zhi Lin, agradeço a prontidão com que sempre respondeu aos meus diversos pedidos e à preciosa ajuda na síntese dos materiais, nomeadamente na preparação da coluna de ETS-4.

À Investigadora do CESAM Marta Otero, agradeço o seu interesse e entusiasmo pelo meu trabalho e as discussões sempre proveitosas que tivemos ao longo do trabalho.

Ao Professor Doutor Carlos Silva e à Patrícia Lito, agradeço os ensinamentos na área da engenharia química e a preciosa ajuda no desenvolvimento do modelo baseado nas equações de Nernst-Planck.

À Joana Coimbra, agradeço a sua contribuição na parte inicial do trabalho.

À Doutora Teresa Caldeira e ao Senhor Ivo Mateus, que com a sua experiência e conhecimento me ajudaram a concretizar este trabalho. À D. Dina e D. Helena agradeço a disponibilidade sempre demonstrada.

A todos os colegas do grupo de Química Analítica e Ambiental, agradeço a boa disposição, amizade e companheirismo. Um agradecimento especial à Ana, à Anabela, à Cláudia, ao Daniel, à Lídia, à Marta Veríssimo, à Olga, ao Pedro Coelho, ao Pedro Pato e à Sónia, pelas conversas banais e científicas que tivemos e por todos os bons momentos passados dentro e fora do laboratório.

Aos amigos de sempre, Susana, Tânia, Nelson e Maria do Carmo, simplesmente por existirem e por saber que posso contar sempre com a vossa amizade e estímulo, quer estejam por perto ou longe.

Por último, um agradecimento muito especial aos meus pais e ao Carlos pelo apoio incondicional e estímulo constante, que me ajudaram a singrar no meu percurso.

A todos o meu grande
Bem Haja.

palavras-chave

Mercúrio, materiais microporosos, titanosilicato ETS-4, remoção, remediação ambiental.

resumo

O Mercúrio é um dos metais pesados mais tóxicos existentes no meio ambiente, é persistente e caracteriza-se por bioamplificar e bioacumular ao longo da cadeia trófica. A poluição com mercúrio é um problema à escala global devido à combinação de emissões naturais e emissões antropogénicas, o que obriga a políticas ambientais mais restritivas sobre a descarga de metais pesados. Consequentemente o desenvolvimento de novos e eficientes materiais e de novas tecnologias para remover mercúrio de efluentes é necessário e urgente. Neste contexto, alguns materiais microporosos provenientes de duas famílias, titanossilicatos e zirconossilicatos, foram investigados com o objectivo de avaliar a sua capacidade para remover iões Hg^{2+} de soluções aquosas.

De um modo geral, quase todos os materiais estudados apresentaram elevadas percentagens de remoção, confirmando que são bons permutadores iónicos e que têm capacidade para serem utilizados como agentes descontaminantes. O titanossilicato ETS-4 foi o material mais estudado devido à sua elevada eficiência de remoção (>98%), aliada à pequena quantidade de massa necessária para atingir essa elevada percentagem de remoção. Com apenas 4 $mg \cdot dm^{-3}$ de ETS-4 foi possível tratar uma solução com uma concentração igual ao valor máximo admissível para descargas de efluentes em cursos de água (50 $\mu g \cdot dm^{-3}$) e obter água com qualidade para consumo humano (<1.0 $\mu g \cdot dm^{-3}$), de acordo com a legislação Portuguesa (DL 236/98). Tal como para outros adsorbentes, a capacidade de remoção de Hg^{2+} do ETS-4 depende de várias condições experimentais, tais como o tempo de contacto, a massa, a concentração inicial de mercúrio, o pH e a temperatura. Do ponto de vista industrial as condições óptimas para a aplicação do ETS-4 são bastante atractivas, uma vez que não requerem grandes quantidades de material e o tratamento da solução pode ser feito à temperatura ambiente. A aplicação do ETS-4 torna-se ainda mais interessante no caso de efluentes hospitalares, de processos de electro-deposição com níquel, metalúrgica, extracção de minérios, especialmente ouro, e indústrias de fabrico de cloro e soda cáustica, uma vez que estes efluentes apresentam valores de pH semelhantes ao valor de pH óptimo para a aplicação do ETS-4. A cinética do processo de troca iónica é bem descrita pelo modelo Nernst-Planck, enquanto que os dados de equilíbrio são bem ajustados pelas isotérmicas de Langmuir e de Freundlich. Os parâmetros termodinâmicos, ΔG° and ΔH° indicam que a remoção de Hg^{2+} pelo ETS-4 é um processo espontâneo e exotérmico. A elevada eficiência do ETS-4 é confirmada pelos valores da capacidade de remoção de outros materiais para os iões Hg^{2+}, descritos na literatura. A utilização de coluna de ETS-4 preparada no nosso laboratório, para a remoção em contínuo de Hg^{2+} confirma que este material apresenta um grande potencial para ser utilizado no tratamento de águas.

keywords

Mercury, microporous materials, ETS-4 titanosilicate, removal, environmental remediation.

abstract

Mercury is one of the most toxic heavy metals, exhibiting a persistent character in the environment and biota as well as bioamplification and bioaccumulation along the food chain. Natural inputs combined with the global anthropogenic sources make mercury pollution a planetary-scale problem, and strict environmental policies on metal discharges have been enforced. The development of efficient new materials and clean-up technologies for removing mercury from effluents is, thus, timely.

In this context, in my study, several microporous materials from two families, titanosilicates and zirconosilicates were investigated in order to assess their Hg^{2+} sorption capacity and removal efficiency, under different operating conditions. In general, almost all microporous materials studied exhibited high removal efficiencies, confirming that they are good ion exchangers and have potential to be used as Hg^{2+} decontaminant agents. Titanosilicate ETS-4 was the material most studied here, by its highest removal efficiency (>98%) and lowest mass necessary to attain it. Moreover, according with the Portuguese legislation (DL 236/98) it is possible to attain drinking water quality (i.e. $[Hg^{2+}]<$ 1.0 $\mu g \cdot dm^{-3}$) by treating a solution with a Hg^{2+} concentration equal to the maximum value admissible for effluents discharges into water bodies (50 $\mu g \cdot dm^{-3}$), using only 4 $mg \cdot dm^{-3}$ of ETS-4. Even in the presence of major freshwater cations, ETS-4 removal efficiency remains high.

Like for other adsorbents, the sorption capacity of ETS-4 for Hg^{2+} ions is strongly dependent on the operating conditions, such as contact time, mass, initial Hg^{2+} concentration and solution pH and, to a lesser extent, temperature. The optimum operating conditions found for ETS-4 are very attractive from the industrial point of view because the application of ETS-4 for the treatment of wastewater and/or industrial effluents will not require larges amounts of adsorbent, neither energy supply for temperature adjustments becoming the removal process economically competitive. These conditions become even more interesting in the case of medical institutions liquid, nickel electroplating process, copper smelter, gold ore tailings and chlor-alkali effluents, since no significant pH adjustments to the effluent are necessary. The ion exchange kinetics of Hg^{2+} uptake is successfully described by the Nernst-Planck based model, while the ion exchange equilibrium is well fitted by both Langmuir and Freundlich isotherms. Moreover, the feasibility of the removal process was confirmed by the thermodynamic parameters (ΔG° and ΔH°) which indicate that the Hg^{2+} sorption by ETS-4 is spontaneous and exothermic.

The higher efficiency of ETS-4 for Hg^{2+} ions is corroborate by the values reported in literature for the sorption capacity of other adsorbents for Hg^{2+} ions. The use of an ETS-4 fixed-bed ion exchange column, manufactured in our laboratory, in the continuous removal of Hg^{2+} ions from solutions confirms that this titanosilicate has potential to be used in industrial water treatment.

List of Contents

List of Figures

List of Tables

Abbreviations

a	Intercept
AAD	Average absolute deviation
b	Slope
C	Liquid-phase concentration
C_i	Concentration of species i (Hg^{2+}/Na^{+}) in bulk solution, ($ng \cdot dm^{-3}$, $\mu g \cdot dm^{-3}$, $mol \cdot m^{-3}$)
$CVAFS$	Cold vapour atomic fluorescence spectrometry
d	Interlay spacings of component atoms and ions
D_i	Self-diffusion coefficient of species i (Hg^{2+}/Na^{+}), ($m^2 \cdot s^{-1}$)
D_{AB}	Inter-diffusion coefficient of pair $A-B$, ($m^2 \cdot s^{-1}$)
F	Faraday constant, ($C \cdot mol^{-1}$)
$FT-IR$	Fourier transform infrared
G	Gibbs free energy, ($kJ \cdot mol^{-1}$)
H	Enthalpy, ($kJ \cdot mol^{-1}$)
J_i	Intra-particle molar flux of species i (Hg^{2+}/Na^{+}), ($mol \cdot m^{-2} \cdot s^{-1}$)
k_1	First-order rate constant, (h^{-1})
k_2	Second-order rate constant, ($g \cdot mg^{-1} \cdot h^{-1}$, $m^3 \cdot s^{-1} \cdot mol^{-1}$)
k_f	Convective mass transfer coefficient, ($m \cdot s^{-1}$)
K_d	Distribution coefficient, ($dm^3 \cdot g^{-1}$)
K_f	Freundlich constant, ($mg^{1-1/n} \cdot (dm^3)^{1/n} \cdot g^{-1}$)
K_L	Langmuir constant, ($dm^3 \cdot mg^{-1}$)
n	Freundlich parameter
q	Adsorbed concentration
q_i	Concentration of counter ion i (Hg^{2+}/Na^{+}) in the particle, ($mg \cdot g^{-1}$, $mol \cdot m^{-3}$)
$\overline{q}_i$	Average concentration of counter ion i (Hg^{2+}/Na^{+}) in the particle, ($mol \cdot m^{-3}$, $mmol \cdot g^{-1}$)
$q_{\max}$	Maximum loading, ($mg \cdot g^{-1}$)
Q_{tot}	Total amount of Hg^{2+} ions sorbed in the microporous material column
r	Radial position in the particle, (m)
$\Re$	Gas constant, ($J \cdot mol^{-1} \cdot K^{-1}$)
R	Particle radius, (m)
R_L	Separation factor
S	Entropy, ($kJ \cdot mol^{-1} \cdot K^{-1}$)
$S_{y/x}$	Standard deviation of y-residuals
t	t-student, in equations 1.1 and 1.2
t	Time, (s, min, h)
T	Absolute temperature, K
v	Flow rate, ($cm^3 \cdot min^{-1}$)
v_1	Initial first-order kinetic rate, ($mg \cdot g^{-1} \cdot h^{-1}$)
v_2	Initial second-order kinetic rate, ($mg \cdot g^{-1} \cdot h^{-1}$)
V_L	Volume of liquid phase, (dm^3, m^3)
V_s	Volume of solid phase, (m^3)

W	Dry weight of microporous material (mg)
XRD	X-ray diffraction
z_i	Charge of component i (Hg^{2+}/Na^{+})

Greek letters

ϕ	Electrostatic potential, (V)
λ	Wavelength of incident X-rays, (nm)
θ	Scattering angle, in equation 5.1

Subscripts

A	Counter ion initially present in bulk solution (Hg^{2+})
B	Counter ion initially present in particle (Na^{+})
NP	Nernst-Planck based model
$2nd-order$	Second-order kinetic model
s	Solid-liquid particle interface
0	Initial condition of experiment
t	Intermediate condition of experiment
e	Equilibrium condition of experiment

Chapter 1

Introduction

1.1. State of art

Water is considered an important and scarce commodity in many countries around the World and even so the contamination of surface and ground water by disposal of effluents containing organic pollutants and heavy metals continues until nowadays.

Heavy metals are well known for their toxicity and amounts in the environment are still increasing every year (Petrus and Warchol, 2003). Metals such as Hg, Cd, Ni, As, Pb, Cr are harmful and toxic to human beings and disturb ecological environments (Yardim et al., 2003; Rao et al., 2009). A wide variety of industries are responsible for the release to the environment of heavy metals through their wastewaters (*e.g.* metal finishing industry, ore mining and smelting, burning of fossil fuels, chemical industry, pharmaceuticals). Ria de Aveiro is an example, among so many others, of an estuarine system with heavy metals contamination due to the discharge of industrials and urban effluents in several of its canals. The contamination of inner areas of Ria de Aveiro by mercury from an industrial complex located in Estarreja has been confirmed (Hall et al., 1987; Duarte et al., 1991; Pereira et al., 1998).

Mercury is generally considered to be the most dangerous and toxic heavy metal released to the environment (Yardim et al., 2003; Walcarius et al., 2004; Di Natale et al., 2006; Yavuz et al., 2006), categorised as non-essential and non-biodegradable (Mishra et al., 2007). Even at very low concentration, mercury causes potential hazards due to its accumulation in the food chain (Di Natale et al., 2006; Rao et al., 2009). A special characteristic of mercury is its strong adsorption onto biological tissues and slow elimination from them (Rao et al., 2009). The European Union considers mercury as a priority and hazardous pollutant and defines a maximum permissible concentration of total mercury as low as 1 $\mu g \cdot dm^{-3}$, for drinking water, and 5 $\mu g \cdot dm^{-3}$, for wastewater discharge (Di Natale et al., 2006).

Due to growing environmental pollution and strict environmental regulations on metal discharges there is a strong demand to develop efficient technologies for heavy metal removal from water. In the literature, numerous processes of treatment have been proposed: coagulation, chemical precipitation, evaporation, electrolysis, ion exchange, adsorption and reverse osmosis (Reddad et al., 2002; Ranganathan, 2003; Chiron et al., 2003; Petrus and Warchol, 2003; Khraished et al., 2004; Peric et al., 2004; Feng et al., 2004; Tüzün et al., 2005; Zhang et al., 2005; Choi et al., 2006a; Grimm et al., 2008; Ghodbane and Hamdaoui, 2008). However, many of these conventional technologies are inadequate and expensive and usually originate secondary problems. From all treatment

processes available for mercury removal from water and wastewater, adsorption is the most attractive principally due to its simplicity and effectiveness (Ranganathan, 2003; Zhang et al., 2005; Lopes et al., 2007). The typical adsorbents for the removal of Hg^{2+} ions are activated carbons, but in the past few years a wide range of materials have been emerging as alternative low-cost adsorbents. Since its first introduction for heavy metal removal, activated carbon has undoubtedly been the most popular and widely used adsorbent in wastewater treatment applications worldwide (Babel and Kurniawan, 2003). Several studies have reported the successful application of activated carbons to remove Hg^{2+} from waters and wastewaters (*e.g.* Mohan et al., 2001; Krishnan and Anirudhan, 2002; Ranganathan, 2003; Yardim et al., 2003; Rao et al., 2009). However, activated carbon remains an expensive material (Babel and Kurniawan, 2003). Thus, there is much interest in finding alternative low-cost adsorbents that may replace activated carbon. In this context, biopolymers, zeolites, clays, natural oxides, carbonaceous wastes, which exhibit capacity to remove heavy metals from contaminated waters with low cost (Babel and Kurniawan, 2003) are attracting attention. Zeolites are among the most promissory materials because of their high ion-exchange capacity, selectivity and environmental compatibility, since the exchangeable ions (Na^{+}, Ca^{2+} e K^{+}) are relatively harmless (Panayotova, 2001; Petrus and Warchol, 2003). Of special importance for environmental protection is their ability to uptake and retain heavy metals species from aqueous media. Microporous materials, such as titanosilicates and zirconosilicates constitute novel zeotype families and their ion-exchange properties have attracted a considerable attention in the last decade since they are stable and exhibit a remarkable selectivity (Al-Attar and Dyer, 2001). Some of these microporous materials have already been applied in the removal of heavy metals (Kuznicki and Thrush, 1991; Zhao et al., 2003; Pavel et al., 2003; Lv et al., 2004; Lv et al., 2005; Choi et al, 2006a; Choi et al, 2006b; Cincotti et al., 2006; Lv et al., 2007) such as Cu, Pb and Cd. Very few papers area available on mercury and most deal with relatively unrealistically high metal concentrations (Zhu and Alexandratos, 2005; Pérez-Quintanilla et al., 2006). Mercury, however, is very toxic even at trace levels (Davis et al., 2000), and the lack of studies is due to the difficulties encountered in its determination at the low concentrations (<100 $\mu g \cdot dm^{-3}$) usually existing in the environment (Andac et al., 2003a). Further complications arise because both, many chemicals and pharmaceutical preparations contain traces of mercury, and certain other ions in solution may interfere with the determination of Hg^{2+} by some analytic techniques (Andac et al., 2003b).

1.2. Mercury

Mercury, also known as quicksilver, is the eightieth element in the periodic table. It occurs in the air, water and soil, as elemental or metallic mercury, inorganic and organo-mercury compounds. The first written record of this element is due to Aristotle who described it as "liquid silver" in the fourth century B.C. (Skoog et al., 1996). From then until now, mercury has been used in a wide range of applications. However, due to the more intensive use in the last century, mercury and its compounds have been notoriously associated with several environment problems and human health, namely, the methyl-mercury poisoning in Minamata (Japan), the organic mercury poisoning in Iraq, the methyl-mercury exposure in the Amazon (Brazil) and the elemental mercury spill in Catamarca (Peru), among other cases of contamination of air and food by both elemental and organic mercury compounds (Gochfeld, 2003).

Nowadays, mercury is considered as a priority and hazardous pollutant and strict environmental policies have been defined on discharged. Mercury's cycle is shown in Figure 1.1.

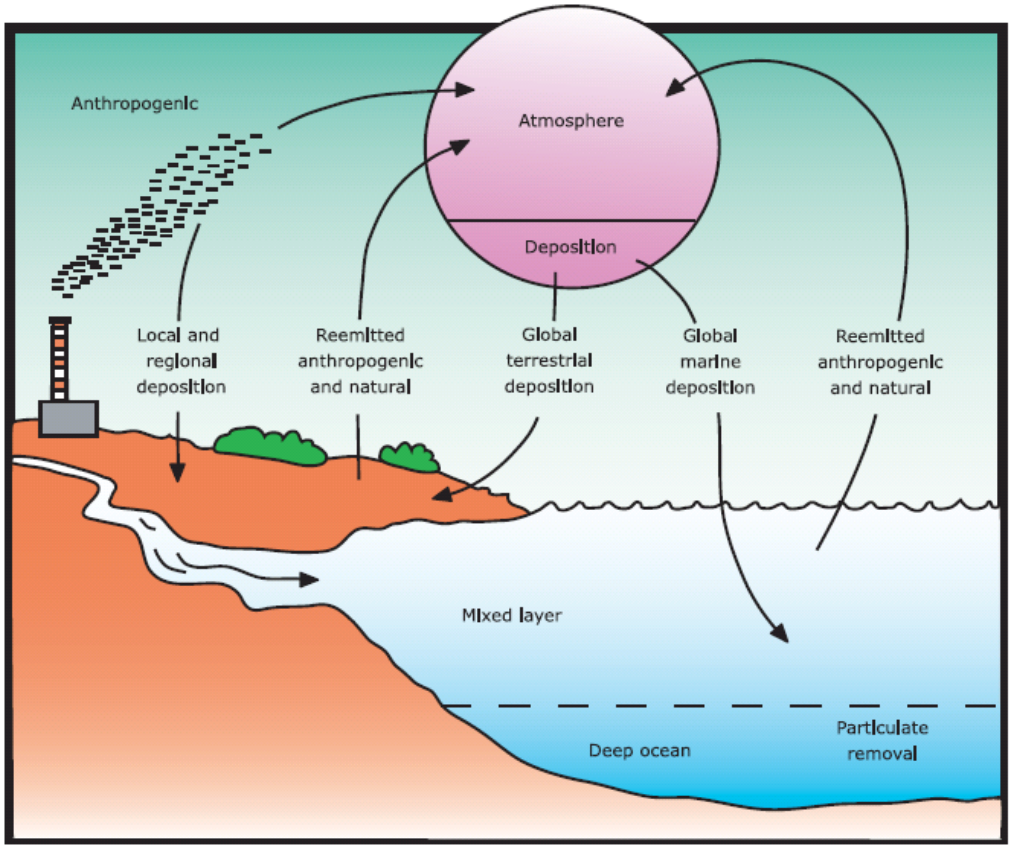

Figure 1.1 – The mercury cycle (EPA, 2006; http://www.epa.gov/mercury/roadmap/htm)

1.2.1. Physical and chemical properties

Mercury is a heavy (density 13.5 $g \cdot cm^{-3}$ at 293 K) silver-white liquid at room temperature (melting point 234.3 K and boiling point 630.4 K) (Andren and Nriagu, 1979). Mercury presents low electrical resistivity (961×10^{-9} ohm·m at 298 K – available at http://en.wikipedia.org/wiki/Mercury_(element), high surface tension, high thermal conductivity (8.30 $W \cdot m^{-1} \cdot K^{-1}$ at 300 K – at http://en.wikipedia.org/wiki/Mercury_(element) and uniform volume expansion over its entire liquid range (Andren and Nriagu, 1979). The mercury vapour pressure depends strongly on temperature, *i.e.*, approximately 14-15 $mg \cdot m^{-3}$ at 293 K according to, respectively, Andren and Nriagu (1979) and IPCS (1991) and 72 $mg \cdot m^{-3}$ at 573 K (Andren and Nriagu, 1979). These and other mercury properties may be found with more detail in Table 1.1.

Mercury occurs in three different oxidation states: 0 (Hg^0 - metallic); 1+ (Hg_2^{2+} - mercurous) and 2+ (Hg^{2+} - mercuric) (IPCS, 1991). Both mercurous and mercuric ions can form numerous inorganic and organic chemical compounds.

Specifically, mercury (0) has the unique distinction of being a volatile liquid at most Earth-surface temperatures and, therefore, it can persist for significant lengths of time in contact with air. The mercurous ion (Hg_2^{2+}) disproportionates in the presence of sulphide, hydroxyl and cyanide ions, according to following equation (Abrams et al., 1997): $Hg_2^{2+} + S^{2-} \leftrightarrow Hg^0 + HgS$.

Mercury (I) salts have low solubility except for the nitrate, chlorate and perchlorate, which behave as strong electrolytes (Abrams et al., 1997). Mercury (II) is the principal form of mercury in aquatic environments, having strong tendency to form complexes with many chemical species in solution (Beneš and Havlík, 1979). In addition to complexes, Hg(II) forms an important group of organomercuric compounds, where one or two organic radicals (R or R') are directly linked via their carbon atom to the mercury atom: R-Hg-X or R-Hg-R' (X is an inorganic ligand) (Beneš and Havlík, 1979). The most common radicals found in these organomercurials are methyl and phenyl and among the most frequently encountered inorganic ligands are chloride, hydroxide, nitrate and sulphate anions (Beneš and Havlík, 1979). Unlike most other metals, mercury exhibits higher tendency to form covalent rather than ionic bonds (Andren and Nriagu, 1979).

In natural waters, mercury is present in several major forms: organic complexes of mercury with low and high molecular weights may form a very significant part of dissolved mercury pool, depending on the concentration and nature of dissolved organics (Beneš and Havlík, 1979).

Table 1.1 – General characterisation and physical properties of mercury.

General		Physical properties		Atomic properties	
Name	Mercury	Phrase	Liquid	Crystal structure	rhombohedral
Symbol	Hg	Density	13.5 g·cm^{-3} (293 K)	Oxidation states	+2; +1; 0
Atomic number	80	Melting point	234.3 K	Electronegativity	2.00 (Pauling scale)
Appearance	Silvery 	Boiling point	630.4 K	Ionisation energies	1st: 1007.1 kJ·mol^{-1}
		Critical point	1750 K, 172.00 MPa		2nd: 1810 kJ·mol^{-1}
		Heat of fusion	2.29 kJ·mol^{-1}		3rd: 3300 kJ·mol^{-1}
Chemical series	Transition metals	Heat of vaporisation	59.11 kJ·mol^{-1}	Atomic radius	150 pm
Group	12	Specific heat capacity	27.983 J·mol^{-1}·K^{-1} (293 K)	Covalent radius	149 pm
Period	6	Vapour pressure	1 Pa (315 K)	Van der Waals radius	155 pm
Block	d		100 Pa (393 K)	Ionic radius (Hg^{2+})	110 pm (Pauling)
Atomic weight	200.59 g·mol^{-1}		10 kPa (523 K)		
Electron configuration	[Xe] $4f^{14}$ $5d^{10}$ $6s^2$		100 kPa (629 K)		

Among soluble inorganic forms of mercury, elementary mercury, neutral molecules of mercuric hydroxide or chloride predominate in fresh waters and anionic chloro-complexes or elementary mercury prevail in sea water (Beneš and Havlík, 1979).

1.2.2. Natural occurrence and anthropogenic sources and applications

The natural mercury background has been enormously augmented by mercury pollution resulting from a variety of human activities, especially the industrial ones. The primary sources of mercury release to the environment (air, water, soils and sediments) can be grouped into four categories (EPA, 2006):

- New releases from naturally occurring sources such as volcanic activity and weathering of rocks.
- Re-releases of historic mercury previously deposited through natural and anthropogenic process in soils, sediments, water bodies, landfills and waste tailings/piles (also called "re-emitted sources").
- New releases of mercury impurities from combustion of fossil fuels, and from smelting of metals such as gold and zinc.
- New releases resulting from uses of mercury in products and manufacturing processes such chlor-alkali manufacturing.

Natural sources of mercury to the environment are weathering of rocks and volcanoes, the latter being responsible for approximately half of atmospheric mercury emissions (http://en.wikipedia.org/wiki/Mercury_(element)). Mercury rarely occurs free in nature and is found mainly in cinnabar ore (HgS). Mercury deposits, which include many mercury minerals, are described in terms of composition and typical occurrence by Nriagu (1979). However, the commercial production of mercury is made almost entirely from cinnabar (mercury sulphide). Some mercury has been obtained from metacinnabar (HgS-$(HgS)_{80}(HgSe)_{20}$), livingstonite ($HgSb_4S_8$), corderoite ($Hg_3S_2Cl_2$) and other mercury minerals, species that are found in association with cinnabar (Nriagu, 1979). Minor amounts of mercury have also been recovered from mercuriferous stibnite and tetrahedrite and as a by-product in the smelting of some zinc ores (Nriagu, 1979). Mercury is extracted by heating cinnabar in a current of air and condensing the vapour: $HgS + O_2 \rightarrow Hg + SO_2$. Nowadays there are strict regulations on the amount of mercury vapour that can be allowed to escape into the air during the smelting operations. Beginning in 1558, with the invention of the patio process to extract silver from ore using mercury, mercury became an essential resource in the economy of Spain and its American colonies

(http://en.wikipedia.org/wiki/Mercury_(element)). More than 100,000 tons of mercury were mined from the region of Huancavelica, Peru. The patio process and later pan amalgamation process continued to create great demand for mercury to treat silver ores until the late 1800s. Former mines in Italy, the United States and Mexico which once produced a large proportion of the world supply have now been completely mined out or, in the case of Slovenia (Idrija) and Spain (Almadén), shut down due to the fall of the price of mercury (http://en.wikipedia.org/wiki/Mercury_(element)). In 2005, China was the top producer of mercury with almost two-thirds global share. Several other countries are believed to have unrecorded production of mercury from copper electrowinning processes and by recovery from effluents (http://en.wikipedia.org/wiki/Mercury_(element)).

A number of key international emissions anthropogenic sources contribute to global cycling and deposition of mercury via air pathways, including: coal-fired combustion sources; mining and metals production, such as smelting; mercury cell chlor-alkali manufacturing facilities; and combustion or incineration of waste products containing mercury (*e.g.* municipal solid waste combustors, medical waste incinerators, crematoria) (EPA, 2006). The United Nations Environmental Program (UNEP) estimates that the total global emissions of mercury (both anthropogenic and natural to the atmosphere) range from 4,400 to 7,500 metric ton per year, while Environmental Protect Agency (EPA) estimates that 50-70 percent of current global anthropogenic atmospheric emissions come from fuel combustion, and much of this is from China, India and other Asian countries (Figure 1.2-a) (EPA, 2006).

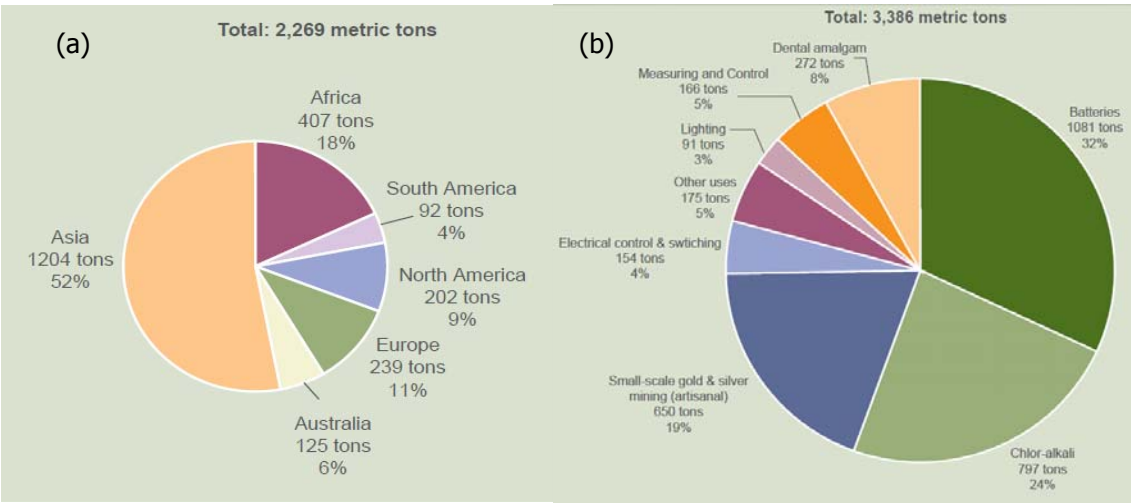

Figure 1.2 – Region distribution of man-made air emissions of mercury cycle (a) and global mercury use (b) in 2000 (EPA, 2006; http://www.epa.gov/mercury/roadmap/htm).

Moreover, these values tend to increase because coal consumption in Asia is expected to increase over the next 20 years (EPA, 2006). Small-scale gold and silver mining is an

important mercury emissions source in numerous Asian, South American and African countries and have been estimated by UNEP to be about 300 metric tons per year, but some experts estimate that total mercury release from this type of gold mining is between 650 and 1,000 metric tons per year on a global basis (EPA, 2006).

After combustion of coal, mercury-cell chlor-alkali factories are the largest source of atmospheric mercury release to global environmental (EPA, 2006). Mercury has been used in the chlor-alkali plants for simultaneous production of chlorine and caustic soda by the electrolysis of brine solutions, using a flowing cathode of metallic mercury (Nriagu, 1979; IPCS, 1991). The sodium, which amalgamates at the cathode, is converted to NaOH with water and the released mercury is recycled into the cell (Nriagu, 1979). However, since this process was not entirely closed and some losses of mercury were observed, modifications of the existing plants have been performed, such as the adoption of diaphragm cells and membrane cells. Chlorine producers across Europe are progressively moving towards the membrane cell process, as this is the most environmentally sound way of manufacturing chlorine (http://www.eurochlor.org/makingchlorine). In 2004, emissions for all mercury cells across Western Europe reached an all-time low of 1.01 grams per tonnes of chlorine capacity (http://www.eurochlor.org/makingchlorine). While the number of mercury-cell chlor-alkali facilities has been greatly reduced in Europe and United States over the last two decades, the process is still prevalent in many parts of the world including Russia, several South American countries, and India, which is estimated to have most of the plants in developing countries (EPA, 2006).

In contrast with atmospheric releases, mercury releases to water and soil have essentially a local impact rather than a global impact. The majority of mercury in surface waters from anthropogenic origin results from air deposition, municipal sewage treatment plants and point sources discharges of industrial facilities (*e.g.* mercury-cell chlor-alkali, silver and gold mining and smelting of metals) (EPA, 2006). The vast majority of land releases are the result of mining activities (*e.g.* gold, silver, zinc mining) (EPA, 2006).

The widespread industrial and agricultural applications of mercury and its compounds, is due to their unusual physicochemical properties (Nriagu, 1979). The liquid state at ordinary temperatures, the high surface tension, uniform volume expansion and inability to wet and adhere to glass have combined to make mercury extremely useful for barometers, manometers, thermometers and many other measuring devices, control instruments, electrical apparatus, batteries and boilers (Nriagu, 1979). Mercury has found commercial use in the production of fluorescent and high intensity arc discharge lamps, rectifiers, oscillators, power control switches, hot-cathode tubes and pool-cathode tubes for high-frequency applications (Nriagu, 1979; IPCS, 1991). Due to its ability to form amalgams or liquid metallic solutions (several metals solubility in mercury at 18-20ºC are compiled in

Andren and Nriagu (1979)), mercury has been used in the industrial recovery of metals (Nriagu, 1979), such as the extraction of gold from ore, mainly in Amazon region, and in the making of dental fillings. However, the use of mercury in lamps and batteries is declining, and, for example, the Nordic Countries, Germany and Austria have strict regulations on the use of amalgam and mercury thermometers (Mukherjee et al., 2004). In the early 70's the catalytic properties of mercury and many of its salts were recognized, the conversion of acetylene to acetaldehyde, as well as the production of polyvinyl chloride (PVC) and polyvinyl acetate (PVA) from vinyl chloride and vinyl acetate, respectively, being the most important industrial processes (Andren and Nriagu, 1979; Nriagu, 1979). The high toxicity of mercury and of its compounds, has led to their widespread use as bactericides, fungicides, insecticides and pharmaceuticals, such as diuretics, antiseptics, skin preparations and preservatives (Nriagu, 1979). Meanwhile, mercury is being effectively replaced by other less toxic materials. Mercury is also a useful coolant due to its high thermal conductivity and it is highly rated as an electrical conductor because of its low electrical resistivity (Nriagu, 1979). Nowadays an emerging research area is the synthesis and preparation of mercury based superconductors and semiconductors. However, mercury-cell chlor-alkali facilities are among the principal users of mercury in the world (Figure 1.2-b) (EPA, 2006). Global estimates for mercury uses in processes and uses range from 2,000 to 3,400 metric tons per year (EPA, 2006).

Over History, drastic changes have occurred in the principal uses of mercury: prior to the 16th century mercury was essentially used in medicine and paint; since then, the growth in applications has paralleled scientific advancements and the number of applications exceeded 3000 (Nriagu, 1979). Nowadays, the two principal uses of mercury are for electrical apparatus and in production of caustic soda and chorine. Since significant progress has been made to reduce industrial emissions of mercury, as well as to reduce or eliminate the amount of mercury used in several processes and products, in the future, perhaps we will have mercury-free processes and products.

1.2.3. Toxicity

According to a study performed by the Agency for Toxic Substances and Disease Registry, mercury is the third most toxic substance (http://www.atsdr.cdc.gov/cercla/07list.html). The high toxicity of mercury is related to two processes: bioaccumulation and biamplification.

Although elemental mercury is toxic to humans when it is ingested or inhaled, the great concern is to monomethylmercury (MeHg), since it is the form to which humans are primarily exposed (EPA, 2006). While all forms of mercury can bioaccumulate, MeHg generally accumulates to a greater extent than other forms (EPA, 2006). Inorganic mercury is relatively insoluble in body tissues and fluids, so it is expelled from the body about ten times faster than organometallic mercury. This, usually in form of alkly compounds such as MeHg, is somewhat soluble in fatty tissues such as the liver (Skoog et al., 1996). MeHg accumulates to toxic levels and is expelled from the body quite slowly (Skoog et al., 1996).

In the environment, inorganic mercury is converted to organometalic mercury by anaerobic bacteria in sludge deposited at the bottom of lakes, streams and other bodies of water. Small animals consume the organometallic mercury and are eaten by larger life forms. As mercury moves up the food chain from microbes, to shrimp, to fish and ultimately to larger animals, the mercury becomes even more concentrated. Thus species that are high on the food chain accumulate body burdens of mercury that can be ten times higher, or more, than the species they consume (Skoog et al., 1996). This process is called biomagnification.

Mercury exposure effects can vary depending on the form of mercury to which a person is exposed and the level and length of exposure (EPA, 2006). Today, human exposure is mainly to two forms of mercury: elemental mercury vapour and MeHg (Clarkson, 1994; EPA, 2006). The former is present in the working environment in certain workplaces where metallic mercury is used, is emitted by dental amalgam tooth fillings, and is present in the ambient atmosphere (Clarkson, 1994) and, the longer people breathe the contaminated air, the larger the risk to their health since lungs are the most important area for adsorption, retaining as much as 80%, in contrast with gastrointestinal adsorption which retains less than 0.01% (Chang et al., 1999). The latter is found principally in fish and tissues of marine mammals (Clarkson, 1994), which may then be consumed by people and wildlife. However, the divalent inorganic mercury, Hg^{2+}, is a metabolic product of both Hg^0 and MeHg and may be the proximate toxic agent for Hg^0 if not for MeHg (Clarkson, 1994).

The toxic effects of mercury depend on its form: mercuric ions (Hg^{2+}) do not cross the blood-brain barrier effectively and are therefore not a potent neurotoxicant (Chang et al., 1999); inorganic mercuric salts, however, are very nephrotoxic, producing necrotizing damage to the renal proximal tubules (Chang et al., 1999); mercury vapour and MeHg, on the other hand, enter the central nervous system readily and are considered highly neurotoxic (Chang et al., 1999).

1.2.4. Regulations

Although there is a global consensus on mercury's toxicity, there is not a standard worldwide regulation on mercury standard limits. In the United States mercury is included in the list of priority pollutants of EPA, and the permitted discharge EPA limit of wastewater for total mercury is 10 $\mu g \cdot dm^{-3}$ and the limit for drinking water is 2 $\mu g \cdot dm^{-3}$.

In the European Union mercury is also considered as a priority and hazardous pollutant and its maximum concentration for wastewater discharge is 5 $\mu g \cdot dm^{-3}$, while for drinking water is 1 $\mu g \cdot dm^{-3}$. Furthermore, under Directive 2000/60/CE, the European Union regulated the cessation or phasing out of discharges, emissions and losses by 2020 (Di Natale et al. 2006).

The Portuguese legislation established 1 $\mu g \cdot dm^{-3}$ as the maximum admissible value (MAV) in surface waters for drinking water production (DL 236/98 available at http://dre.pt) and 50 $\mu g \cdot dm^{-3}$ as the emission limit value (ELV) of wastewaters discharges (DL 236/98 available at http://dre.pt) and as the emission limit value of industrial discharges (DL 52/99 available at http://dre.pt). The ELV is the monthly mean, defined as the arithmetical mean of the daily mean.

The World Health Organization (WHO) recommends a maximum uptake of 0.3 mg per week and 1 $\mu g \cdot dm^{-3}$ as the maximum acceptable concentration in drinking water (Zhang et al., 2005).

1.2.5. Mercury removal from water, effluents and wastewaters

In Nature, soil particles such as clays, oxides, peat moss and humus adsorb mercury from rainfall and remove it from the cycle (Abrams et al., 1997). The tendency of mercury to sink rapidly and combine with sulphide in anaerobic bottom sediments to form cinnabar (HgS) and reaction with organic matter appears to be the major scavenging mechanism (Abrams et al., 1997).

For liquid effluents and wastewaters, several techniques are available for removing mercury. Some of them are merely laboratory curiosities while others are commercially proven techniques, treating mercury-contaminated effluents from a number of industries (Beszedits, 1979). For a more effective removal, most of the available commercial treatment systems combine several removal techniques instead of only one.

1.2.5.1. Biological treatment

Biological methods, in particular activated sludge, have been widely used in municipal and industrial wastewaters treatment since they provide high quality effluents at low operating conditions (Beszedits, 1979). The major disadvantage of these methods is that although the activated sludge can tolerate heavy metals to a certain point, beyond a certain level the metals become toxic to the viable micro-organisms (Beszedits, 1979).

Some studies on heavy metal removal by activated sludge treatment indicate a reduction on mercury levels by about 85% and by 69% (Beszedits, 1979). During the treatment of wastewater in municipal sewage works, some of the mercury is vaporized, some of it passes out in the discharge effluent and a sizeable fraction becomes concentrated in the sludge (Beszedits, 1979).

Although mercury tends to be toxic towards most micro-organisms, *Pseudomonas* strain K62 is a mercury-resistant bacterium able to take up and vaporize organic and inorganic mercury (Beszedits, 1979).

1.2.5.2. Precipitation and complexation

Chemical precipitation is the most popular method for the removal of inorganic forms and can be conducted in batch or continuous mode (Beszedits, 1979). Lime (calcium oxide), caustic soda and sodium carbonate are among the chemicals most widely used (Beszedits, 1979). The former is the most frequently employed because of its relative simplicity and low cost (Beszedits, 1979). However, since metal sulphides are generally more insoluble in water than the corresponding hydroxides, sulphide precipitation has gained wide acceptance. On the other hand, sulphide precipitation suffers from one notable deficiency: an excess of sulphide in solution tends to react with water to form noxious hydrogen sulphide but if an insufficient amount is added, the concentration of metal remaining will be high (Beszedits, 1979). The presence of complexing agents can reduce drastically the metal removal, so breaking down the complex before chemical precipitation is helpful (Beszedits, 1979).

1.2.5.3. Ion exchange

Ion exchange is one of the most effective techniques for removing heavy metals from solutions (Beszedits, 1979). It is employed extensively for metal finishing bath purification, polishing effluents after primary treatment and recovering precious metals. Numerous ion

exchange resins are specific, having a high capacity for individual ions. To avoid fouling in the resins beds, suspended solids must be removed from the influent waste stream (Beszedits, 1979). Certain type of resins can be deteriorated under oxidizing conditions (Beszedits, 1979).

Inorganic mercury forms and MeHg have been successfully removed by a chelating resin called Ionac SRXL in the pH range of 1-9 (Beszedits, 1979). Though this particular resin is no longer commercially available, another one purportedly identical, Strafion NMRR, has a capacity of 680 kg Hg/1000 kg adsorbent when mercury is dissolved in water (Beszedits, 1979). However, performance of the resin is strongly influenced by pH: above 5 for inorganic mercury and between 6 and 9 for MeHg removal (Beszedits, 1979).

Many other resins are commercially available for mercury removal; some of them take advantage of thiol and sulphur functional groups for the removal of heavy metals from wastewaters.

1.2.5.4. Activated carbon adsorption

Powdered and granular activated carbon has been used for years in the treatment of municipal and industrial wastewaters (Beszedits, 1979). Adsorptive capacity of activated carbon is a function of such parameters as carbon pore size, surface area, temperature, pH and initial concentration of the solution treated (Beszedits, 1979). Formation of sulphide in activated carbon columns through the action of sulphate reducing bacteria under anaerobic conditions has been well documented, but the presence of sulphide enhances the removal of metals (Beszedits, 1979).

Several studies have reported the successful application of activated carbons to remove Hg^{2+} from waters and wastewaters (*e.g.* Mohan et al., 2001; Krishnan and Anirudhan, 2002; Ranganathan, 2003; Yardim et al., 2003; Rao et al., 2009). Despite its efficient use, activated carbon remains an expensive material and the higher the quality of activated carbon, the greater its cost (Babel and Kurniawan, 2003).

1.2.5.5. Solvent extraction

Solvent extraction of metals from solutions has received a tremendous increase by the introduction of selective complexing agents in the early 1960's (Beszedits, 1979). The recovery of metals from primary sources and craps by the use of organic extractants is a well-established process (Beszedits, 1979). Since this technique is widely used in several countries for copper recovery, considerable attention has been focused on the application

of the technique for removal and recovery of metals from sludges and even from dilute water solutions (Beszedits, 1979).

In the case of mercury, it was found that high molecular weight amines were effective for its removal from industrial wastewater (Beszedits, 1979). A study with several amines reveals that two commercially available amines, Aliquat 336-S (tricaprylmethylammonium chloride) and Adogen 464 (methyltri (C_8-C_{10}) ammonium chloride) are most versatile since they could remove mercury from acid as well as alkaline brine solutions (Beszedits, 1979). Extraction with these amines results in a mercury level reduction by more than 99%. This technique is also effective for the removal of mercury from wide variety of aqueous solutions. Furthermore, since both amines have solubility of less than 5 ppm in water, they do not pose any toxicity hazards towards aquatic fauna; however, many complexing agents commonly used in solvent extraction are deadly to fish even at low concentrations (Beszedits, 1979).

1.2.5.6. Electrolytic process

Electrolytic processes are quite versatile and metals recovered by this technique are of high purity (Beszedits, 1979). These processes can be used for plating out metals, destroy cyanides and reducing chromium (Beszedits, 1979). The removal of mercury and several other metals from wastewaters can be performed by an electrochemical process employing a fluidised bed packed with conductive particles. Bed packing may consist of metal particles or metal-coated ceramic spheres and the collector metal is usually tin (Beszedits, 1979). A low voltage d.c. current is applied across the bed and the metallic pollutants deposit on the particles as the waste stream flows in an upward direction through the bed (Beszedits, 1979). The only pre-treatment required is pH adjustment to around 7 and regeneration can be accomplished by chemical (usually nitric acid) or electrochemical stripping (Beszedits, 1979).

1.2.5.7. Reverse osmosis

Reserve osmosis may be used by itself or it can supplement other treatment methods. Combined reverse osmosis and ultra-filtration find widespread application in the recovery of valuable constituents from waste streams (Beszedits, 1979). Moreover, in the metal finishing industry reverse osmosis is employed for the recovery of precious and common metals (Beszedits, 1979).

1.2.5.8. Liquid membranes

The liquid membranes process can reduce the mercury level in wastewaters by more than 99% even if the initial concentration is as high as several hundred ppm (Beszedits, 1979). Liquid membranes are water-immiscible emulsions made up of an oil phase composed of surfactants and additives in hydrocarbon solvent which encapsulates tiny droplets of an aqueous solution of appropriate reagents for removing (stripping) and trapping wastewater contaminants (Beszedits, 1979). In many respects the liquid membrane process is similar to solvent extraction but it combines extraction and stripping into a single operation. In the case of heavy metals, which do not have an appreciable oil solubility a suitable carrier ion is added to the oil phase to facilitate the transport (Beszedits, 1979). The Alamine 336, a C_8-C_{10} tertiary amine has been successfully employed as carrier ion in the case of mercury removal (Beszedits, 1979).

1.2.5.9. Agriculture products

Numerous agricultural products and by-products have the ability to adsorb heavy metals and due to their relative abundance and low cost, considerable attention has been given to their application in removing mercury and other metals from industrial effluents (Beszedits, 1979). Although many of these agriculture materials have demonstrated an exceptional affinity for organometallic and inorganic mercury in laboratory studies, only a few are currently used in commercial pollution control equipment (Beszedits, 1979). Feng et al. (2004) and Rao et al. (2009) have reported the successful application of agricultural by-product waste to remove Hg^{2+} from waters.

1.2.5.10. Ozonation

Ozonation is one of the most versatile wastewater treatment techniques, widely used for disinfections of water supplies and sewage, decolourisation of wastewaters and the destruction of bio-refractory organics (Beszedits, 1979). Ozonation can often enhance the biodegradability of industrial effluents and can be very effective in the removal of toxic compounds (Beszedits, 1979). The ozonation is particular useful for the destruction of metal-organic complexes and the liberated metal can be removed by precipitation (Beszedits, 1979).

1.2.5.11. Mercury recovery from sludge

Overall, the removal of mercury from various processes described previously and effluent streams can create voluminous sludges and proper disposal of these sludges can be troublesome and expensive (Beszedits, 1979). However, sludge disposal problems are greatly mitigated if the mercury is recovered, which can be done by hypochlorite and chlorine oxidation, electrolytic oxidation and roasting (Beszedits, 1979).

1.2.6. Analytical techniques for mercury determination

The most common techniques to determine the mercury content on environmental samples include cold vapour atomic absorption spectrometry (CVAAS), cold vapour atomic fluorescence spectroscopy (CVAFS), gold trap pre-concentration, gas chromatography with electron capture detection (GC/ECD) and neutron activation analysis (NAA) (Rood and Sanford, 1999). The sample matrix and mercury content must always be considered when selecting the analytical technique. The analytical technique selected for mercury determinations in my study was cold vapour atomic fluorescence spectroscopy, since is usually a hundred times more sensitive than atomic absorption, allowing the measurement of 1 $ng \cdot dm^{-3}$ of mercury.

1.2.6.1. Theoretical fundamentals of cold vapour atomic fluorescence spectroscopy

Cold vapour atomic fluorescence spectroscopy, also referred to by the acronym CVAFS, is a subcategory of the analytical technique known as atomic fluorescence (AFS). Atomic fluorescence spectroscopy is, together with flame emission and atomic absorption spectroscopy, one of the most common elemental analysis techniques and is based on the fluorescence of atomic vapours (Horlick, 1986). Atomic fluorescence occurs when excited atoms return from an excited electronic state of higher energy to their ground electronic state emitting a fluorescent radiation (Horlick, 1986; Braun, 1987; Skoog et al., 1996). The intensity of the emitted radiation is measured perpendicularly to the incident beam, in order to avoid interference of the transmitted excitation light and guaranteeing that only the light scattered by the sample causes stray light. There are three types of fluorescence: the most common resonance and non-resonance fluorescence, and the sensitized fluorescence which is rarely encountered (Horlick, 1986; Braun, 1987). Resonance fluorescence is used most often for quantitative analysis by AFS and occurs when the

absorption and fluorescence wavelengths are identical, while the non-resonance fluorescence occurs when the exciting wavelength and the wavelength of the emitted fluorescence line are different (Figure 1.3) (Horlick, 1986; Braun, 1987).

The main difference between AFS and CVAFS is that in the latter is not necessary to use sources (*e.g.* flame or electro-thermal atomizers) to generate atomic vapour. CVAFS is used in the determination of volatile heavy-metal, such as mercury, because it makes use of its appreciable vapour pressure (0.266 Pa at 298 K), that allows vapour measurement at room temperature. The mercury atoms are excited by an ultraviolet light source at 253.7 nm and then fluoresce back to the ground electronic state, at the same wavelength (resonance fluorescence). Unlike the directional excitation radiation, fluorescence is omnidirectional and may, thus, be detected using a photomultiplier or UV photodiode.

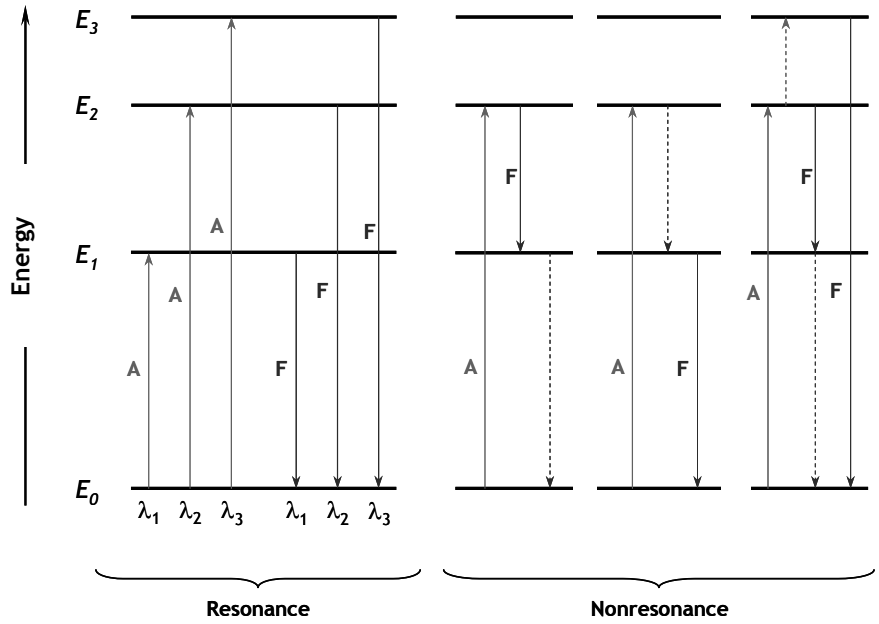

Figure 1.3 – Energy-level diagram illustrating the energetic transitions that occur during resonance and nonresonance atomic fluorescence. A - Absorption; F - Fluorescence; the dashed lines depict radiationless transitions.

1.2.6.2. Instrumentation and analytical procedure

The CVAFS system used in this work is presented in Figure 1.4 and includes three distinct liquid fluxes (sample, blank and reducer), two peristaltic pumps holding up the pump tubes, a mixing valve, a gas-liquid separation cell, a drying membrane, a fluorescence detector and a computer with appropriate software.

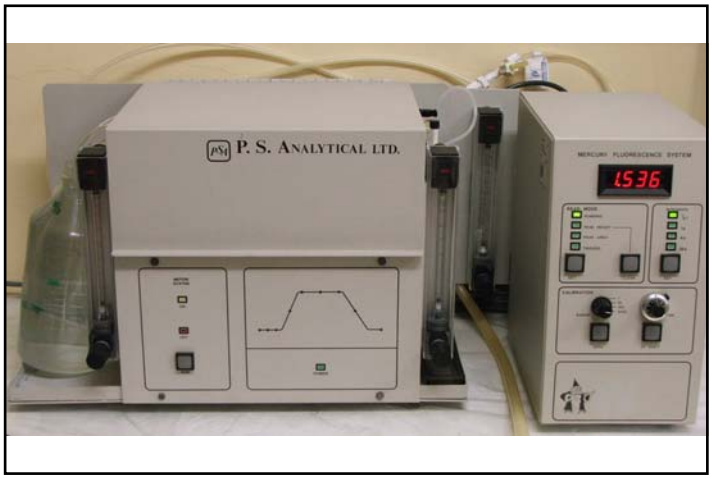

Figure 1.4 – CVAFS equipment for mercury determination.

The reducing agent used was tin (II) chloride (2% (w/v) in hydrochloric acid 10% (v/v)) and the blank was always high-purity water (Milli-Q water). The sample, the water and the reducing solutions were pumped from the storage containers by a peristaltic pump, which works continuously at constant speed, pumping the solutions in the correct proportions required by the chemical reaction (Figure 1.5). Afterwards, the solutions were mixed in the mixing valve (reducer + water or reducer + sample) and the Hg^{2+} ions present in the sample were reduced to elemental mercury (Hg^0) (Figure 1.5). Then, the resultant mixture and the gaseous products formed were continuously pumped into the gas-liquid separation cell and, by bubbling up an argon flux (carrier gas), the generated Hg^0 was removed from the separation cell and passed through a drying membrane, to remove any water vapour that could be carried out and could cause fluorescence quenching. The membrane was dried in air K (dryer). Finally, mercury vapour reached the detector cell for quantification, where another argon flux (sheath gas) kept the measure conditions as uniform as possible, reducing memory effects (Figure 1.5). The set up conditions in the AFS detector are shown in Table 1.2.

The Hg^{2+} concentration in the samples was quantified by a calibration curve. The standards were prepared daily by diluting the stock solution of $Hg(NO_3)_2$ to the desired concentration in nitric acid 2% (v/v). The concentration of the standards ranged from 0.0 to 50 $ng \cdot dm^{-3}$, in the range 1000, and from 0.0 to 0.5 $\mu g \cdot dm^{-3}$, in the range 100. The samples were always analysed in triplicate and at the end of the working day it was necessary to rinse all the system by pumping water into the three liquid fluxes and to pass air K into the membrane.

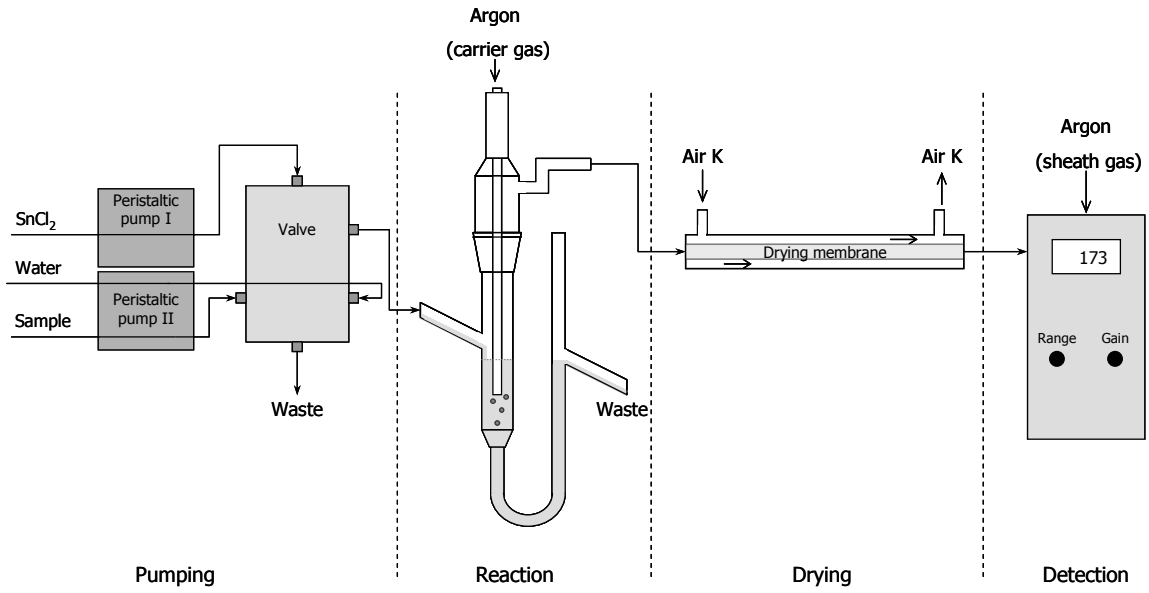

Figure 1.5 – Representation of mercury (II) analysis in the CVAFS system.

Table 1.2 – AFS-detector measure conditions.

Parameter	**Value**
Range	100 or 1000
Fine Gain	10.0
Delay time	10 s
Rise time	30 s
Analysis time	30 s
Memory time	50 s
Sample flow	7.2 – 7.4 $cm^3 \cdot min^{-1}$
Blank (water) flow	7.2 – 7.4 $cm^3 \cdot min^{-1}$
Reducer ($SnCl_2$) flow	2.4 – 3.0 $cm^3 \cdot min^{-1}$
Carrier gas (argon) flow	300 $cm^3 \cdot min^{-1}$
Sheath gas (argon) flow	300 $cm^3 \cdot min^{-1}$
Dryer (air K) flow	2 500 $cm^3 \cdot min^{-1}$

1.2.6.3. Quality control and assurance of Hg^{2+} determinations

The Hg^{2+} concentration in the samples was quantified using a five standards calibration curve (*e.g.* Figure 1.6) and a standard was analysed every three samples to check for the equipment drift. The samples were always analysed in triplicate and blank analysis was performed per each calibration curve.

Since the slope and the intercept of the calibration curves changed daily (Table 1.3), new calibration curves were performed when the Hg^{2+} determinations were done. This resulted in almost four hundred calibration curves measured in this work.

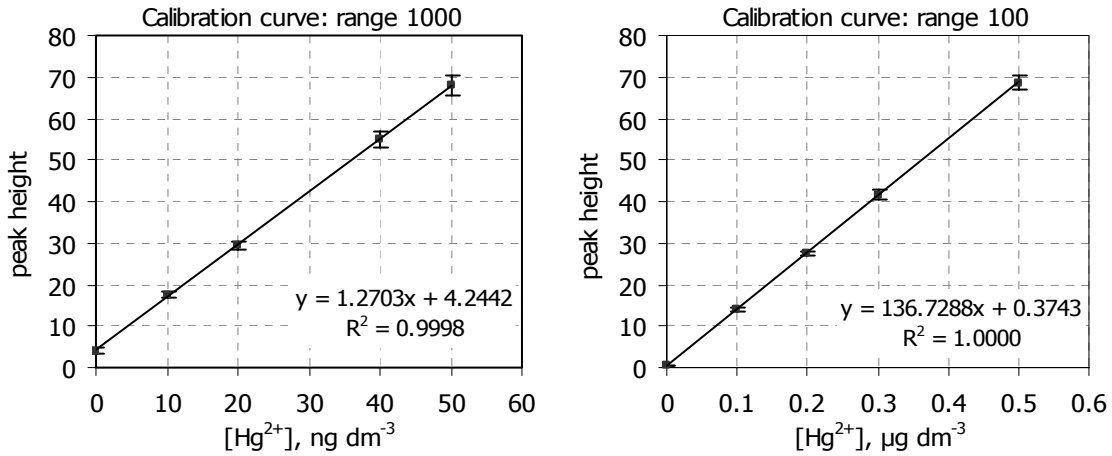

Figure 1.6 – Examples of a calibration curve for the range 1000 (ng·dm^{-3}) and 100 (µg·dm^{-3}).

The slope (b) together with the confidence limits were:

$$b \pm t \frac{S_{y/x}}{\sqrt{\sum_i (x_i - \bar{x})^2}} \qquad (1.1)$$

where the *t*-value is taken at the desired confidence level and (n-2) degrees of freedom (Miller and Miller, 1993). Likewise, the intercept (a) together with the confidence limits were determinated as:

$$a \pm t S_{y/x} \sqrt{\frac{\sum_i x_i^2}{n \sum_i (x_i - \bar{x})^2}} \qquad (1.2)$$

To calculate the confidence levels for the slope and intercept, it is necessary to calculate first the standard deviation of y-residuals ($S_{y/x}$), which is given by:

$$S_{y/x} = \sqrt{\frac{\sum_i (y_i - \hat{y}_i)^2}{n-2}} \quad (1.3)$$

This equation uses the y-residuals, $y_i - \hat{y}_i$, where the $\hat{y}_i$ values are the points on the calculated regression line corresponding to the individual x-values, *i.e.* the fitted y-values.

Table 1.3 – Slope and intercept, with the respective confidence intervals at 95% confidence level, Pearson correlation coefficient and detection limits for calibration curves performed in different days.

Range 1000				
Day	Slope ± 95% confidence limits	Intercept ± 95% confidence limits	Correlation coefficient	Detection limit ($ng \cdot dm^{-3}$)
1	1.35 ± 0.09	3.37 ± 2.65	0.9998	2.52
2	1.18 ± 0.07	2.18 ± 2.17	0.9997	2.38
3	1.42 ± 0.09	3.07 ± 2.67	0.9997	2.43
4	1.10 ± 0.08	1.51 ± 2.44	0.9993	2.86
5	1.27 ± 0.09	4.24 ± 2.87	0.9999	2.91
6	1.39 ± 0.09	3.62 ± 2.74	0.9998	2.54
7	1.21 ± 0.07	2.97 ± 2.10	0.9999	2.23
Range 100				
Day	Slope ± 95% confidence limits	Intercept ± 95% confidence limits	Correlation coefficient	Detection limit ($\mu g \cdot dm^{-3}$)
1	159.69 ± 8.49	-0.70 ± 2.37	0.9996	0.019
2	152.00 ± 6.31	-0.54 ± 1.76	0.9998	0.015
3	115.59 ± 3.13	0.14 ± 0.87	0.9999	0.010
4	139.66 ± 5.57	-0.19 ± 1.55	0.9998	0.014
5	136.50 ± 6.66	-0.70 ± 1.86	0.9997	0.018
6	124.96 ± 1.26	0.02 ± 0.35	1.0000	0.004
7	118.75 ± 1.89	0.13 ± 0.53	1.0000	0.006

The detections limits (Table 1.3) were estimated from the calibration curve as the concentration giving a blank signal, which was estimated as the calculated intercept

because blank signals did not differ from baseline, plus three times the standard derivation of the blank, which was estimate as $S_{y/x}$.

Precision was evaluated by calculating the variation between replicates. However, it was not possible to do a more comprehensive validation for the Hg^{2+} determinations due to the lack of certified reference materials (CRM). Nevertheless, an Hg^{2+} solution control was always performed together with the experiments and recoveries were found to be between 76-93%.

1.3. Microporous Materials

1.3.1. Zeolites

In 1756 a Swedish mineralogist, Cronstedt, recognized a new mineral species which he called 'zeolite' on the basis of its intumescence (Dyer, 1988). He found it in relatively small cavities in rocks of volcanic origin (a classical zeolite occurrence) (Dyer, 1988). Zeolites are a class of crystalline aluminosilicates based on rigid anionic frameworks with well-defined channels and cavities (Smart and Moore, 1992). These cavities contain exchangeable metal cations, usually Na^+ or K^+, and can also hold removable and replaceable guest molecules (water in naturally occurring zeolites) (Smart and Moore, 1992). Cronstedt observed that on heating with a blowtorch zeolites hissed and bubbled as though they were boiling and named them zeolites from the Greek words zeo, to boil and $lithos$, stone (Smart and Moore, 1992). Natural zeolites are formed in a variety of geological environments mainly from volcanic debris; approximately 40 naturally occurring zeolites have been recorded and characterized and more than 100 entirely synthetic structures have been developed (Dyer, 1988; Smart and Moore, 1992). The general formula for the composition of a zeolite is

$$M_{x/n}\left[(AlO_2)_x(SiO_2)_y\right]\cdot mH_2O$$

where cations M of valence n neutralize the negative charges on the aluminosilicate framework.

Zeolites are crystalline, hydrated aluminosilicates with open three-dimensional structures built of $[SiO_4]^{4-}$ and $[AlO_4]^{5-}$ tetrahedra linked to each other by sharing all the oxygens (Figure 1.7) to form regular intracrystalline cavities and channels of molecular dimensions (Dyer, 1988; Smart and Moore, 1992; Rocha and Anderson, 2000).

Silicon-oxygen tetrahedra are electrically neutral when connected together in a three-dimensional network as in quartz (SiO_2), however the replacement of Si^{4+} by Al^{3+} in such structure creates an electrical imbalance and, to preserve the overall electrical neutrality,

each AlO_4 tetrahedron needs a balancing positive charge that is provide by exchangeable cations held electrostatically within the zeolite (Rocha and Anderson, 2000).

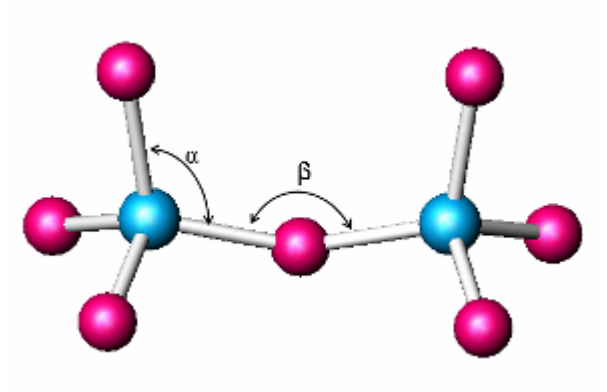

Figure 1.7 – The zeolite building units. [SiO_4] and [AlO_4] tetrahedra linked by corner-sharing where α is the O-Si/Al-O bond angle and β is the Si/Al-O-Si/Al bond angle (http://wikis.lib.ncsu.edu/index.php/Zeolites)

It is possible for the tetrahedra (primary building units) to link by sharing two, three or all four corners, thus forming a variety of different structures (Smart and Moore, 1992) denominated secondary building units (Sbu). The secondary building units consist of n-ring structures which can contain as many as 20 tetrahedra and as little as 4 (http://wikis.lib.ncsu.edu/index.php/Zeolites). This is shown schematically in Figure 1.8. Each corner in the secondary building units represents the centre of a primary building unit (tetrahedron). Secondary building units can be linked to form cages or channels within the structure. Connecting rings of different sizes leads to many different structures.

The zeolite structure may be classified by secondary building units content, structure type (IUPAC nomenclature), name (prefix 'zeolite' indicate that the material is known only as synthetic material) and typical unit cell content (Dyer, 1988).

Due to their structure, these materials exhibit remarkable physical and chemical properties, such as selective sorption, ion exchange and catalytic activity (Rocha and Anderson, 2000) and because of them these materials have considerable potential for environmental and industrial applications (Pavel et al., 2003) as cation exchangers (*e.g.* used in water softening), molecular sieves for separating molecules of different sizes and shapes (used in separation of gases and drying agents) and catalysts. Of special importance for environmental uses is their ability to uptake and retain heavy metals species from aqueous media.

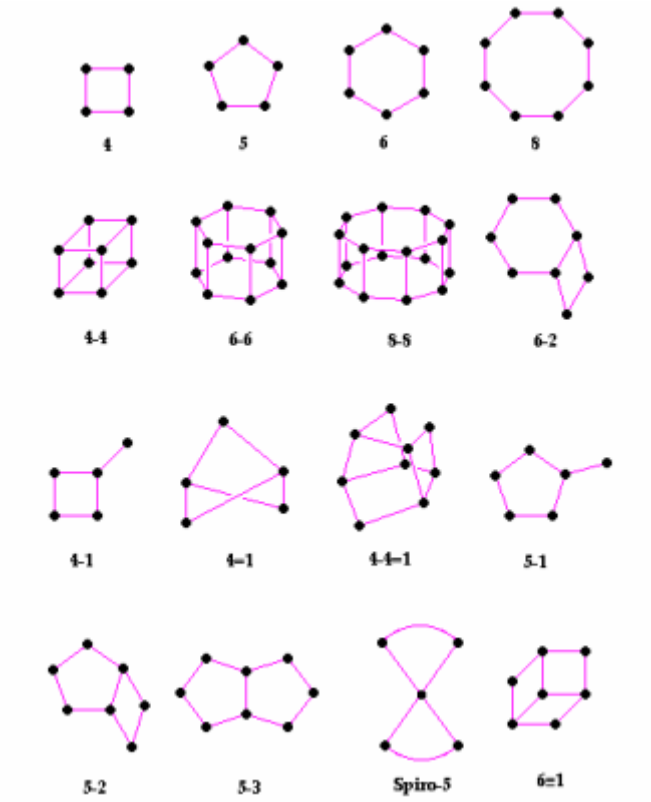

Figure 1.8 – The secondary building units of zeolite structures. (http://wikis.lib.ncsu.edu/index.php/Zeolites)

Many zeolite structures are based on the sodalite unit (or β-cage) (Figure 1.9) which is a combination of two secondary building units: 4- and 6-rings linked together to form a basket-like structure also called a truncated octahedron (Smart and Moore, 1992; Ferreira, 1997).

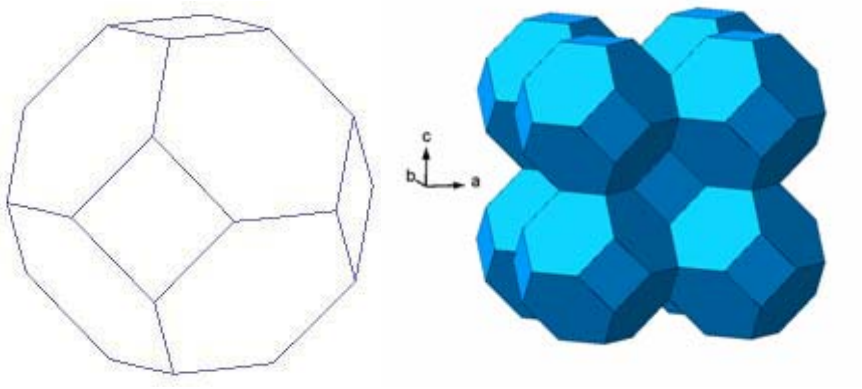

Figure 1.9 – The β-cage, common in many zeolite structures and describable as a truncated octahedron. O has been omitted, and the vertices represent Al/Si. (a) The mineral sodalite structure, which is itself composed of these units, with each 4-ring shared by two β-cages (b). (http://wikis.lib.ncsu.edu/index.php/Zeolites)

Zeolite-A and zeolite-X (Figure 1.10) are two examples of synthetic zeolites well characterised, with their structure based on the sodalite unit, commercially available and with industrial applications. The Na^+ form of zeolite-A is used as a water softener by exchanging the Na^+ ions with Ca^{2+} in hard water; it also can be added to detergents to replace polyphosphates which are not environmentally friendly; it can be used to recover radioactive strontium; while zeolite-X is most frequently seen in industrial settings, such as petroleum cracking, due to the presence of large channels. Moreover, zeolites were heavily used in the clean-up operations after the Chernobyl and Three-Mile Island incidents (Smart and Moore, 1992).

Zeolite-A is a fairly typical example where the Si/Al ratio is unity as it can be found in the crystal structure where Si and Al atoms strictly alternate, while zeolite-X structure has Si/Al ratios between 1 and 1.5 (Smart and Moore, 1992). Clearly changing the Si/Al ratio of a zeolite also changes its cation content; the fewer aluminium atoms there are, the fewer exchangeable cations will be present (Smart and Moore, 1992). Table 1.4 displays the structure classification of zeolites A and X.

Table 1.4 – Zeolite structure classification (Dyer, 1988).

Name	Secondary building unit	Structure type	Typical unit cell content
Zeolite-A	Double 4 ring (D4R)	LTA	$Na_{12}[(SiO_2)_{12}(AlO_2)_{12}]\cdot 27H_2O$
Zeolite-X	Double 6 ring (D6R)	FAU	$Na_{88}[(SiO_2)_{104}(AlO_2)_{88}]\cdot 220H_2O$

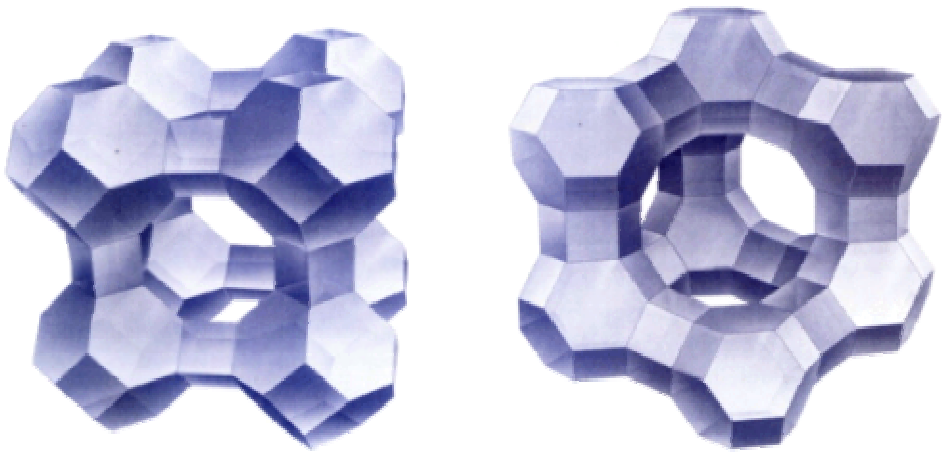

Zeolite-A Zeolite-X

Figure 1.10 – Zeolite-A (LTA) and zeolite-X (FAU) 3-D structure (http://www.sinolbc.com)

One of the most important structural features of zeolites is the network of linked cavities or pores forming a system of channels throughout the structure (Smart and Moore, 1992). These cavities are of molecular dimensions and can adsorb species small enough to

gain access to them (Smart and Moore, 1992). The size of the window or pore-opening into the channel is the factor controlling the molecules that can be adsorbed in the cavities (Smart and Moore, 1992). For example, the pore-opening in zeolite-A is 410 pm, determined by an 8-ring window which is considerably small when compared with the diameter of the internal cavity (1140 pm) (Smart and Moore, 1992). On the other hand, zeolite-X has a 12-ring window, whose diameter is 740 pm (Hyatt, et al., 2004).

The well-known name of molecular sieve given to these crystalline aluminosilicates is due to the windows and channels, which form a three-dimensional sieve with mesh widths between about 300 and over 1000 pm, able to separate mixtures such as straight-chain and branched-chain hydrocarbon (Smart and Moore, 1992).

1.3.2. Zeotype materials: titano- and zircono-silicates

During the 1980s a variety of novel microporous frameworks were synthesised based on an aluminophosphate system (Rocha and Anderson, 2000). However, in their pure form these materials exhibit little catalytic potential and absence of ion-exchange properties, since the overall framework has no net charge (Rocha and Anderson, 2000). The frameworks of aluminophosphates (AlPOs) consist of alternating corner-sharing of $[PO_4]$ and $[AlO_4]$ tetrahedra; nevertheless framework substitutions are possible and lead to silico-aluminophosphates (SAPOs) and metal-substituted aluminophosphates (MeAPOs) (Rocha and Anderson, 2000). Metals, such as magnesium, manganese, ion, cobalt, zinc and vanadium are the most widely used in the framework substitutions (Rocha, 1996a). In all these materials the framework metal is apparently in tetrahedral coordination (Rocha and Anderson, 2000).

However, during the 1990s some attention was given to a much less explored, compositional possibility for microporous frameworks, structures consisting of interlinked octahedra and tetrahedra (Rocha and Anderson, 2000). Two of the most relevant examples of this type of materials are microporous titanosilicates and zirconosilicates. Both, titanosilicates and zirconosilicates form an important class of materials that occur naturally and can also be synthesised. Usually, the structure of these materials is built of SiO_4 tetrahedra and TiO_6 and ZrO_6 octahedra, respectively (Rocha, 1996a; Zubkova and Pushcharovsky, 2008).

In Nature, titanosilicates usually have a dense structure but, although their deposits are rare a few natural microporous titanosilicates are known (Rocha, 1996a; Ferreira, 1997). Probably the most familiar of natural microporous titanosilicates is the mineral zorite,

$Na_6[Ti(Ti_{0.9}Nb_{0.1})_4(Si_6O_{17})_2(O, OH)_5]\cdot 11H_2O$, that was discovered in 1973 by Mer'kov and co-works, in trace quantities in the Kola Peninsula (Siberian Tundra) (Rocha, 1996a; Ferreira, 1997; Rocha and Anderson, 2000). The structure of this mineral was solved in 1979 by Belov and Sandomirskii and is characterised by a highly disordered framework with ostensibly a 2-dimensional channel system. Two orthogonal sets of channels are defined by 12-T/O atom and 8-T atom rings (T = tetrahedral silicon; O = octahedral titanium) (Rocha and Anderson, 2000). In reality, the disorder in zorite results in larger 12-ring channels becoming partitioned into sections (Rocha and Anderson, 2000). Other examples of natural titanosilicates are the minerals penkvilksite, $Na_4[Ti_2Si_8O_{22}]\cdot 4H_2O$, and vinogradovite, $Na_8[Ti_8Si_{16}O_{52}]$ (Ferreira, 1997).

Zirconium silicates occur widely in Nature and their formation is mainly connected with hydrothermal conditions (from *ca.* 200 to 500 ºC) (Rocha and Anderson, 2000; Zubkova and Pushcharovsky, 2008). More than 20 natural and synthetic zirconium silicates are known and for about one-third of them the crystal structures have been solved (Rocha and Anderson, 2000).

Some of the first hydrothermal syntheses of zirconosilicates were carried out by Maurice in 1949, while the first synthesis of a material containing titanium was only presented in 1967 by Young, however, later studies reveal that this material had a considerable dense structure to be considered a microporous material (Ferreira, 1997; Rocha and Anderson, 2000).

Chapman and Roe (1990) published the synthesis and X-ray diffraction pattern of three microporous titanosilicates, one of which seemed to have the structure of mineral zorite, while Engelhard Corporation filed a series of patents describing a similar small-pore material, which was named ETS-4 (Engelhard titanosilicate-4), and a second solid named ETS-10 (Kuznicki, 1989; Kuznicki, 1990). The latter has been receiving much attention owing to its wide-pore nature and thermal stability. As to the other two titanosilicates reported by Chapman and Roe (1990), one it is an analogue of mineral vinogradovite and the other is the analogue to mineral pharmacosiderite (Ferreira, 1997). Later, Clearfield and co-workers studied by powder X-ray diffraction methods the structure of pharmacosiderite analogues with composition $HM_3TiO_4(SiO_4)_3\cdot 4H_2O$ ($M = H^+, K^+, Cs^+$) and in 1994 reported the synthesis, crystal structure and ion exchange properties of a novel porous titanosilicate of ideal composition $Na_2Ti_2O_3SiO_4\cdot 4H_2O$ (Rocha and Anderson, 2000). Rocha and Anderson and co-works have been able to prepare a series of synthetic analogues of nenadkevichite, which is a rare mineral first found in the Lovozero region (Russia) with the composition (Na, Ca)(Nb, Ti)$Si_2O_7\cdot H_2O$, with Ti/Nb molar ratios ranging from 0.8 to 17.1 and a purely titaneous sample (Rocha et al., 1996b; Rocha et al., 1996c). When attempting to prepare novel microporous framework titanosilicates several groups

have obtained novel microporous and/ layered materials, some of which have very interesting and unusual structures, showing potential to be used in a number of applications such as ion exchange (Rocha and Anderson, 2000). For example, Ferreira (1997) observed the co-precipitation of other materials during the synthesis of ETS-10. The new materials were denominated AM-n (Aveiro-Manchester, n=1, 2, 3, 4), the two cities where the work was developed. One such material, know as AM-1 (Lin et al., 1997) or JDF-L1 (Roberts et al., 1996) has the composition $Na_4Ti_2Si_8O_{22}{\cdot}4H_2O$ and is an unusual non-centrosymetric tetragonal layered solid (Rocha and Anderson, 2000). Others, like AM-2 and AM-3, do not contain Ti-O-Ti linkages that in many porous framework titanosilicates often form infinite chains. AM-2 is a synthetic potassium titanosilicate analogue of the mineral umbite, a rare zirconosilicate found in the Khibiny alkaline massif (Russia) and AM-3 is a sodium titanosilicate analogue of the mineral penkvilksite found in Mont Saint-Hilaire, Québec (Canada) and the Kola Peninsula (Russia) (Rocha and Anderson, 2000). AM-4, $Na_3(Na,H)Ti_2O_2(Si_2O_6)_2{\cdot}2H_2O$, is yet another example of a layered titanosilicate (Rocha and Anderson, 2000). Clearfield et al. (1997) reported the synthesis of a layered titanosilicate that seems to be closely related with AM-4; the same group has also carried out a considerable number of studies on the evaluation of synthetic ion exchangers for cesium and strontium removal from contaminated groundwater and wastewater using among others, several microporous and layered titanosilicates (Rocha and Anderson, 2000).

After the first records on hydrothermal syntheses of zirconosilicates by Maurice, Baussy and co-works in 1974 summarise the early work in this field and reported the hydrothermal syntheses of analogues of minerals catapleiite ($Na_2ZrSi_3O_9{\cdot}2H_2O$) and elpidite ($Na_2ZrSi_6O_{15}{\cdot}3H_2O$) at 350-500 ºC (Rocha and Anderson, 2000). More recently, Jale et al., (1999) reported the hydrothermal synthesis of a potassium analogue of elpidite at relatively low temperature (200 ºC). In 1997 Clearfield and co-workers, reported the synthesis, characterisation, and properties of three novel layered materials and five other zirconosilicates, in particular a synthetic analogue of mineral gaydonnayite (ideal formula $Na_2ZrSi_3O_9{\cdot}2H_2O$) (Bortun et al., 1997). This material has also been synthesised by Rocha and Anderson and co-works (Lin et al., 1999) (AV-4) and by Jale et al., (1999). Another interesting microporous zirconosilicate is petarasite a rare mineral, $[Na_5Zr_2Si_6O_{18}(Cl,OH){\cdot}2H_2O]$, and its synthetic analogue AV-3 (Rocha and Anderson, 2000).

Microporous titanosilicates and zirconosilicates constitute novel zeotype families and the ion exchange properties of these materials have attracted a considerable attention during the last decade since they are stable, have large pore sizes, remarkable selectivity and consist of a variety of framework structures (Al-Attar and Dyer, 2001).

1.3.2.1. ETS-10

ETS-10 (Engelhard TitanoSilicate material number 10), $[(Na,K)_2TiSi_5O_{13}\cdot 4H_2O]$ is one of the most important microporous titanosilicate known. The most interesting aspect of the structure of ETS-10 is that contains infinite –O–Ti–O–Ti–O chains which run in two orthogonal directions surrounded by silicate rings (Anderson et al. 1994; Rocha and Anderson, 2000). The pore structure of ETS-10 consists of 12-rings, seven rings, five rings and three rings and has a three-dimensional large-pore channel system whose minimum diameter is define by 12-ring apertures (Figure 1.11) (Rocha et al., 1998).

Since ETS-10 contains corner-sharing TiO_6 octahedra and corner sharing SiO_4 tetrahedra, there is an associated charge of -2 per Ti^{4+} ion, which is balanced by extra-framework cations (Rocha et al., 1998).

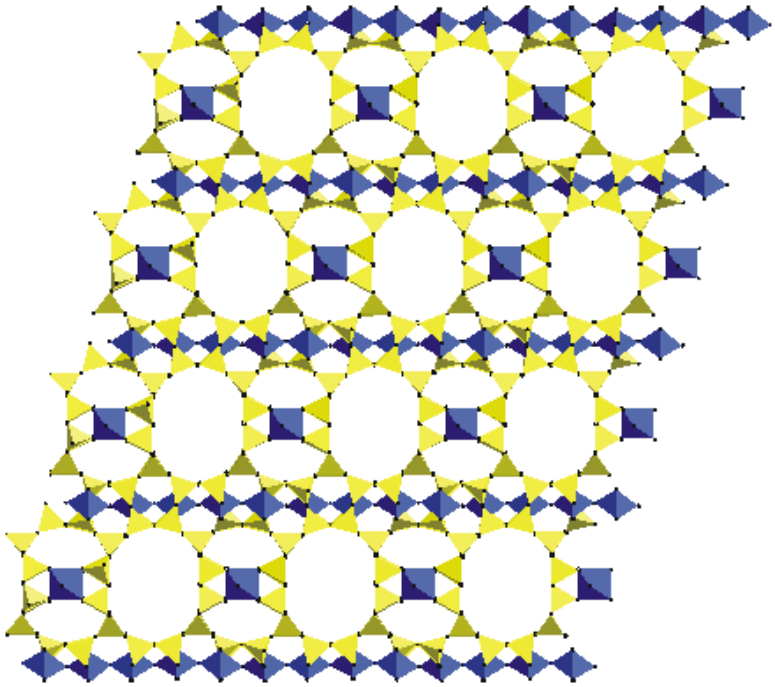

Figure 1.11 – Projection of the structure of ETS-10 polymorph A along [110] direction; blue Ti octahedra, yellow Si tetrahedra, black spheres oxygens.

The synthesis of ETS-10 was firstly reported by Kuznicki (1989). Using a slight modification of the initial method, highly pure and crystalline ETS-10 has been obtained by Anderson et al. (1994). The ETS-10 sample used in this study was synthesised according to the procedure described by Rocha et al., 1998, using $TiCl_3$ as precursor: a sodium silicate aqueous solution (20.0 g, 8 w/w% Na_2O, 27 w/w% SiO_2) was mixed with 15.4 g distilled water, 2.47 g sodium hydroxide (pro analysis), 2.33 g sodium chloride and 3.63 g potassium chloride. This mixture was stirred thoroughly until a solution was obtained. A

titanium trichloride (10.7 g) aqueous solution (1.9 M in 2.0 M HCl) was then added with stirring, and a homogeneous gel formed. ETS-10 seeds (0.1 g) were added to this gel. Static crystallisation was carried out in Teflon-lined autoclaves at 503 K (230 °C) for 24 h. The products were washed with distilled water (*ca.* 500 cm^3, two slurries) filtered and dried overnight at 383 K (110 °C). The gel composition was $4.7Na_2O:1.5K_2O:TiO_2:5.5SiO_2:122H_2O$.

ETS-10 is a white powder with density of 1.8 $kg{\cdot}dm^{-3}$, the particle size is 5 μm and pore size is *ca.* 0.49×0.76 nm. The theoretical cation exchange capacity of ETS-10 is 3.38 $meq{\cdot}g^{-1}$.

Owing to its wide-pore structure and framework charge ETS-10 exhibits considerable potential for being used as ion-exchanger, especially for divalent cations (Rocha and Anderson, 2000). Indeed several studies have demonstrated its unusual ion exchange capacity for heavy metal ions, such as Pb^{2+}, Cd^{2+}, Cu^{2+}, Co^{2+},Mn^{2+}, Zn^{2+}(Pavel et al., 2003, Lv et al., 2005; Choi et al., 2006a; Choi et al., 2006b; Lv et al., 2007; Lv et al., 2008).

1.3.2.2. ETS-4

ETS-4, $[Na_9Ti_5Si_{12}O_{38}(OH){\cdot}12H_2O]$ is a small-pore member of the Engelhard TitanoSilicate (ETS) family of mixed octahedral/tetrahedral microporous framework materials. The powder X-ray diffraction pattern of ETS-4 suggests strong similarities with the structure of the mineral zorite (Rocha and Anderson, 2000). Two orthogonal sets of channels are defined by 12-T/O atom and 8-T atom rings (T = tetrahedral silicon; O = octahedral titanium) (Rocha and Anderson, 2000). In reality, the disorder in zorite results in larger 12-ring channels becoming partitioned into sections (Rocha and Anderson, 2000). This may be a hindrance to its adsorption characteristics since a molecule diffusing into its 12-T/O channel must make detours through the 8-T channel in order to pass freely (Rocha and Anderson, 2000). ETS-4 framework comprises corner-sharing SiO_4 tetrahedra, TiO_5 pentahedra and TiO_6 octahedra (Figure 1.12). Each titanium ion has an associated -2 charge, which is neutralised by extra-framework cations usually Na^+ and K^+. ETS-4 lacks thermal stability because its structure contains structural water bound in chains along the channel system; at temperatures of 200ºC this water is lost and the structure collapses (Rocha and Anderson, 2000).

In 1990 two independent reports by Kuznicki (1990) and Chapman and Roe (1990) discussed the synthesis of a microporous titanosilicates with a structure similar of mineral zorite. The synthesis of the ETS-4 used in this study was performed as follows: an alkaline solution was made by dissolving 33.16 g of metasilicate, 2.00 g NaOH, and 3.00 g KCl into

25.40 g of H_2O. Then, 31.88 g of $TiCl_3$ (15 % m/m $TiCl_3$ and 10 % m/m HCl,) were added to this solution and stirred thoroughly. This gel, with a molar composition $5.9Na_2O{:}0.7K_2O{:}5.0SiO_2{:}1.0TiO_2{:}114H_2O$, was transferred to a Teflon-lined autoclave and treated at 503 K (230 ºC) for 17 hours under autogenous pressure without agitation. The product was filtered off, washed at room temperature with distilled water, and dried at 343 K (70 ºC) overnight, the final product being an off-white microcrystalline powder. ETS-4 is a white powder with density of 2.2 $kg{\cdot}dm^{-3}$, particle size range from 0.5-0.9 μm and pore size 0.4 nm. The theoretical cation exchange capacity of ETS-4 is 5.54 $meq{\cdot}g^{-1}$.

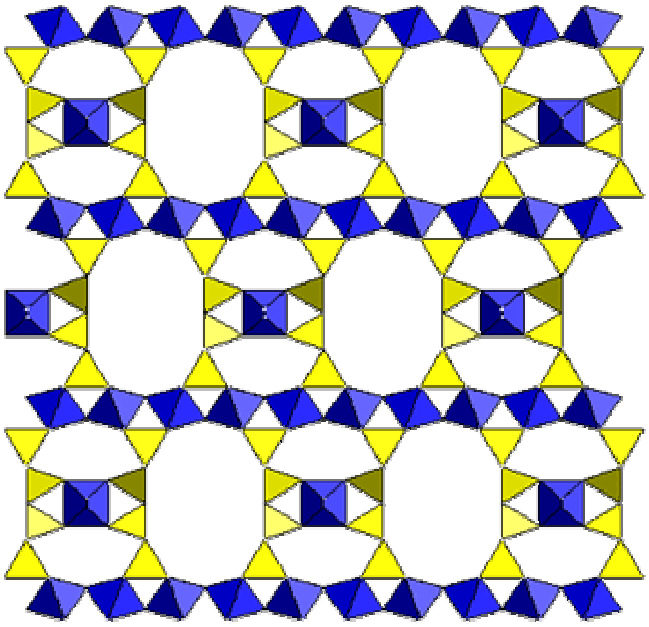

Figure 1.12 – Projection of the structure of ETS-4 along [001] direction; blue Ti octahedra, yellow Si tetrahedra.

In contrast to ETS-10, few studies exist until the moment on ETS-4 ion exchange capacity. Al-Attar and Dyer (2001) have studied the sorption of uranium onto titanosilicate materials, among them ETS-4 and Popa et al. (2006) applied ETS-4 in the purification of waste waters containing radioactive ions ($^{60}Co^{2+}$, $^{115m}Cd^{2+}$ and $^{203}Hg^{2+}$).

1.3.2.3. AM-2

AM-2 (Aveiro-Manchester material number 2), $[K_2TiSi_3O_9{\cdot}H_2O]$ is a synthetic potassium titanosilicate analogue of mineral umbite. AM materials (n=1, 2, 3 and 4) are often seen as low-level impurities contaminating ETS-10, ETS-4, and synthetic nenadkevichite and were

discovered as a result of a systematic study of Rocha and co-works (Lin et al., 1997) at finding novel microporous titanosilicates. AM-1 and -4 are two new layered titanosilicates and microporous AM-2 and -3 are the synthetic analogues of minerals umbite and penkvilksite, respectively (Lin et al., 1997). Interestingly, AM-1, -2 and -3 contain no Ti-O-Ti linkages and, hence, differ in a fundamental way from all the above mentioned titanosilicates, which (like many others) contain infinite Ti-O-Ti chains. Umbite is a very rare potassium zirconium silicate that occurs in the Khibiny alkaline massif on Kola Peninsula (Russia). Although the ideal formula of umbite is $K_2ZrSi_3O_9{\cdot}H2O$, a pronounced substitution of Ti for Zr occurs (Lin et al., 1997).

In the structure of umbite (Figure 1.13), the M-octahedra, $(Zr,Ti)O_6$, and T-tetrahedra, SiO_4, form a three-dimensional MT-condensed framework (Lin et al., 1997). The M octahedron is coordinated to six T tetrahedra and, therefore, does not form Ti-O-Ti chains (Lin et al., 1997). In addition to the M-O-T bonds these tetrahedra form also T-O-T links with each other; the resulting T radical has an identity period of three T tetrahedra and forms an infinite chain (Lin et al., 1997). Among all the known silicates and their T analogues, the umbite structure seems to be the first one to display such a MT-condensed framework (Lin et al., 1997). AM-2 is stable up to 550-600 °C, losing water and rehydrating back after being kept in air for a few hours at room temperature (Lin et al., 1997).

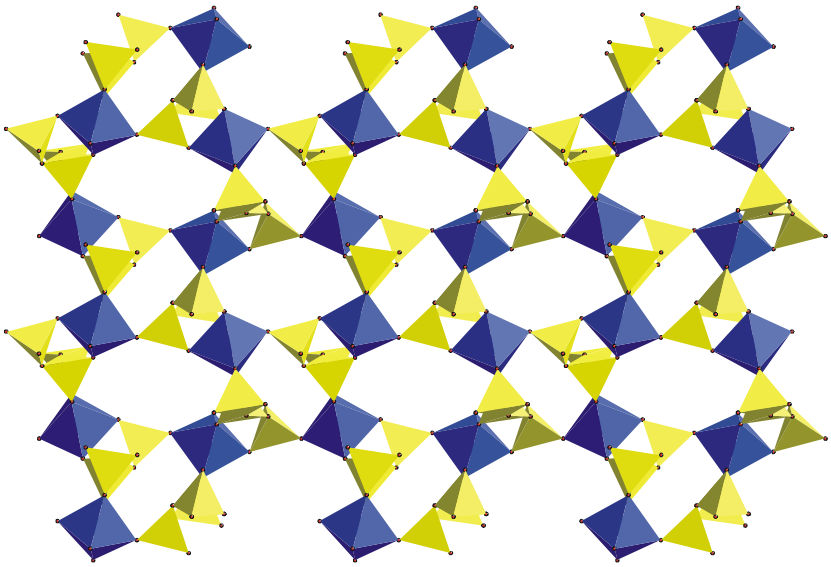

Figure 1.13 – Projection of the structure of AM-2 along [001] direction; blue Zr,Ti octahedra, yellow Si tetrahedra, red spheres oxygens.

The AM-2 titanosilicate employed in this study was prepared by the procedure reported by Lin et al., 1997: an alkaline solution was made by mixing 4.16 g of precipitated silica, 9.90 g of KOH (85% m/m), 2.74 g of KCl and 29.4 g of H_2O. $TiCl_3$ (11.42 g; 23.5% m/m

solution of $TiCl_3$ in 5.9% m/m HCl), was added to this solution and stirred thoroughly. The gel, with a composition $6.1K_2O{:}4.0SiO_2{:}1.0TiO_2{:}120H_2O$, was autoclaved under autogenous pressure at 503 K (230 ºC) for 4 days.

AM-2 is a white powder with density of 2.7 $kg{\cdot}dm^{-3}$, particle size 1.4 μm and pore size *ca.* 0.27×0.55 nm. The theoretical cation exchange capacity of AM-2 is 5.37 $meq{\cdot}g^{-1}$.

1.3.2.4. Pharmacosiderite

Synthetic titaneous pharmacosiderite, $[HK_3Ti_4O_4(SiO_4)_3{\cdot}4H_2O]$ is a microporous titanosilicate, whose structure was studied by powder X-ray diffraction methods in 1990s by Clearfield and co-works (Behrens et al., 1996). This material possesses a most interesting structure built up from TiO_6 octahedra, which share faces to form Ti_4O_4 cubes around the unit-cell corners and have silicate tetrahedra joining the titanium octahedra to form a three-dimensional framework (Figure 1.14) (Rocha and Anderson, 2000).

The synthesis of pharmacosiderite titanium silicate was performed as follows: an alkaline solution was made by dissolving 15.00 g of sodium silicate solution (27% m/m SiO_2, 8% m/m Na_2O), 11.20 g KOH (85% m/m) into 15.00 g H_2O. Then 4.00 g anatase (98% m/m) was added to this alkaline solution. This gel, with a molar composition $0.4Na_2O{:}1.7K_2O{:}1.4SiO_2{:}1.0TiO_2{:}30H_2O$ was transferred to a Teflon-lined autoclave and treated at 473 K (200 ºC) for 4 days under autogenous pressure without agitation.

Pharmacosiderite is a white powder with density of 2.5 $kg{\cdot}dm^{-3}$, particle size 0.2-0.4 μm and pore size 0.36 nm. The theoretical cation exchange capacity of pharmacosiderite is 5.54 $meq{\cdot}g^{-1}$.

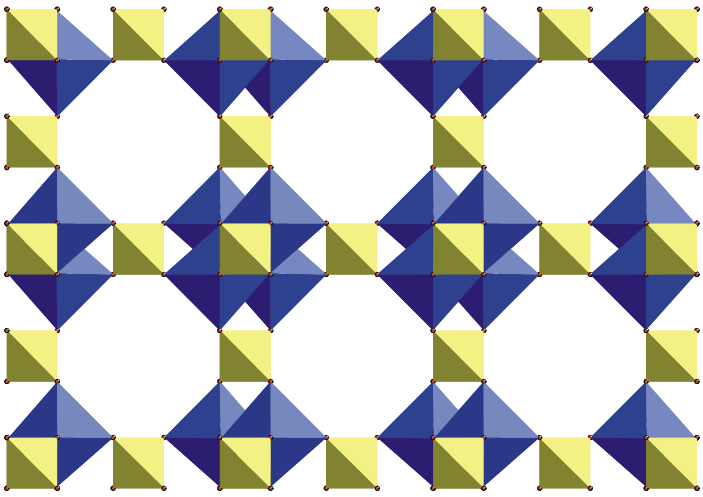

Figure 1.14 – Projection of the structure of pharmacosiderite along [100] direction; blue Ti octahedra, yellow Si tetrahedra, red spheres oxygens.

1.3.2.5. Petarasite

Petarasite (Mont St. Hilaire, Québec, Canada) is a rare mineral with the formula $[Na_5Zr_2Si_6O_{18}(Cl,OH)\cdot 2H_2O]$ and AV-3 is its synthetic analogue (Aveiro microporous material number 3). This microporous zirconosilicate possesses a very unusual structure consisting of an open three-dimensional framework built of corner-sharing six-membered rings and ZrO_6 octahedra (Figure 1.15) (Rocha and Anderson, 2000).

Elliptical channels defined by mixed six-membered rings, consisting of pairs of SiO_4 tetrahedra linked by zirconium octahedral, run parallel to the b and c axes; other channels limited by six-membered silicate rings run parallel to the c axis (Rocha and Anderson, 2000). The sodium, chloride and hydroxyl ions and the water molecules reside within the channels, and the framework does not collapse until the release of Cl^- at *ca*. 800 ºC (Rocha and Anderson, 2000).

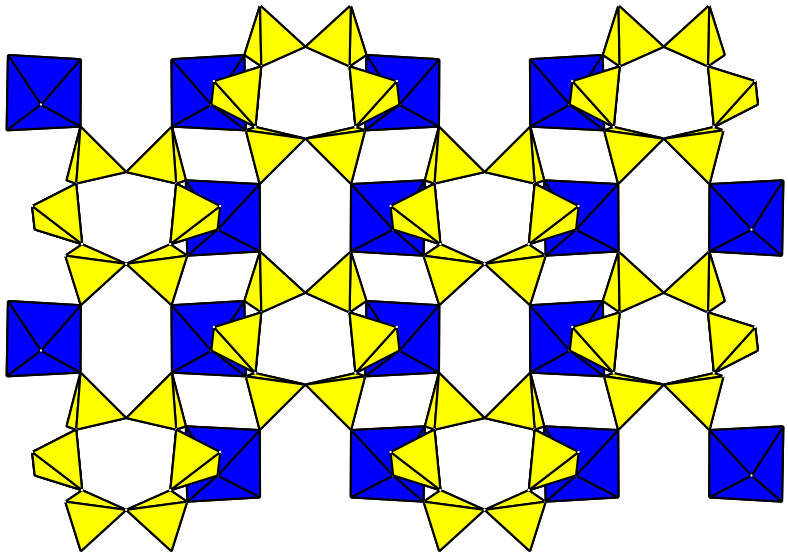

Figure 1.15 – Projection of the structure of Petarasite and AV-3 along [001] direction; blue Zr octahedra, yellow Si tetrahedra.

AV-3 zirconosilicate was synthesised according to the method reported by Lin et al., 1999: an alkaline solution was made by mixing 5.35 g of sodium silicate solution (27% m/m SiO_2, 8% m/m Na_2O), 7.21 g of H_2O, 1.43 g of NaOH, 2.00 g of NaCl and 1.00 g of KCl. An amount of 0.84 g of $ZrCl_4$ was added to this solution and the mixture was stirred thoroughly. The gel, with a composition $1.75Na_2O{:}0.28K_2O{:}1.0SiO_2{:}0.15ZrO_2{:}25H_2O$, was autoclaved under autogenous pressure for 10 days at 503 K (230 °C).

Petarasite (AV-3) is a white powder with density of 2.9 kg·dm^{-3}, particle size 0.2 μm and pore size 0.19×0.38 nm. The theoretical cation exchange capacity of petarasite is 5.94 meq·g^{-1}.

1.3.2.6. AV-13

AV-13 analogue (Aveiro microporous material number 13) is yet another microporous zirconosilicate with formula $Na_{2.27}ZrSi_3O_9Cl_{0.27}.2H_2O$ (Ferreira et al., 2003). The three-dimensional framework structure of AV-13 consists of corner-sharing ZrO_6 octahedra and SiO_4 tetrahedra. The latter form six-membered $[Si_6O_{18}]^{12-}$ rings, which are interconnected by ZrO_6 octahedra (Figure 1.16).

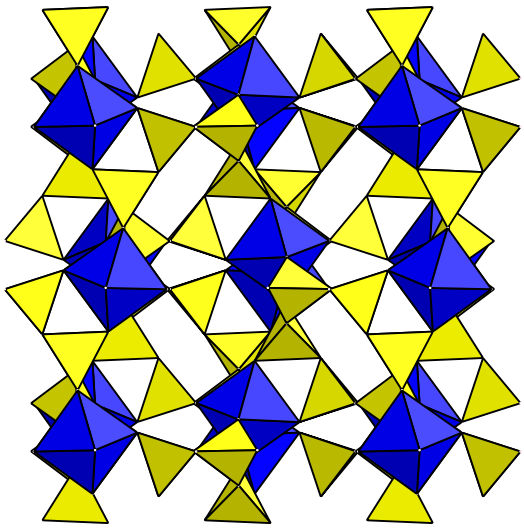

Figure 1.16 – Projection of the structure of AV-13 along [100] direction. Blue Zr octahedra, yellow Si tetrahedra. For clarity, Na^+, Cl^- and H_2O molecules are omitted.

AV-13 zirconosilicate was synthesised according to the procedure reported by Ferreira et al., 2003: an alkaline solution was made by dissolving 20.0 g of sodium metasilicate (Na_2SiO_3·$5H_2O$, BDH) into 22.27 g H_2O. A solution of 7.33 g $ZrCl_4$ in 11.73 g H_2O was added to the alkaline solution while stirring thoroughly. The formed gel, with a molar composition $3.0Na_2O:3.0SiO_2:1.0ZrO_2:80H_2O$, was transferred to a Teflon-lined autoclave and treated at 503 K (230 ºC) for 14 days under autogenous pressure, without agitation. The product was filtered off, washed at room temperature with distilled water, and dried at 343 K (70ºC) overnight.

AV-13 is a white powder with density of 2.7 kg·dm^{-3}, particle size 2 μm and pore size 0.23×0.32 nm. The theoretical cation exchange capacity of AV-13 is 5.44 meq·g^{-1}.

Particle sizes were estimated from SEM images (Hitachi S-4100), density and pore size were calculated from crystallographic data and theoretical cation exchange capacity (CEC) was calculated from molecular weight and exchangeable cations.

1.4. Equilibrium and kinetics studies: theory and models

When a certain mass of microporous material (solid phase) is contacted with a given volume of a solution, with a certain Hg^{2+} concentration (liquid phase), the uptake of Hg^{2+} by the material starts, reducing the Hg^{2+} concentration. This process occurs until the equilibrium between the two phases is achieved. At equilibrium, the Hg^{2+} distribution between the microporous material and the solution depends on the capacity of the material and experimental/operational conditions. The kinetics of the removal process indicates the rate of the uptake/removal process since the material and the solution are put in contact (t_0) until the equilibrium (t_e). In this time interval, the Hg^{2+} concentration in the microporous material (q_t) increases while the Hg^{2+} concentration in the liquid phase (C_t) decreases. After the equilibrium is attained at time t_e, q_t and C_t do not change along time. Thus, equilibrium is characterized by a certain Hg^{2+} concentration in the material (q_e) and in the liquid phase (C_e) (Cooney, 1998).

In the particular case of the microporous materials used in this work, it is known that the uptake of Hg^{2+} is based on an ion exchange process. Ion exchange is essentially a chemical reaction (Misak, 1995; Shah and Devi, 1998; Rao et al., 2002; Gode and Pehlivan, 2003; Lin and Juang, 2005) and may be represented by conventional chemical equilibrium (Helfferich, 1995).

In batch experiments, a selected weight (W) of microporous material is put into a certain volume (V_L) of an Hg^{2+} solution with an initial concentration (C_0), and magnetically stirred at constant temperature.

The amount of Hg^{2+} taken up by the microporous material must equal the amount of Hg^{2+} removed from solution, or, in mathematical terms (Cooney, 1998):

$$q_t W = V_L (C_0 - C_t) \tag{1.4}$$

A consistent set of units for the quantities in this mass balance is required. Our set of units was: W =milligrams of microporous materials, V_L =litres of Hg^{2+} solution, C_0 and C_t =micrograms of Hg^{2+} per litre of solution and q_t =micrograms of Hg^{2+} sorbed per

milligram of microporous materials, or milligrams of Hg^{2+} sorbed per gram of microporous materials.

Since the values of W, V_L and C_0 are known and C_t may be experimentally assessed by solution CVAFS analysis, from equation 1.4 it is possible to compute q_t values corresponding to C_t determined along time until the equilibrium values (q_e and C_e) are achieved. At the equilibrium, the percentage removal of Hg^{2+}, also called *uptake* percentage, may be evaluated as follows:

$$\%\ \ removal\ \ of\ \ Hg^{2+} = \left(C_0 - C_e\right) \times 100 / C_0 \qquad (1.5)$$

1.4.1. Kinetic study

Most of the sorption/desorption transformation processes of various solid phases are time-dependent. To understand the dynamic interactions of solutes with solid phases and to predict their fate with time, knowledge of the kinetics of these processes is important.

The kinetics of Hg^{2+} removal was studied for several microporous materials and the experimental results interpreted by two simple kinetic models commonly used: the semi-empirical pseudo-first order, also called the Lagergren rate equation, and the pseudo-second order kinetic equation.

1.4.1.1. Lagergren model

The first order rate equation used for the sorption of liquid/solid systems based on solid capacity was the Lagergren rate equation (Lagergren, 1898). This equation, one of the most extensively used for the sorption of a solute from a liquid phase, is expressed by:

$$\frac{dq_t}{dt} = k_1\left(q_e - q_t\right) \qquad (1.6)$$

Rearranging equation 1.6, gives:

$$\frac{dq_t}{\left(q_e - q_t\right)} = k_1 dt \qquad (1.7)$$

Integrating equation 1.7 for the boundary conditions $t = 0$ to $t = t$ and $q_t = 0$ to $q_t = q_t$, gives:

$$\int_0^{q_t} \frac{1}{\left(q_e - q_t\right)} dq_t = \int_0^t k_1 dt$$

Evaluating the integrals gives:

$$\ln(q_e - q_t) - \ln q_e = -k_1 t \quad (1.8)$$

$$\ln\left(\frac{q_e - q_t}{q_e}\right) = -k_1 t \text{ or } \log\left(\frac{q_e - q_t}{q_e}\right) = \frac{-k_1}{2.303} t \quad (1.9)$$

the integrated rate law for a pseudo-first order reaction, where k_1 is the rate constant of pseudo-first sorption (h^{-1}).

Equation 1.9 may be rearranged in order to obtain a linear form

$$\log(q_e - q_t) = \log(q_e) - \frac{k_1}{2.303} t \quad (1.10)$$

The validity of the model is shown by the linear trend observed when graphing experimental $\log(q_e - q_t)$ as a function of t. The rate constant (k_1) is determined from the slope of the linear regression, as well as the intercept should match the q_e value previously introduced. However, it is well known that Lagergren model may not represent the sorption evolution along the full time range (Ho and McKay, 1999a; Ho and McKay, 1999b; Reddad et al., 2002; Chiron et al., 2003; Aksu, 2005).

Ho and McKay (1999a) refer that the equation applicable to experimental results generally differs from a true first-order equations in two ways: (i) $k_1(q_e - q_t)$ does not represent the number of available sites; (ii) $\log(q_e)$ is an adjustable parameter, which often differs from the intercept of the $\log(q_e - q_t)$ against t a plot, although in a true first-order process it should be equal to this intercept.

1.4.1.2. Pseudo second-order model

The pseudo-second order equation is also based on the sorption capacity of the solid phase and, in contrast with the first model, usually predicts the system behaviour over the whole range of sorption (Namasivayam and Senthilkumar, 1998; Ho and McKay, 1999b; Aksu, 2005). Assuming that the sorption capacity is proportional to the number of active sites occupied on the sorbent, the kinetic rate law may be written as follows (Ho and McKay, 1999b):

$$\frac{dq_t}{dt} = k_2(q_e - q_t)^2 \quad (1.11)$$

where k_2 ($g \cdot mg^{-1} \cdot h^{-1}$) is the rate constant of pseudo-second sorption. Separating the variables in equation 1.11 gives:

$$\frac{dq_t}{(q_e - q_t)^2} = k_2 dt \quad (1.12)$$

Integrating this equation for the boundary conditions $t = 0$ to $t = t$ and $q_t = 0$ to $q_t = q_t$, gives:

$$\int_0^{q_t} \frac{1}{(q_e - q_t)^2} dq_t = \int_0^t k_2 dt$$

$$\int_0^{q_t} \frac{1}{\left(q_e^2 - 2q_e q_t + q_t^2\right)} dq_t = k_2 \int_0^t dt$$

Evaluating of the integrals gives:

$$\left[\left(\frac{-2}{2q_t - 2q_e}\right) - \left(\frac{-2}{-2q_e}\right)\right] = k_2 t \quad (1.13)$$

$$\frac{1}{(q_e - q_t)} - \frac{1}{q_e} = k_2 t \quad (1.14)$$

which is the integrated rate law for a pseudo-second order reaction. Equation 1.14 may be rearrange to obtain the linear form

$$\frac{t}{q_t} = \frac{1}{k_2 q_e^2} + \frac{1}{q_e} t \quad (1.15)$$

For the applicability of the model, the plot of t/q_t versus t should be linear and the constants k_2 and q_e are obtained from the corresponding intercept and slope. Unlike, the Lagergren equation, no parameter needs to be known beforehand.

1.4.1.3. Nernst-Planck based model

The kinetic performance of ion exchange is mostly interpreted by semi-empirical pseudo first- and second-order equations (Lagergren, 1989, Ho and McKay, 1999a; Ho and McKay, 1999b; Reddad et al., 2002; Yardim et al., 2003; Chiron et al., 2003; Aksu, 2005; Zhang et al., 2005; Lopes et al. 2007). A more reliable approach deals with the application of the Nernst-Planck equations to describe mass transport in ionic systems, in which both concentration and electric potential gradients, induced by the different counter ions motilities, are accounted for (Helfferich, 1995; Rodrígez et al., 1998; Valverde et al., 2004).

In this study, a model based on the Nernst-Planck equations was developed in collaboration with Chemical Engineering group of the University of Aveiro and is particularly focused on modelling the ion exchange process between the Na^+ present in the ETS-4 framework and the Hg^{2+} ions present in the liquid phase; the model combines both intra-particle and film resistances to mass transport, and involves three parameters: the self-diffusivities of Hg^{2+} and Na^+, and the convection mass transfer coefficient.

Model equations have been derived assuming the following hypothesis: (i) film and intra-particle mass transfer resistances; (ii) spherical solid particles; (iii) perfectly stirred tank; (iv) isothermal and isobaric operation; (v) co-ions are excluded from the zeolite particles (Donnan exclusion); and (vi) ideal solution behaviour.

1) Nernst-Planck equations

The ion-exchange may be represented by conventional chemical equilibrium (Helfferich, 1995) between two counter ions. For the case where the ETS-4 is initially in B (Na^+) form and the counter ion in solution is A (Hg^{2+}), the reaction is:

$$z_A \overline{B^{Z_B}} + z_B A^{z_A} \Leftrightarrow z_B \overline{A^{z_A}} + z_A B^{z_B} \tag{1.16}$$

where z_A and z_B are the electrochemical valences.

The flux of each counter ion in dilute ionic solutions may be described by the Nernst-Planck equations (Helfferich, 1995):

$$J_A = -D_A\left(\frac{\partial q_A}{\partial r}\right) - D_A z_A q_A \frac{F}{\Re T}\left(\frac{\partial \phi}{\partial r}\right) \tag{1.17}$$

$$J_B = -D_B\left(\frac{\partial q_B}{\partial r}\right) - D_B z_B q_B \frac{F}{\Re T}\left(\frac{\partial \phi}{\partial r}\right) \tag{1.18}$$

where D_A and D_B are the self-diffusion coefficients of species A and B, q_A and q_B are the molar concentration of counter ions in the particle, F is Faraday constant, R is gas constant, T is absolute temperature, ϕ is the electrostatic potential and r is the radial position.

The general expression for the flux of A may be recast as a special form of the Fick's first law, where a coupled inter-diffusion coefficient, D_{AB}, appears:

$$J_A = -D_{AB}\left(\frac{\partial q_A}{\partial r}\right), \text{ and } D_{AB} \equiv \frac{D_A D_B\left(z_A^2 q_A + z_B^2 q_B\right)}{D_A z_A^2 q_A + D_B z_B^2 q_B} \tag{1.19}$$

D_{AB} depends on D_A, D_B, and the ionic composition of the ETS-4, which varies in the course of ion-exchange.

2) Material balances and initial and boundary conditions

The material balances to the vessel and over a spherical shell of the ETS-4 particle are, respectively:

$$\frac{\partial C_A}{\partial t} = -\frac{V_s}{V_L}\frac{\partial \bar{q}_A}{\partial t} \tag{1.20}$$

$$\left(\frac{\partial q_A}{\partial t}\right) = -\frac{1}{r^2}\frac{\partial}{\partial r}\left(r^2 J_A\right) \tag{1.21}$$

where the average loading per unit particle volume is:

$$\bar{q}_A = \frac{3}{R^3}\int_0^R r^2 q_A dr \tag{1.22}$$

The above differential equations are subjected to the following initial and boundary conditions.

$$t = 0, \quad q_A = \bar{q}_A = 0 \text{ and } C_A = C_{A0} \tag{1.23}$$

$$r = R, \quad q_A = q_{As} \tag{1.24}$$

$$r = 0, \quad \left(\frac{\partial q_A}{\partial r}\right) = 0, \tag{1.25}$$

The equality of internal and film ionic fluxes must be observed at particle surface, and uniquely determines interface concentrations (hereafter denoted by subscript s):

$$\left(\frac{\partial q_A}{\partial r}\right)_{r=R} = \frac{k_f}{D_{AB}}\left(C_A - C_{As}\right) \tag{1.26}$$

where k_f is the convective mass transfer coefficient.

For a complete description of the development of the Nernst-Planck based model please see Supplementary material chapter.

1.4.2. Equilibrium study

Experimentally, at a constant temperature and for different initial ratios between mass of microporous material and mass of Hg^{2+} in a certain volume of solution, several q_e *vs.* C_e experimental values may be obtained. Many models have been proposed to describe sorption equilibrium data ($q_e vs. C_e$). Among them, isotherm equations are mathematical expressions that relate the amount of solute adsorbed on the solid phase and the concentration of the solute in the liquid phrase, at a given constant temperature (Cooney, 1998). In this way, the relationship between q_e and C_e values may be mathematically expressed, which allows to design batch and fixed-bed reactors (Cooney, 1998).

The Langmuir and Freundlich isotherms are the equations most used to describe the sorption equilibrium in environmental studies (Kocaoba, 2007). They are two-parameter equations and, by far, the most common single-solute expressions used, because in almost every case, one of them fits the data quite well and, consequently, there is no need for more complex isotherm equations, particularly those involving three or more parameters (Cooney, 1998).

Although the Langmuir and Freundlich models were originally established for adsorption processes, they have been assessed in this work for equilibrium representation in the very same way many researchers have done for differential materials, particularly zeolites (Zhao et al., 2003; El-Kamash et al., 2005; Sprynskyy et al., 2006; Kocaoba, 2007). At the equilibrium, the ion-exchange material is thought of as a charged adsorbent and, thus, the 'adsorption' isotherm equations may be applicable (Lin et al., 2008). The use of Langmuir and Freundlich equations in this work allow the simple determination of the isotherm parameters corresponding to the equilibrium data of Hg^{2+} removal by microporous materials, and permit to compare them with those published for other sorbent materials.

1.4.2.1. Langmuir isotherm

The Langmuir equation assumes that adsorption occurs at definite localized sites on the surface, each site being able to bind a single molecule of the adsorbing species. The energy of adsorption is equal for all sites and there are no interaction forces between adjacently adsorbed molecules (Stumm, 1992; Cooney, 1998). Theoretically, a saturation value is reached, beyond which no further sorption can take place, which is represented by a plateau in the equilibrium isotherm. This observation corresponds to the assumption of one complete monomolecular layer of coverage of the adsorbing species on the adsorbent (Cooney, 1998; Kocaoba, 2007).

The Langmuir equation applies to the ion exchange process with certain assumptions (Shah and Devi, 1998; Gode and Pehlivan, 2003; Lin et al., 2008): (i) maximum exchange depends on the saturation level of a monolayer of solute molecules on the material surface; (ii); solid surface is provided with uniform distribution on the exchangeable sites; (iii) each exchanged matter on the site has the same affinity; and (iv) concentration of one of the ions or of the total solution is constant for homovalent and heterovalent exchange.

The deduction of the Langmuir equation assumes that the rate of adsorption is proportional to the solute concentration in the liquid phase (C_e) and to the fraction of available sites of the adsorbent (1-θ), where θ is the fraction of sites covered:

$$rate \quad of \quad adsorption = kC_e(1-\theta) \tag{1.27}$$

where k is a constant. Otherwise, the rate of desorption is assumed to be proportional to the amount of solute on the adsorbent:

$$rate \quad of \quad desorption = k'\theta \tag{1.28}$$

where k' is a second constant. At equilibrium, both rates are equal; equating equations 1.27 and 1.28 gives:

$$kC_e(1-\theta) = k'\theta \tag{1.29}$$

$$\theta = \frac{kC_e}{(k' + kC_e)} \tag{1.30}$$

the equation 1.30 can be written as:

$$\theta = \frac{K_L C_e}{(1 + K_L C_e)} \tag{1.31}$$

where $K_L = k/k'$.

Since the amount of solute adsorbed per unit weight of adsorbent (q) and θ are proportional to each other, it is preferable to work in terms of q rather than θ.

$$q_e = \frac{K_L q_{\max} C_e}{1 + K_L C_e} \tag{1.32}$$

where K_L ($dm^3 \cdot mg^{-1}$) is the Langmuir sorption equilibrium constant and $q_{\max}$ ($mg \cdot g^{-1}$) is the concentration of the adsorbed species on the adsorbent when one complete monomolecular layer of coverage is achieved (Cooney, 1998).

The constants K_L and $q_{\max}$ are obtained from experimental data on q_e *vs.* C_e by noting that the equation may be written in the linear form:

$$\frac{1}{q_e} = \frac{1}{q_{\max}} + \frac{1}{K_L q_{\max} C_e} \tag{1.33}$$

Plotting $1/q_e$ *vs.* $1/C_e$ yields a straight line with slope $1/K_L q_{\max}$ and intercept $1/q_{\max}$. Knowing the slope and intercept values it is possible to determine the K_L and $q_{\max}$ values.

The Langmuir equation is also used to obtain R_L, the dimensionless equilibrium parameter also called the separation factor (Yavuz, et al., 2006):

$$R_L = \frac{1}{1 + K_L C_0} \tag{1.34}$$

where C_0 is the initial concentration of the adsorbed species. Often, the solute has a higher affinity for the solid phase than for the liquid phase, which indicates a good adsorption and $R_L < 1$. Otherwise, $R_L > 1$ indicates that the solute species prefer the liquid phase over the solid phase and the isotherm presents a concave shape. When $R_L = 1$ the isotherm is linear, *i.e.*, $q_e = mC_e$, where m is a constant.

1.4.2.2. Freundlich isotherm

The Freundlich equation is more empirical than the Langmuir equation but it is frequently used in correlating aqueous phase experimental data. The Freundlich model does not assume that the material coverage must approach a constant value corresponding to one complete solute monomolecular layer as C_e gets larger (Cooney, 1998). In fact, inspection of the Freundlich equation:

$$q_e = K_f C_e^{1/n} \tag{1.35}$$

reveals that q_e monotonously increases with increasing C_e which, being physically impossible, means that the Freundlich equation should fail to describe the experimental data at high C_e values (Cooney, 1998). However, real adsorption processes are considered sufficiently diluted, in order to avoid the process entering the region where the Freundlich equation breaks down (Cooney, 1998).

In the Freundlich model, the energy distribution of the adsorption sites is essentially of an exponential type, rather than of the uniform type assumed in the Langmuir development. According with Cooney (1998), there is much experimental evidence that real energy distributions, while not being strictly exponential, are indeed approximately of this type. Thus, some sites are highly energetic and bind the adsorbed species strongly, whereas some are much less energetic and bind the adsorbed species weakly. The rates of adsorption/desorption vary with the strength or energy of the sites, which leads to the possibility of more than just one monomolecular layer of coverage, and to a different shape of the isotherm equation (Cooney, 1998).

Like the Langmuir equation, the Freundlich one may be written in the linear form, by taking the logarithm of each side of equation 1.35:

$$\log q_e = \log K_f + \left(\frac{1}{n}\right) \log C_e \tag{1.36}$$

where K_f ($mg^{1-1/n} \cdot (dm^3)^{1/n} \cdot g^{-1}$) and n are the Freundlich parameters. K_f is a constant indicative of the relative adsorption capacity of the adsorbent, and n is a constant

indicative of the intensity of the adsorption, usually ranging from 1 and 10. Both constants characterise the extent of adsorption and the degree of non-linearity between solution and concentration, respectively (Kocaoba, 2007).

Plotting $\log q_e$ *vs.* $\log C_e$ will yield a straight line with slope of $1/n$ and intercept $\log K_f$, from which the Freundlich parameters K_f and n are easily calculated.

1.5. Work innovation and general objectives

The main goal of this study is to contribute to the development of novel technologies for the removal of mercury (II) from water, with potential for future application in industrials effluents, waste water plants and/or drinking water treatment.

The main innovative aspect of my work is the use of new microporous transition metal silicates for mercury (Hg^{2+}) removal from aqueous solutions where the metal concentrations are similar to those found in real systems, and in the presence of competitive ions. The concentrations of the latter are similar to those in natural systems, some two or three orders of magnitude higher than that of Hg^{2+}.

The specific objectives of my study are:

- To assess and compare the ability of certain microporous titanosilicates and zirconosilicates to remove Hg^{2+} from aqueous solutions, identifying the best material.
- To evaluate the effect of the competition between Hg^{2+} and other cations for the exchangeable sites of the microporous materials.
- To evaluate the influence of certain experimental parameters, such as initial Hg^{2+} concentration, mass of adsorbent, stirring rate, contact time, temperature and pH, on the removal efficiency.
- To model the kinetics and equilibrium experimental data.
- To obtain the equilibrium equation and to calculate thermodynamic parameters for the ion-exchange process.
- To study the modifications occurring in the structure of the microporous materials after being used in Hg^{2+} uptake, aiming at their regeneration and reuse.
- To compare the removal efficiency of the microporous materials studied and commercial adsorbents.

Chapter

2

Evaluating the potential of microporous materials for Hg^{2+} removal from aqueous solutions and experimental procedure optimisation

2.1. Introduction

As discussed in chapter 1, zeolites and zeolitic materials are among the most promising materials to be use as adsorbents in heavy metals removing processes, replacing materials such as activated carbon and resins. Microporous materials have certain properties, such as high ion-exchange capacity, thermal and chemical selectivity, and environmental compatibility (Panayotova, 2001; Petrus and Warchol, 2003), which afford them considerable potential to be use as decontaminant agents for waters polluted with heavy metals. Moreover, some microporous materials have already been successfully applied to the removal of some heavy metals (Choi et al., 2006a; Choi et al., 2006b; Cincotti et al., 2006), mainly copper, lead and cadmium. However, very little is available in the particular case of mercury and most of the published work deals with relatively high and unreal (for natural waters) mercury concentrations (Zhu and Alexandratos, 2005; Pérez-Quintanilla et al., 2006). These facts prompted us to study the applicability of microporous materials as adsorbents[1] for Hg^{2+} removal from polluted natural waters.

This chapter describes my preliminary studies on two types of microporous materials, titanosilicates and zirconosilicates, assessing their potential for uptaking Hg^{2+} from aqueous solutions, depicted in terms of removal percentage and sorption capacity (q).

From a wide range of microporous materials, four titanosilicates (ETS-10, ETS-4, AM-2 and synthetic pharmacosiderite) and two zirconosilicates (synthetic petarasite and AV-13) were selected and their potential for water Hg^{2+} decontamination investigated. The work was planned in order to simulate the conditions prevalent in poorly-polluted estuarine systems. Because the Hg^{2+} concentration in estuarine waters rarely exceeds a few hundred $ng \cdot dm^{-3}$, a concentration of 500 $ng \cdot dm^{-3}$ was chosen. However, due to the low concentration of Hg^{2+} in natural waters relatively to the concentrations of other ions, it is also important to assess the sorption capacity of these materials to remove Hg^{2+} in the presence of other major ions. Hence, this chapter reports on the Hg^{2+} uptake efficiency of different microporous materials at metal levels that mimic those found in natural waters, and the effect of competing ions Mg^{2+}, Na^{+} and Cl^{-}. However, due to the low ionic strength of the samples, a significant part of Hg^{2+} was found to be lost during the experiments. Thus, a posterior optimisation of the experimental procedure was performed, with the purpose of minimising Hg^{2+} losses.

[1] *Adsorbent* is a general term to denote solids which bind molecules by a variety of means: physical attractive forces, chemical bonds, ion exchange, etc. (Cooney, 1999).

2.2. Chemical reagents and equipment

All reagents (Table 2.1) were of analytical reagent grade, obtained from chemical commercial suppliers and used without further purification. The water used for preparing the mercury (II) solutions was always high-purity (18.2 MΩ·cm), with low total-organic carbon content (< 5 $\mu g \cdot dm^{-3}$) with no particles larger than 0.22 μm. This water was obtained from a Millipore system, that combines the models Elix 5 and Milli-Q Plus 185. The equipment used in this work is shown on (Table 2.1).

Table 2.1 – Reagents and equipment used in the work.

Chemical	**Commercial supplier**	**Application**
Mercury (II) nitrate (1000 $mg \cdot dm^{-3}$)	Spectrosol® BDH	Standard preparation
Nitric acid 65% p.a. max. 0.005 ppm Hg	Merck	pH adjustment
Nitric acid 65% p.a.	Merck; Fluka	Standard preparation
Tin (II) chloride dehydrate p.a.	Merck	Mercury analysis
Hydrochloric acid 37% puriss.	Riedel-deHaën/Merck	Mercury analysis
Equipment	**Brand Make**	**Model**
Cold vapour atomic fluorescence spectroscopy:		
▪ Cold vapour generator	PSA	10.003
▪ Fluorescence detector	PSA	Merlin 10.023
Microbalance	Sartorius	M5P
Analytical balance	Mettler	AE 200
pH meter	Anatron	300
Water distiller	GFL	2008
Ultra-pure water system	Millipore	Milli-Q Plus 185
Drying oven	LEEC	
Magnetic hotplate stirrers	Selecta	Agimatic-N
	Heidolph	MR 3001 K
Water bath	Heidolph	
Electronic contact thermometers	Heidolph	EKT 3001

2.3. Evaluating the potential of microporous materials for Hg^{2+} removal

2.3.1. Experimental conditions

The experiments were carried out in batch conditions, at room temperature (294±1 K). In each test *ca.* 0.5 g of microporous materials and 50 cm^3 of 500 $ng \cdot dm^{-3}$ Hg^{2+} solution were used (Table 2.2). Titanosilicates and zirconosilicates powders and aqueous solutions were maintained in contact for 60 hours with stirring.

To study the competition between Hg^{2+} and other ions present in seawater, removal experiments were also performed in the conditions described above but using three different support solutions: $MgSO_4$ solution (6.1 $g \cdot dm^{-3}$), NaCl solution (35 $g \cdot dm^{-3}$) and synthetic seawater prepared according to Parsons et al (1984).

Table 2.2 – Mass of microporous materials used in the experiments for the different solutions (Milli-Q water, $MgSO_4$ and NaCl solutions and artificial seawater).

Microporous Materials	**Mass** (g ± 0.0001 g)			
	Support solution			
	Water	$MgSO_4$	NaCl	Sea-water
ETS-10 (T)	0.4993	0.5004	0.5000	0.5019
ETS-4 (T)	0.5001	0.5017	0.5000	0.5006
AM-2 (T)	0.5001	0.5007	0.5003	0.5010
Pharmacosiderite (T)	0.5007	0.5001	0.5008	0.5005
Petarasite (Z)	0.4998	0.5014	0.5009	0.5002
AV-13 (Z)	0.5002	0.5008	0.5000	0.4994

(T) titanosilicate; (Z) zirconosilicate

The major problem encountered in these experiments was the low Hg^{2+} concentration (500 $ng \cdot dm^{-3}$), since adsorption processes onto the vessels and contaminations may seriously compromise the results. For this reason and in order to quantify the amount of Hg^{2+} that was lost due to adsorption to the vessels and during the filtration process, control experiments were carried out.

2.3.2. Control experiments

In all Hg^{2+} removal experiments, control trials were performed and all the results were corrected taking into account the losses due to laboratory procedures.

It is important to know where the main Hg^{2+} losses take place, so that in future studies, they are eliminated or minimized. In order to identify where the main Hg^{2+} losses occur, a set of eight Hg^{2+} controls was performed in the same experimental conditions described in section 2.3.1, but without adding microporous material. Hg^{2+} measurements were made before and after filtration. This procedure allowed identifying and quantifying the two main sources of Hg^{2+} loss: the Hg^{2+} adsorption to the reaction and store containers and the filtration process. The results obtained indicated that filtration is the main source of Hg^{2+} loss (*ca*. 27±4%), while adsorption by containers represents *ca.* 10% (Figure 2.1).

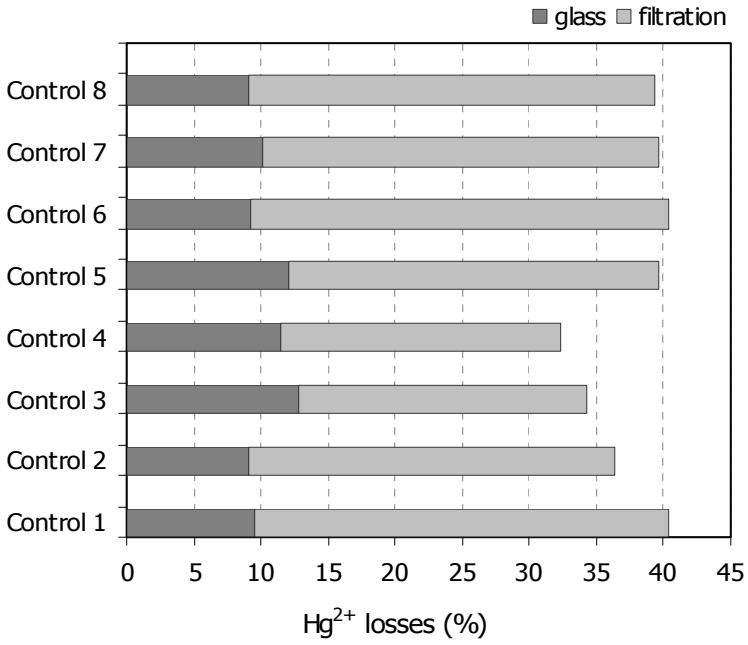

Figure 2.1 – Hg^{2+} losses (%) distribution.

2.3.3. Hg^{2+} removal by microporous materials in the absence of competition ions

The results obtained in the Hg^{2+} removal experiments with the different microporous titano and zirconosilicates, in absence of competing ions, indicate that all microporous materials efficiently remove Hg^{2+} from aqueous solutions (removal > 85%). However, it is clear that Hg^{2+} has different affinity for the different materials. Table 2.3 depicts the residual Hg^{2+} concentration in the liquid-phase, the experimental Hg^{2+} removal by the

materials and the amount of Hg^{2+} removed per gram of material, for an available Hg^{2+} concentration of 362 $ng \cdot g^{-1}$, after blank correction.

Table 2.3 – Hg^{2+} removal by microporous titano and zirconosilicates in absence of competing ions: residual Hg^{2+} concentration (C_{res}), removal percentage (%) and amount of Hg^{2+} removed per gram of microporous material (q).

Microporous Materials	C_{res} ($ng \cdot dm^{-3}$)	Removal (%)	q ($ng \cdot g^{-1}$)
ETS-10 (T)	5.60 ± 0.27	98.5 ± 0.1	35.7 ± 0.0
ETS-4 (T)	49.3 ± 1.9	86.4 ± 0.5	31.3 ± 0.2
AM-2 (T)	10.1 ± 1.4	97.2 ± 0.4	35.2 ± 0.1
Pharmacosiderite (T)	46.0 ± 3.5	87.3 ± 1.0	31.6 ± 0.4
Petarasite (Z)	5.48 ± 0.37	98.5 ± 0.1	35.7 ± 0.0
AV-13 (Z)	6.01 ± 0.26	98.3 ± 0.1	35.6 ± 0.0

(T) titanosilicate; (Z) zirconosilicate; mean ± standard deviation

Even though all materials display high removal percentages, ETS-10, petarasite and AV-13 are the best materials (in the absence of competing ions), with the highest removal efficiencies and removing nearly all metal in solution (Figure 2.2). Although titanosilicate AM-2 also efficiently removes Hg^{2+} from solution, its performance is slightly lower than that of those materials. The least efficient of all materials are ETS-4 and pharmacosiderite, displaying the lowest removal capacities, respectively, 31.3 and 31.6 $ng \cdot g^{-1}$. Zirconosilicates seem to perform better than titanosilicates, however only two examples of the former were studied and, thus, a note of caution is required. Both zirconosilicates have comparable sorption capacities but, in contrast, titanosilicates ETS-10, ETS-4, AM-2 and pharmacosiderite seem to have distinct sorption behaviour.

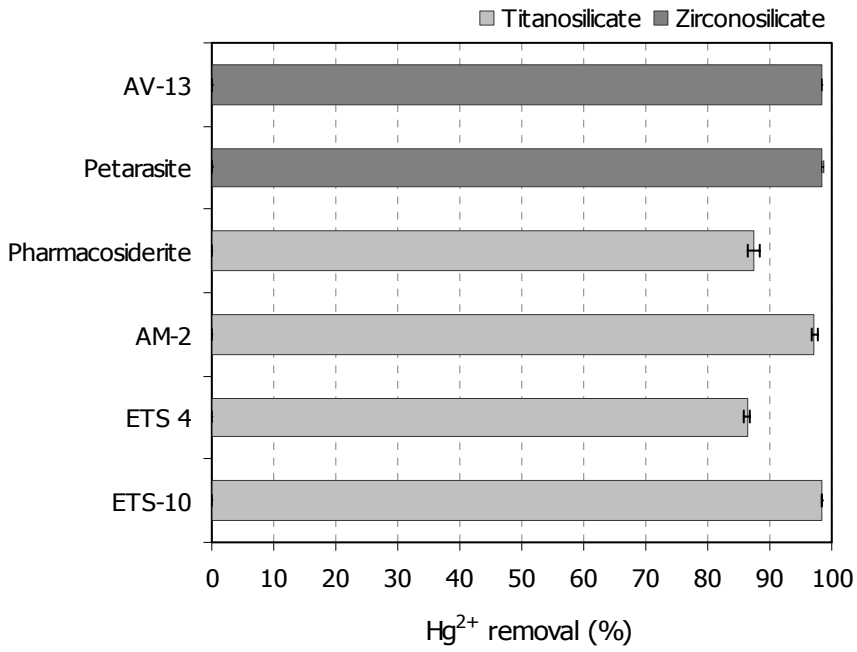

Figure 2.2 – Mean and standard deviation of Hg^{2+} removal by titanosilicates and zirconosilicates, in the absence of competing ions (Milli-Q water support solution).

2.3.4. Hg^{2+} removal by microporous materials in the presence of competing ions

Figure 2.3 displays the removal percentage of Hg^{2+} in the different support solutions studied ($MgSO_4$ and NaCl solutions and artificial seawater). In the presence of the Mg^{2+} ion, zirconosilicates AV-13 and petarasite are the best microporous materials for removing Hg^{2+}. Their removal efficiencies remain at almost the same value as when only Hg^{2+} is in solution, even when the Mg^{2+} concentration is much larger (1×10^4) than the Hg^{2+} one. Among titanosilicates, ETS-10, ETS-4 and AM-2 exhibit similar removal efficiencies, AM-2 being the best material (97.0%), while pharmacosiderite is the least efficient (72.4%) of all materials in removing Hg^{2+} in the presence of Mg^{2+} (Table 2.4). These results show that the presence of a divalent cation, such as Mg^{2+}, does not influence much the Hg^{2+} removal by microporous titano and zirconosilicates, except in the case of the pharmacosiderite analogue, which has an uptake decrease >10%, relatively to the Hg^{2+} removal in absence of competing ions. Zirconosilicates, petarasite and AV-13, exhibited slightly better Hg^{2+} removal efficiency than titanosilicates. Once again, a note of caution is required since only two examples of the zirconosilicates were studied and the difference in the amount of Hg^{2+} removed by gram of microporous material, excluding pharmacosiderite, is only 0.3 $ng{\cdot}g^{-1}$ (Table 2.4).

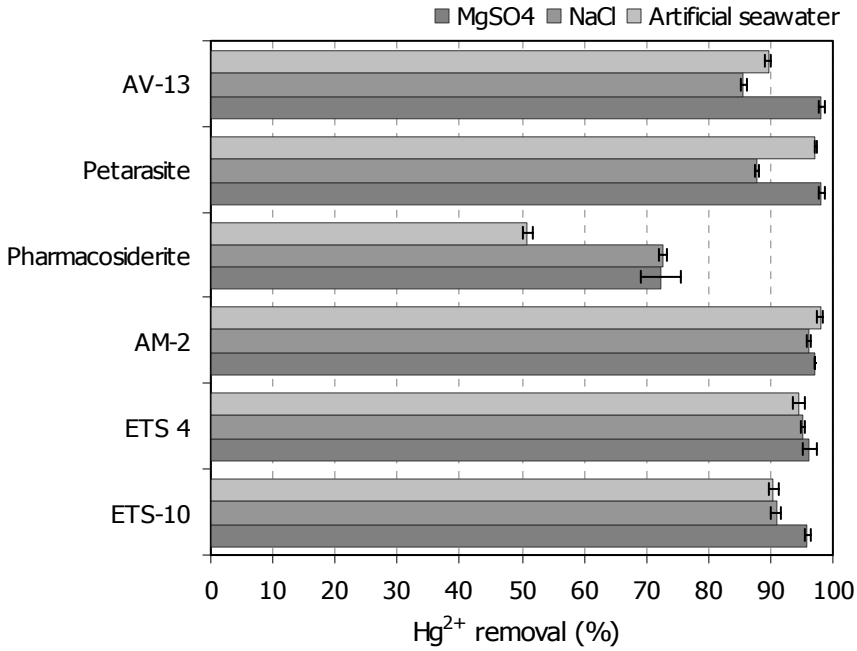

Figure 2.3 – Mean and standard deviation of Hg^{2+} removal by titanosilicates and zirconosilicates, in different removal systems: $MgSO_4$ solution, NaCl solution and artificial seawater.

In the presence of NaCl, the titanosilicates AM-2 and ETS-4 are the best materials for Hg^{2+} removal, respectively 39.0 and 38.7 $ng \cdot g^{-1}$, although ETS-10 also exhibits a large removal capacity (36.9 $ng \cdot g^{-1}$) (Table 2.4). In contrast with the results obtained in the previous support systems (Milli-Q water and $MgSO_4$ solution), in the presence of NaCl, microporous zirconosilicates exhibited Hg^{2+} removal efficiencies lower than titanosilicates (except pharmacosiderite). The uptake for petarasite reaches 87.8%, while for AV-13 the uptake is 85.6%. Pharmacosiderite has, again, the worst performance of all materials, with the lowest uptake efficiency (72%). Comparing the results obtained for the Hg^{2+}/Mg^{2+} and Hg^{2+}/Na^{+} systems I conclude that the titanosilicates removal percentages decrease slightly or remain constant (pharmacosiderite) from changing the competing ion from Mg^{2+} (divalent) to Na^{+} (monovalent), whereas for zirconosilicates the removal percentages decrease >10%. This indicates that petarasite and AV-13 are less selective to Hg^{2+} (divalent ion) in the presence of monovalent cations.

In the most complex system (Hg^{2+}/artificial seawater) studied here, because it includes both Mg^{2+} and Na^{+} ions in the same concentrations as in the previous systems, AM-2 is the most efficient material for Hg^{2+} removal. Its removal efficiency remains at almost the same value as in the other studies (only Hg^{2+}, Hg^{2+}/Mg^{2+} and Hg^{2+}/Na^{+}). Petarasite has also a good performance, its removal efficiency remains at almost the same value as in the studies with only Hg^{2+} and with Hg^{2+}/Mg^{2+}. The ETS-4 uptake is also high (94.5%) and the results obtained for titanosilicate ETS-10 and zirconosilicate AV-13 are similar, respectively

90.5 and 89.7%. In this adsorption system, pharmacosiderite exhibited the poorest sorption results of all materials, with only 50.9% removal efficiency (Figure 2.3).

Table 2.4 – Hg^{2+} removal by titano and zirconosilicates in the presence of competing ions: available Hg^{2+} concentration after blank correction (C_{corr}), residual Hg^{2+} concentration (C_{res}), removal percentage (%) and amount of Hg^{2+} removed per gram of microporous material (q).

Microporous Materials	C_{corr} (ng·dm^{-3})	C_{res} (ng·dm^{-3})	Removal (%)	q (ng·g^{-1})
I. MgSO4 support solution				
ETS-10 (T)	178 ± 82	7.28 ± 0.94	95.9 ± 0.5	17.1 ± 0.1
ETS-4 (T)		6.61 ± 1.88	96.3 ± 1.1	17.1 ± 0.2
AM-2 (T)		5.28 ± 0.00	97.0 ± 0.0	17.2 ± 0.0
Pharmacosiderite (T)		49.3 ± 5.6	72.4 ± 3.2	12.9 ± 0.6
Petarasite (Z)		3.28 ± 0.94	98.2 ± 0.5	17.4 ± 0.1
AV-13 (Z)		3.29 ± 0.94	98.2 ± 0.5	17.4 ± 0.1
II. NaCl support solution				
ETS-10 (T)	406 ± 14	36.9 ± 3.5	90.9 ± 0.9	36.9 ± 0.4
ETS-4 (T)		19.6 ± 1.8	95.2 ± 0.4	38.7 ± 0.2
AM-2 (T)		15.7 ± 1.8	96.4 ± 0.4	39.0 ± 0.2
Pharmacosiderite (T)		111 ± 2	72.6 ± 0.6	29.4 ± 0.2
Petarasite (Z)		49.6 ± 1.3	87.8 ± 0.3	35.6 ± 0.1
AV-13 (Z)		58.5 ± 1.8	85.6 ± 0.4	34.8 ± 0.2
III. Artificial seawater support solution				
ETS-10 (T)	253 ± 14	24.1 ± 1.8	90.5 ± 0.7	22.8 ± 0.2
ETS-4 (T)		14.0 ± 2.4	94.5 ± 1.0	23.9 ± 0.2
AM-2 (T)		5.07 ± 1.17	98.0 ± 0.5	24.7 ± 0.1
Pharmacosiderite (T)		124 ± 2	50.9 ± 0.8	12.9 ± 0.2
Petarasite (Z)		7.01 ± 0.67	97.2 ± 0.3	25.6 ± 0.1
AV-13 (Z)		26.1 ± 1.2	89.7 ± 0.5	22.7 ± 0.1

(T) titanosilicate; (Z) zirconosilicate; mean ± standard deviation

Under the experimental conditions used, the presence of monovalent and divalent cations does not seem to influence greatly the removal of Hg^{2+} by microporous titanosilicates and zirconosilicates. This probably happens because the concentration of ions in the studied solutions is relatively low and, thus, the full ion-exchange capacity of the materials is never even approached. The notable exception is pharmacosiderite, since its Hg^{2+} removal capacity in the presence of competing ions decreases almost 40%. For all these reasons there is a clear indication that some of these inorganic materials may have an important environmental application, since they may be used to remove Hg^{2+} from contaminated waters.

2.4. Experimental procedure optimisation

In the previous section I reported that some microporous materials are able to remove Hg^{2+} from aqueous solutions, showing thus a possible environmental applicability, for example in waste water treatment. However, due to the low ionic strength of the samples, a significant part of Hg^{2+} was found to be lost during the experiments (section 2.3.2). Thus, my first goal was to optimise the experimental procedure, with the purpose of minimising Hg^{2+} losses.

On the basis of the results obtained in the preliminary study my main concerns are the filtration process and the Hg^{2+} adsorption onto the storage containers. In order to resolve these operational problems, simple and quick experiments were planned and performed. The optimisation experiments were designed considering the results obtained in the preliminary study, and also the targets of future studies. For these sets of experiments the concentration of 50 $\mu g \cdot dm^{-3}$ was chosen, as this is the limit value for discharges from industrial sectors, in accordance with the Portuguese legislation (DL 236/98 available at http://dre.pt).

2.4.1. Filtration

The filtration process is largely recognised as a source of error in trace metal determinations in water (Gardner and Comber, 1997). This statement was confirmed with the results obtained in the study reported in section 2.3.2, according to which, 27±4% of Hg^{2+} is lost during the filtration.

In order to minimize Hg^{2+} losses during the filtration process, a first set of four experiments was planned and the results are shown in Figure 2.4. These experiments

consisted in investigating differences in Hg^{2+} concentration of one solution with distinct experimental procedures (with and without filtration). For this proposal a Hg^{2+} solution with initial pH *ca.* 4 was prepared by diluting the Hg^{2+} stock solution to the desired concentration (50 $\mu g \cdot dm^{-3}$) and then the Hg^{2+} concentration of that solution was evaluated before and after filtration for different times. Afterwards, the Hg^{2+} solution was acidified with concentrated HNO_3 acid (Hg free), to pH<2 and once again the Hg^{2+} concentration of that solution was compared before and after filtration. The scheme of the experimental procedure is described in Table 2.5.

The results from experiments I and II clearly indicate that filtration is a source of Hg^{2+} loss. A significance test statistically confirms that there are no significant differences (P=0.05) between the initial Hg^{2+} concentration and the mean Hg^{2+} concentration of the solution which is not filtrated before analysis (Experiment II). In contrast, there are significant differences (P=0.05) between the initial Hg^{2+} concentration and the mean Hg^{2+} concentration of the solution which is filtrated before analysis (Experiment I).

Table 2.5 – Scheme of the experimental procedure for the first set of experiments.

Designation	**Time** (min)	**Description**
Experiment I	0.5; 15	An aliquot was taken from the Hg^{2+} solution (50 $\mu g \cdot dm^{-3}$; **pH *ca.* 4**), **filtered** through a 0.45 µm Millipore membrane, transferred to a storage vessel and then immediately analysed by CVAFS.
Experiment II	5; 20	An aliquot was taken from the Hg^{2+} solution (50 $\mu g \cdot dm^{-3}$; **pH *ca.* 4**), transferred to a storage vessel and then immediately analysed by CVAFS.
Experiment III	25; 50; 60	An aliquot was taken from the Hg^{2+} solution (50 $\mu g \cdot dm^{-3}$; **pH <2**), transferred to a storage vessel and then immediately analysed by CVAFS.
Experiment IV	35; 55	An aliquot was taken from the Hg^{2+} solution (50 $\mu g \cdot dm^{-3}$; **pH <2**), **filtered** through a 0.45 µm Millipore membrane, transferred to a storage vessel and then immediately analysed by CVAFS.

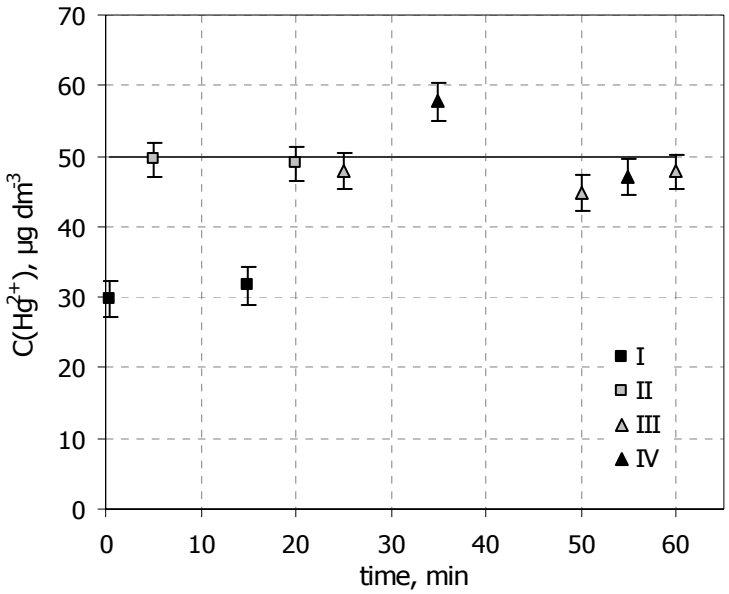

Figure 2.4 – Hg^{2+} concentration ($\mu g \cdot dm^{-3}$) and the respective confidence interval for distinct experimental procedure: I - with filtration, II - without filtration; III - without filtration and solution pH<2 and IV - with filtration and solution pH<2.

However, if the pH of the Hg^{2+} solution is <2 (Experiments III and IV), there are no statistical differences (P=0.05) between filtrated and unfiltrated samples. Furthermore, there are no significant differences (P=0.05) between the initial Hg^{2+} concentration and the mean Hg^{2+} concentration after analysis (with and without filtration). This fact suggests that the presence of H^+ can help decreasing Hg^{2+} losses during the filtration process.

After being identified as a one of the major sources of Hg^{2+} loss, the filtration process was studied in detail and divided in three steps:

Step 1: To collect aliquots (25 cm^3) from the reaction vessel, using a glass syringe

Step 2: To filtrate the sample through a 0.45 µm Millipore membrane

Step 3: To collect the filtrated sample from the filtration unit to a storage container

In order to investigate in which step of the filtration process, the main Hg^{2+} takes place, a second set of seven experiments were done and the results are shown in Figure 2.5. These experiments consisted in comparing Hg^{2+} concentrations of one solution when the filtration steps are performed separately and combined. For this purpose, another Hg^{2+} solution, with initial pH *ca.* 4 and concentration of 50 $\mu g \cdot dm^{-3}$, was prepared and then single and different combinations of the filtration steps were performed according with the scheme of the experimental procedure described in Table 2.6.

Table 2.6 – Scheme of the experimental procedure for the second set of experiments.

Designation	Time (h)	Description
Experiment V	0.15; 2.32; 4.80	An aliquot **was taken** from the Hg^{2+} solution (50 $\mu g \cdot dm^{-3}$; pH *ca*. 4), **filtered** through a 0.45 µm Millipore membrane, **transferred** to a storage vessel and then immediately analysed by CVAFS. (All steps).
Experiment VI	0.25; 3.80; 5.12	The Hg^{2+} solution (50 $\mu g \cdot dm^{-3}$; pH *ca*. 4) was analysed by CVAFS **directly** from the reaction vessel. (Any step).
Experiment VII	0.80; 1.70; 2.63	An aliquot **was taken** from the Hg^{2+} solution (50 $\mu g \cdot dm^{-3}$; pH *ca*. 4) then immediately analysed by CVAFS. (Step 1).
Experiment VIII	1.3	An aliquot **was taken** from the Hg^{2+} solution (50 $\mu g \cdot dm^{-3}$; pH *ca.* 4), **filtered** through a 0.45 µm Millipore membrane and then immediately analysed by CVAFS directly from the filtration unit. (Steps 1 and 2). The **filtration unit was washed with plenty of water** between samples.
Experiment IX	3.2	An aliquot **was taken** from the Hg^{2+} solution (50 $\mu g \cdot dm^{-3}$; pH *ca*. 4), **filtered** through a 0.45 µm Millipore membrane and then immediately analysed by CVAFS directly from the filtration unit. (Steps 1 and 2). The **filtration unit was washed with HNO_3 2%** (v/v) between samples.
Experiment X	4.95	An aliquot **was taken** from the Hg^{2+} solution (50 $\mu g \cdot dm^{-3}$; pH *ca*. 4), passed through the filtration unit but **without membrane**, **transferred** to a storage vessel and then immediately analysed by CVAFS. (Steps 1 and 3).
Experiment XI	4.30; 5.32	An aliquot **was taken** from the Hg^{2+} solution (50 $\mu g \cdot dm^{-3}$; pH *ca.* 4), **filtered** through a 0.45 µm Millipore membrane, **transferred** to a storage vessel and then immediately analysed by CVAFS. (All steps). The **membrane was previously washed with HNO_3 2%** (v/v).

Experiments V and VI definitely confirm that the major Hg^{2+} losses occur during the filtration process, *ca.* 30% against *ca.* 3% without filtration.

To investigate if the assemblage (syringe + tube) that collects the Hg^{2+} solution from the reaction vessel contributes to Hg^{2+} losses, the Hg^{2+} solution was analysed immediately after being collected, *i.e.* without being filtrated through a membrane (Experiment VII).

The results show that sampling with the syringe is not responsible for Hg^{2+} losses during the filtration process (Figure 2.5). Moreover, there are no significant differences (P=0.05) between the initial Hg^{2+} concentration and the mean Hg^{2+} concentration of the sub-samples that were collected with the assemblage syringe + tube.

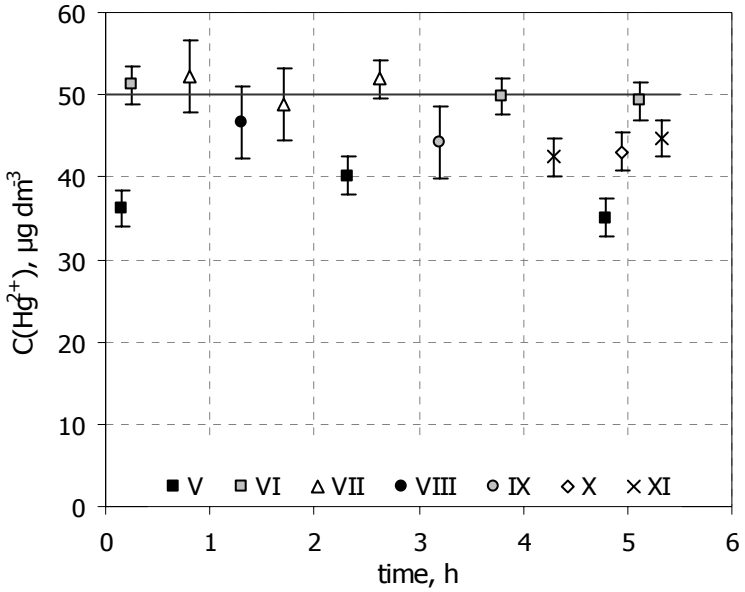

Figure 2.5 – Hg^{2+} concentration ($\mu g \cdot dm^{-3}$) and the respective confidence interval for different steps of the filtration process: V - with filtration (all steps), VI - without filtration; VII - with filtration (step 1); VIII - with filtration using a filtration unit washed with water; IX - with filtration using a filtration unit washed with HNO_3; X - with filtration but without membrane; XI - with filtration with a membrane previously washed with HNO_3.

One other possible cause for Hg^{2+} loss is its adsorption on the filtration unit. Usually, the filtration unit is washed with plenty of water between samples. In experiments VIII and IX two cleaning procedures were tested: the usual (Experiment VIII) and with HNO_3 acid 2% (v/v) (Experiment IX). The results from these experiments indicate both procedures originate losses of the same order (Figure 2.5) and lower (7-12%) than complete filtration (all steps). So, it may be concluded that a minor part of Hg^{2+} is lost by adsorption on the filtration unit. Previous results suggest that the major Hg^{2+} loss occurs between filtration step 1 and step 3, indicating that the membrane could be the major cause for Hg^{2+} losses. To test this hypothesis the membrane was removed from the filtration unit and the Hg^{2+} concentration measured (Experiment X). The results reveal that when the filtration is done without membrane only ca. 14% of Hg^{2+} is lost against ca. 30% with membrane, confirming that the membrane is one of the major causes of Hg^{2+} losses. An attempt to minimize the losses by the membrane was to wash it with HNO_3 2% (v/v) before filtration

(Experiment XI), and with this procedure the total losses were reduced in 57% and represented *ca.* 13% (Figure 2.5).

2.4.2. Material type

Another source of error in metal determinations is the adsorption of the metal to the storage containers. Teflon or high density polythene containers are recognised as the preferred materials for both sampling and storage because adsorptive losses appear to be lower than for other materials (Batley and Gardner, 1977).

In order to test if Teflon containers give lower Hg^{2+} losses than glass containers, a third set of four experiments was performed. Hg^{2+} solutions were prepared in several Teflon vessels and after a certain contact time between the Hg^{2+} solution and the Teflon vessel, the Hg^{2+} concentration in them and in the glass containers used in the previous experiments were compared. For this aim, four Hg^{2+} solutions, with initial pH *ca.* 4 and concentration of 50 $\mu g \cdot dm^{-3}$, were prepared in each of the four different Teflon containers available in the laboratory. The scheme of the experimental procedure is described on Table 2.7.

Table 2.7 – Scheme of the experimental procedure for the third set of experiments.

Designation	**Time** (h)	**Description**
Experiment XII	0.80	The Hg^{2+} solution (50 $\mu g \cdot dm^{-3}$; pH *ca.* 4) was analysed by CVAFS directly from the **Teflon container 1**. (Without filtration).
Experiment XIII	0.63	The Hg^{2+} solution (50 $\mu g \cdot dm^{-3}$; pH *ca.* 4) was analysed by CVAFS directly from the **Teflon container 2**. (Without filtration).
Experiment XIV	0.20; 0.40; 2.13	The Hg^{2+} solution (50 $\mu g \cdot dm^{-3}$; pH *ca.* 4) was analysed by CVAFS directly from the **Teflon container 3**. (Without filtration).
Experiment XV	0.32; 1.97	The Hg^{2+} solution (50 $\mu g \cdot dm^{-3}$; pH *ca.* 4) was analysed by CVAFS directly from the **Teflon container 4**. (Without filtration).

The results shown in Figure 2.6 are not satisfactory since the reproducibility is poor and the Hg^{2+} losses in experiments XII, XIII and XIV are very large (31-74%). Although in the literature Teflon is the recommended material to be used in trace metal storage, the results

from experiments XII-XV reveal that the Teflon containers available in our laboratory are ineffective.

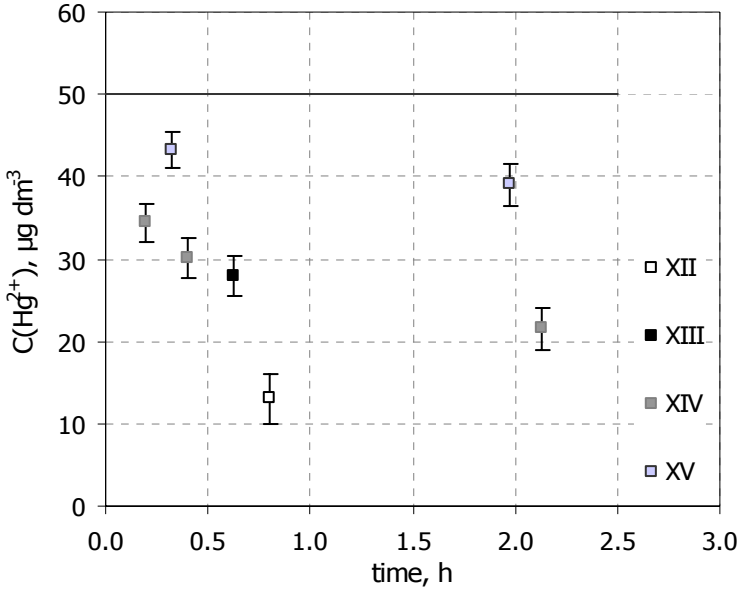

Figure 2.6 – Hg^{2+} concentration ($\mu g \cdot dm^{-3}$) and the respective confidence interval for different Teflon containers: XII - Teflon 1, XIII - Teflon 2; XIV - Teflon 3; XV - Teflon 4.

2.5. Experimental set-up and procedure adopted after optimisation

2.5.1. Glassware cleaning procedures

All glassware used in the experiments was always acid-wash before being use. The reaction vessels (2 dm^3 volumetric flasks) were initially washed several times with water and then were filled with nitric acid 2% (v/v) for 24 hours. Afterwards, the reaction vessels were rinsed several times with distilled water and then rinsed with high-purity water (Milli-Q water). The storage vessels (25 cm^3 Schott Duran® bottles) were firstly washed several times with water and then filled with concentrated nitric acid for 24 hours. Afterwards the storage vessels were rinsed several times with distilled water and then filled with nitric acid 25% (v/v) for 24 hours. After that, and to finish the cleaning procedure, the storage vessels were rinsed several times with distilled water and with high-purity water. The filtration unit was always rinsed between samples with water, then with distilled water and afterwards with nitric acid 2% (v/v). The glassware was dried at room temperature or a 313 K in a drying oven and then was stored, protected from air.

2.5.2. Experimental set-up and procedure

The experimental set-up (Figure 2.7) used in the batch experiments consisted of: (i) volumetric flask (2 dm^3), where the removal process takes place and a magnetic hotplate stirrer, (ii) sampling assemblage to collect aliquots from the bulk solution, encompassing a glass syringe (20 cm^3) connected to a 20 cm Technicon tube (internal Ø 2.54 mm) and (iii) filtration unit composed of a Buchner funnel (Ø 47 mm) and a filtering flask (250 cm^3).

Batch experiments were performed isothermally by contacting under agitation the Hg^{2+} solution and known masses of microporous materials, in closed volumetric flasks to avoid evaporation. Mercury (II) solutions were prepared daily by diluting the stock solution ($Hg(NO_3)_2$, 1000 $mg \cdot dm^3$) to the desired concentration, in high-purity water. The experiments started at the time when known masses of microporous materials were added to Hg^{2+} solutions and stirring was initiated. Aliquots (25 cm^3) were collected at fixed or increasing times, depending on the experiment, filtered through an acid-washed 0.45 µm Millipore membrane, adjusted to pH<2 with *Hg free* HNO_3 and then analysed by cold vapour atomic fluorescence spectrometry (CVAFS). A control Hg^{2+} solution was always run in parallel under the same experimental conditions, in order to assess the magnitude of the Hg^{2+} losses.

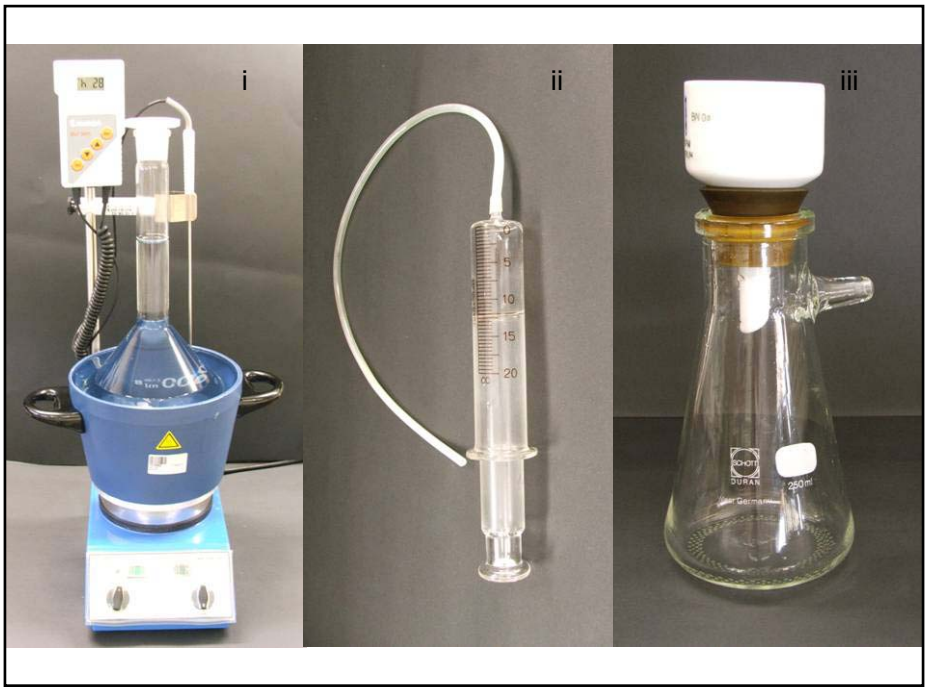

Figure 2.7 – Experimental set-up used in the batch experiments.

2.6. Conclusions

In this preliminary study I have measured and compared the removal of Hg^{2+} from aqueous solutions by microporous titanosilicates (ETS-10, ETS-4, AM-2 and pharmacosiderite) and zirconosilicates (petarasite and AV-13) and the results obtained reveal the potential of some of these microporous materials for removing Hg^{2+} from aqueous solutions both in presence and absence of competing ions. However, the materials performance may be optimised by changing the batch factor and adjusting the Hg^{2+} concentration to be handled (Al-Attar et al., 2000; Koudsi and Dyer, 2001; Petrus and Warchol, 2003).

The Hg^{2+} adsorptive losses during the experimental procedure are now well identified and can be minimized. The experiments assemblage has demonstrated that the filtration process is the major cause of Hg^{2+} losses, especially the membrane, because of the low ionic strength of the samples. However, washing the membrane on the filter holder with dilute nitric acid is an efficient procedure to reduce Hg^{2+} losses in 57%. The acidification of the sample with nitric acid to pH<2 immediately after filtration is also recommended to prevent adsorption losses to the storage containers. In our case, glass containers are preferable since they give better results than the Teflon ones.

Although Hg^{2+} losses have been minimised with the procedure describe previously, a control experiment (without microporous material) is recommended as the only means of assessing adsorptive losses.

Chapter

3

Hg^{2+} removal from aqueous solutions by selected titanosilicates: ETS-10, ETS-4 and AM-2

3.1. Introduction

After both, having obtained very promissory results on Hg^{2+} removal solutions with a low level of contamination, using microporous materials as adsorbents, and having optimised the experimental procedure in order to reduce Hg^{2+} losses (Chapter 2), my study will focus on assessing which is the best material to remove Hg^{2+} from solutions. The criterion that I chose to select the best material was the lowest mass necessary to remove more than 95% of Hg^{2+} ions present in solution, in a fair time. To achieve this purpose and based on the work reported on the previous chapter, some adjustment of the experimental conditions was done and the number of microporous materials in study was reduced. Firstly, it was decided to continue the study only with one type of material and therefore I decided to exclude zirconosilicates and to continue only with titanosilicates. This choice was not due to a less good performance of these materials, which in fact is similar for titano and zirconosilicates, but because the former are already available commercially (at least ETS-4 and ETS-10). The selection of the microporous titanosilicates ETS-10, ETS-4 and AM-2 was based on the results reported on chapter 2. The Hg^{2+} concentration was also adjusted to a more realistic one, observed in effluent discharges. Since the maximum value admissible by the Portuguese legislation for discharges of effluents by industries into water bodies is 50 $\mu g \cdot dm^{-3}$, this was the chosen concentration for future studies. Consequently, it is also important to assess the Hg^{2+} sorption capacity of titanosilicates in the presence of major ions of water bodies. Moreover, the mass of microporous titanosilicate to be used was optimised as a result of experimental conditions adjustments.

This chapter reports an evaluation of the potential of ETS-10, ETS-4 and AM-2 for being used in the decontamination of waters polluted with low Hg^{2+} levels and the effect on the process of fresh water competing ions. The evaluation of the materials sorption capacity is carried out on the basis of current procedures for studying metal adsorption: experimental determination of concentration curves along time, to later determine the corresponding kinetic equation, which will allow predicting the materials behaviour in real systems (Nam and Tavlarides, 2005).

3.2. Experimental conditions

The experiments were carried out in batch conditions, at room temperature (294±1 K). For each experiment a corresponding amount of microporous titanosilicate and 2000 cm^3 of

50 μg·dm^{-3} Hg^{2+} solution were kept in contact, with stirring (1400 rpm), until the Hg^{2+} concentration in solution remained constant. The concentration of 50 μg·dm^{-3} was chosen because this is the actual maximum value accepted for discharges from industrial sectors. Several masses of each titanosilicate were test in order to determinate the optimum value to be use to achieve appropriate Hg^{2+} removal and to reach equilibrium in a fair time (Table 3.1).

Table 3.1 – Masses of titanosilicates used in the experiments.

Microporous Materials	**Trial n.º**	**Mass** (mg ± 0.001 mg)
ETS-10	1	10.104
	2	24.735
ETS-4	3	25.028
	4	8.062
AM-2	5	41.206
	6	45.500

Due to the low Hg^{2+} concentration in natural waters relatively to that of other ions, it is crucial to asses the microporous titanosilicates capacity to remove Hg^{2+} in presence of the latter. Thus, the competitive effect was studied for the titanosilicate presenting the best results in absence of ionic competition.

The competitive effect was studied separately and for the ions whose concentration was that recommended by the United States Environmental Protection Agency for the preparation of synthetic fresh water (EPA, 1994). The competition tests were performed in the same conditions described above and in four different solutions: $NaHCO_3$ solution (96 mg·dm^{-3}), $MgSO_4$ solution (123 mg·dm^{-3}), $CaSO_4{\cdot}H_2O$ solution (60 mg·dm^{-3}) and KCl solution (4 mg·dm^{-3}). In order to model seawater, a NaCl solution (3 g·dm^{-3}) was also prepared and to assess the effect of Cl^- in the previous solution, another one, containing cation and anion in equimolar concentrations was prepared with $NaNO_3$ (4.35 g·dm^{-3}). Table 3.2 depicts the masses of ETS-4 employed in each competition test.

Table 3.2 – Mass of ETS-4 used in the competition experiments performed in the presence of different ions.

Microporous Materials	**Mass** (mg ± 0.001 mg)					
	$NaHCO_3$	$MgSO_4$	$CaSO_4{\cdot}H_2O$	KCl	NaCl	$NaNO_3$
ETS-4	8.058	8.128	8.028	8.115	8.076	8.059

3.3. Selection of the appropriate mass of titanosilicate

For the new experimental conditions (initial Hg^{2+} concentration and batch factor, *i.e.,* ratio between volume and mass), no background information was available on the best mass of titanosilicate to get suitable Hg^{2+} removal and to reach equilibrium in a reasonable time. Therefore, the most appropriate mass of titanosilicate to be used was determinated by trial-error.

The first material to be tested was ETS-10 and in the first trial, 10 mg of material were used. With this amount, a solution almost completely free of Hg^{2+} was obtained. Although the residual Hg^{2+} concentration in the liquid phase was of only 3.47 $\mu g{\cdot}dm^{-3}$, which corresponds to 93% of removal, the kinetics of the removal process was quite slow (Figure 3.1). This fact is noticeable because, although there is a lack of data between 48 and 240 hours, it takes 240 hours to obtain a residual Hg^{2+} concentration of 3.47 $\mu g{\cdot}dm^{-3}$.

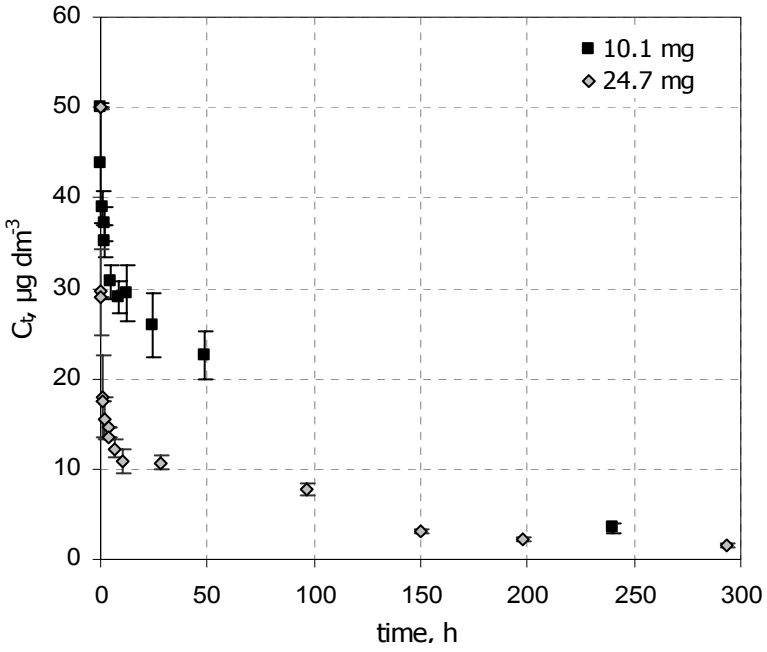

Figure 3.1 – Variation of the Hg^{2+} concentration and respective confidence interval in the liquid phase as function of time, for different masses of ETS-10.

Moreover, after 24 hours it was already noticeable that the kinetics was slow because only 48% of the Hg^{2+} in solution had been removed (Figure 3.1).

In order to reach the equilibrium in a shorter time, a second trial was performed with 24.7 mg of ETS-10 (Figure 3.1).

For the second mass of ETS-10 tested (24.7 mg) the kinetic of the removal process was considerably faster than for the first one (10.1 mg): 78% removal against 48% of Hg^{2+} after 24 hours. Moreover, with 25 mg of ETS-10 and after 293 hours, an even lower residual Hg^{2+} concentration in the liquid phase was obtained (1.49 $\mu g \cdot dm^{-3}$), corresponding to 97% of Hg^{2+} removal. Hence, *ca*. 25 mg of ETS-10 is a suitable mass to employ for the the experimental conditions indicated in the 3.2 section.

An analogous study was performed for ETS-4, using 25 mg in the first trial (Figure 3.2). The results obtained were surprising because after only 16 minutes the residual Hg^{2+} concentration in the liquid phase was as low as 0.84 $\mu g \cdot dm^{-3}$, *ca.* 98% of Hg^{2+} removal. In this trial it was not possible to record the kinetic curve of the process and, thus, a second trial was performed using less material. Reducing the mass of ETS-4 to 8 mg was possible to follow the kinetics of Hg^{2+} removal and to attain equilibrium in a short time. The Hg^{2+} residual concentration in the liquid phase and the removal percentage were, respectively, 1.69 $\mu g \cdot dm^{-3}$ (Figure 3.2) and 97% after 5 hours and 23 minutes.

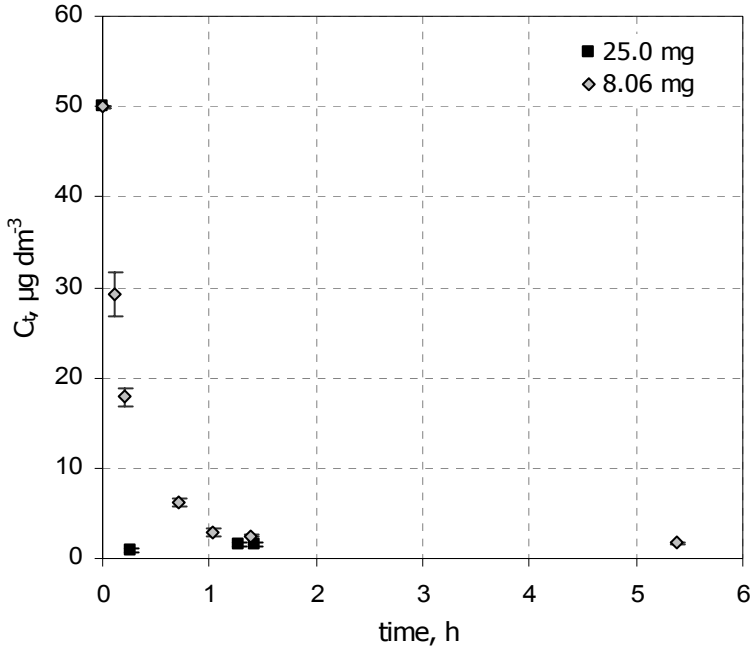

Figure 3.2 – Hg^{2+} concentrations and the respective confidence interval in the liquid phase as function of time, for different masses of ETS-4.

As for ETS-10 and ETS-4, a preliminary study was performed to determine the mass of AM-2 that should be used to attain a low residual Hg^{2+}concentration and to study the kinetics of the removal process. In the first trial, 41 mg of AM-2 were used. Although only two determinations were done they suggested that this mass is adequate (Figure 3.3).

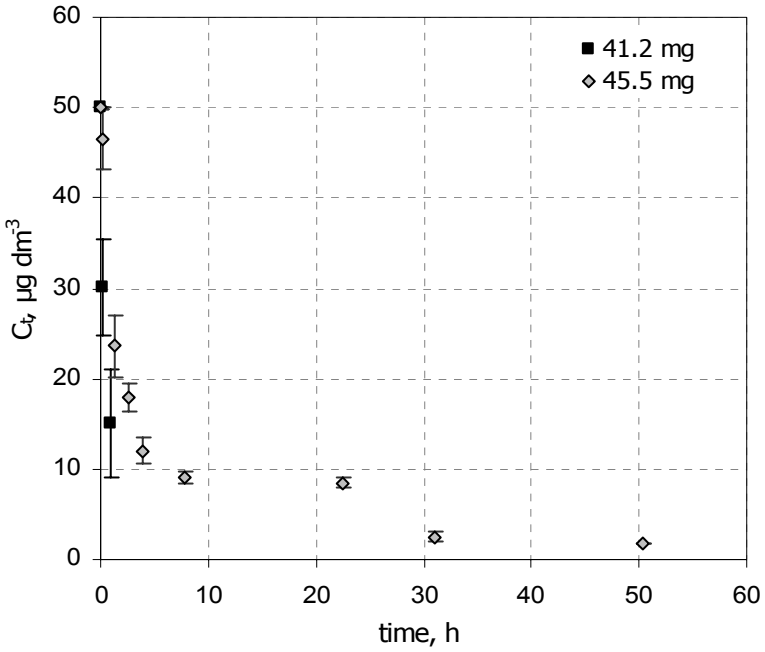

Figure 3.3 – Hg^{2+} concentrations and the respective confidence interval in liquid phase as function of time, for different masses of AM-2.

To confirm this, a more complete study on the AM-2 Hg^{2+} removal efficiency was carried out for 50 hours, with 45.5 mg of AM-2. The second trial confirmed the results obtained in the first trial. After 50 hours of contact time, the amount of AM-2 used removed 96% of the Hg^{2+} in solution, corresponding to a residual Hg^{2+} concentration of 1.77 µg·dm^{-3} (Figure 3.3).

3.4. Hg^{2+} sorption efficiency

The variation of the concentration of Hg^{2+} as a function of time and the corresponding amounts of Hg^{2+} sorbed onto each titanosilicate, for the most appropriate mass of titanosilicate are shown in Figure 3.4. For all materials, a decrease with time of the Hg^{2+} concentration in the liquid phase was observed, even when starting from a low (50 µg·dm^{-3}) Hg^{2+} concentration. Although Hg^{2+} has different affinity for the various titanosilicates, it

is possible to obtain water of drinking quality ([Hg^{2+}] ≤ 2 μg·dm^{-3}) (http://www.inspect-ny.com/water/levels.htm) using all of them.

Table 3.3 depicts the experimental Hg^{2+} uptake by the titanosilicates, the amount of Hg^{2+} removed, the equilibrium Hg^{2+} concentration, the contact time and the mass required for Hg^{2+} removal. Clearly, ETS-4 exhibits the highest affinity for Hg^{2+}, and a relatively small mass of this material is able to remove nearly all the metal in solution. ETS-10 performs slightly better than AM-2, with a q_e value almost twice than that of the latter.

Table 3.3 – Experimental Hg^{2+} uptake, q_e, C_e, contact time and mass of titanosilicate used.

	Microporous titanosilicates		
Experimental parameters	**ETS-10**	**ETS-4**	**AM-2**
Hg^{2+} uptake (%)	97.0 ± 0.5	98.4 ± 0.4	97.7 ± 0.5
q_e (mg·g^{-1})	3.92 ± 0.02	12.2 ± 0.0	2.15 ± 0.01
C_e (μg·dm^{-3})	1.49 ± 0.21	0.93 ± 0.05	1.14 ± 0.20
Time (h ± 0.02* h)	293.18	145.57	141.57
Mass (mg ± 0.001* mg)	24.735	8.062	45.500

* tolerance; value ± standard deviation

The first- and second-order rate constants (k_1 and k_2), the q_e values in equations (1.10) and (1.15) and the corresponding correlation coefficients(R^2) are presented in Table 3.4 for the different materials and were obtained using GraphPad Prism 5 program using the least squares as fitting method and the Marquardt and Levenberg algorithm for minimizing the function.

The experimental kinetic data are shown in Figure 3.5 together with the modelled curves obtained from pseudo-first- and pseudo-second-order equations. The second-order model fits the experimental data slightly better than the first-order one, and the q_e values found assuming the second-order kinetic model slightly overestimate the experimental values, while those assuming the first-order kinetic model are underestimated.

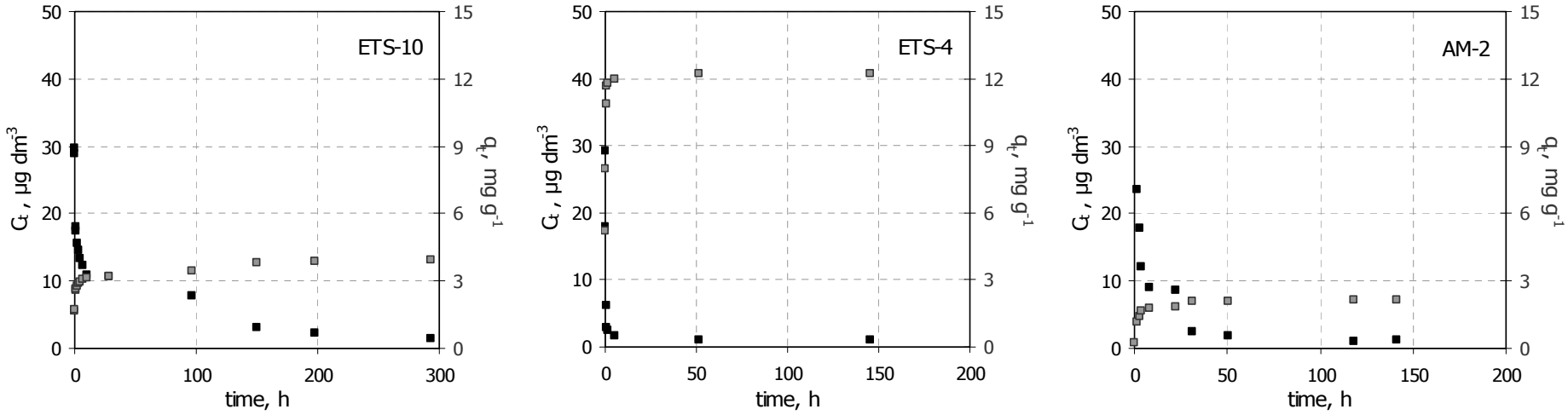

Figure 3.4 – Hg^{2+} concentrations in the liquid phase (C_t) and/or sorbed on the titanosilicate (q_t) as a function of time. Error bars for Hg^{2+} measurements are omitted for clarity. Black symbols – Hg^{2+} in solution; Grey symbols – Hg^{2+} sorbed.

Table 3.4 – First- and second-order sorption rate constants obtained for the removal of Hg^{2+} from the liquid phase. For comparison, the experimental q_e is shown together with that obtained from fitting first- and second-order kinetic curves.

		First-order kinetics			Second-order kinetics		
Microporous titanosilicates	q_e (mg·g^{-1})	k_1 (h^{-1})	R^2	q_e - *fitted* (mg·g^{-1})	k_2 (g·mg^{-1}·h^{-1})	R^2	q_e - *fitted* (mg·g^{-1})
ETS-10	3.92	1.569	0.886	3.31	96.91	0.949	3.51
ETS-4	12.2	5.062	0.994	11.86	14984	0.989	12.5
AM-2	2.15	0.502	0.974	2.024	7.779	0.991	2.13

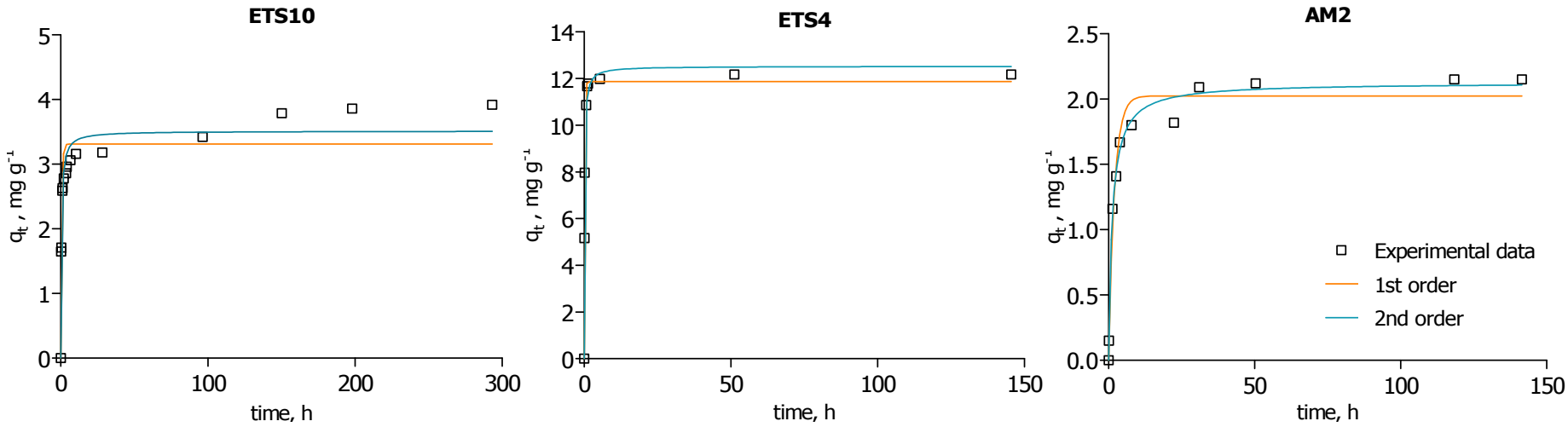

Figure 3.5 – Experimental and modelled kinetic results using pseudo-first- and pseudo-second-order equations for ETS-10, ETS-4 and AM-2.

The kinetics shows that the removal of Hg^{2+} is probably based on two different mechanisms: ion exchange, which is fast, and chemisorption, which is slower. Thus, the kinetics of Hg^{2+} removal by these titanosilicates is ultimately determined by chemisorption, which it seems to be better described by the second-order equation rather than by the first-order one. As revealed by the kinetic constants, ETS-4 displays the faster Hg^{2+} sorption kinetics. In addition, the fitted and experimental q_e values of this material are larger than those of other titanosilicates.

3.5. Hg^{2+} removal under cationic competition

In the previous section, I have shown that ETS-4 is the most efficient titanosilicate studied for removing Hg^{2+} from water. Competitive sorption studies were, hence, carried out using this material. Figure 3.6 shows experimental kinetic results of the Hg^{2+} sorption onto ETS-4 in the presence of major freshwater competitive ions (K^+, Na^+, Mg^{2+} and Ca^{2+}). The experimental Hg^{2+} uptake and sorption capacity corresponding to the single sorption of Hg^{2+} together with data obtained under ionic competition are depicted in Table 3.5.

The competitive effect of the different ions is very different. The cations that affect less the sorption of Hg^{2+} on ETS-4 are Mg^{2+} and Ca^{2+}, because C_e and q_e are almost the same values found when only Hg^{2+} is present in the solution (even when the salt concentration was much high larger than that of Hg^{2+}). For $NaHCO_3$, there is a reduction in the sorption of Hg^{2+}, which may be due to the modification of the pH (Table 3.5). In the presence of KCl, a slight decrease in the sorption of Hg^{2+} was observed, which may be related to the formation of mercury chloro-complexes (neutral or even negatively charged).

In the presence of a relatively high NaCl concentration (3 $g \cdot dm^{-3}$) the Hg^{2+} sorption was suppressed, further indicating that the formation of chloro-complexes restrains the use of ETS-4 (and possibly other titanosilicates) for Hg^{2+} purification. In contrast, the presence of $NaNO_3$, even at high concentration (4.35 $g \cdot dm^{-3}$), does not reduce significantly the sorption of Hg^{2+}, thus showing that Na^+ is not responsible for the considerable competitive effect of NaCl.

The experimental kinetic data of the sorption of Hg^{2+} on ETS-4 under competition of other cations, together with the modelled curves obtained from pseudo-first- and pseudo-second-order equations are shown in Figure 3.7. The first- and second-order rate constants (k_1 and k_2), the q_e values in equations (1.10) and (1.15) and the corresponding correlation coefficients(R^2) are presented in Table 3.6. The results are well described by

the first and second-order kinetics models, which are further supported by the comparison between the experimental and fitted q_e values. This does not hold for the experiment which mimics sea water, for which description neither first- nor second-order models are satisfactory. Both models confirm that $MgSO_4$ and $CaSO_4$ are the salts which affect less the sorption of mercury by ETS-4. For these salts, the experimental q_e is well predicted by both kinetics equations and is nearly equal to that observed in the absence of competitive ions. However, although the corresponding second-order kinetic constants are larger than those obtained for the rest of the titanosilicates (Table 3.6), they are smaller than those found for ETS-4 under no competition. This indicates that the removal of Hg^{2+} is slower when there are competitive ions in solution, which is more evident for CaSO4. The competitive effects of the salts are more evident on the kinetics of Hg^{2+} removal than on the ETS-4 q_e.

Table 3.5 – Experimental Hg^{2+} uptake, sorption capacity (q_e), residual Hg^{2+} concentration (C_e), final pH, contact time and concentration of salt in the experiments using ETS-4 to remove Hg^{2+} in the presence of competing ions.

	Salts						
	none	KCl	$NaHCO_3$	$MgSO_4$	$CaSO_4$	NaCl	$NaNO_3$
[salt] ($mg \cdot dm^{-3}$)	---	4.059 ± 0.001	96.15 ± 0.03	122.7 ± 0.04	59.80 ± 0.02	3000 ± 1	4350 ± 1
Hg^{2+} uptake (%)	98.4 ± 0.4	79.4 ± 1.6	76.7 ± 4.0	97.0 ± 0.6	96.0 ± 0.7	8.0 ± 7.6	78.4 ± 0.4
q_e ($mg \cdot g^{-1}$)	12.2 ± 0.0	9.78 ± 0.20	9.52 ± 0.50	11.9 ± 0.1	12.0 ± 0.1	0.99 ± 0.94	9.73 ± 0.04
C_e ($\mu g \cdot dm^{-3}$)	0.93 ± 0.05	10.3 ± 0.8	11.6 ± 2.0	1.52 ± 0.26	2.00 ± 0.29	46.0 ± 3.8	10.8 ± 0.1
pH (±0.1*)	4.3	4.3	7.7	4.3	4.5	‡	‡
Time (h ±0.02*h)	145.57	127.68	75.62	44.25	46.67	25.7	70.48

* tolerance; value ± standard deviation; ‡ pH values not measure

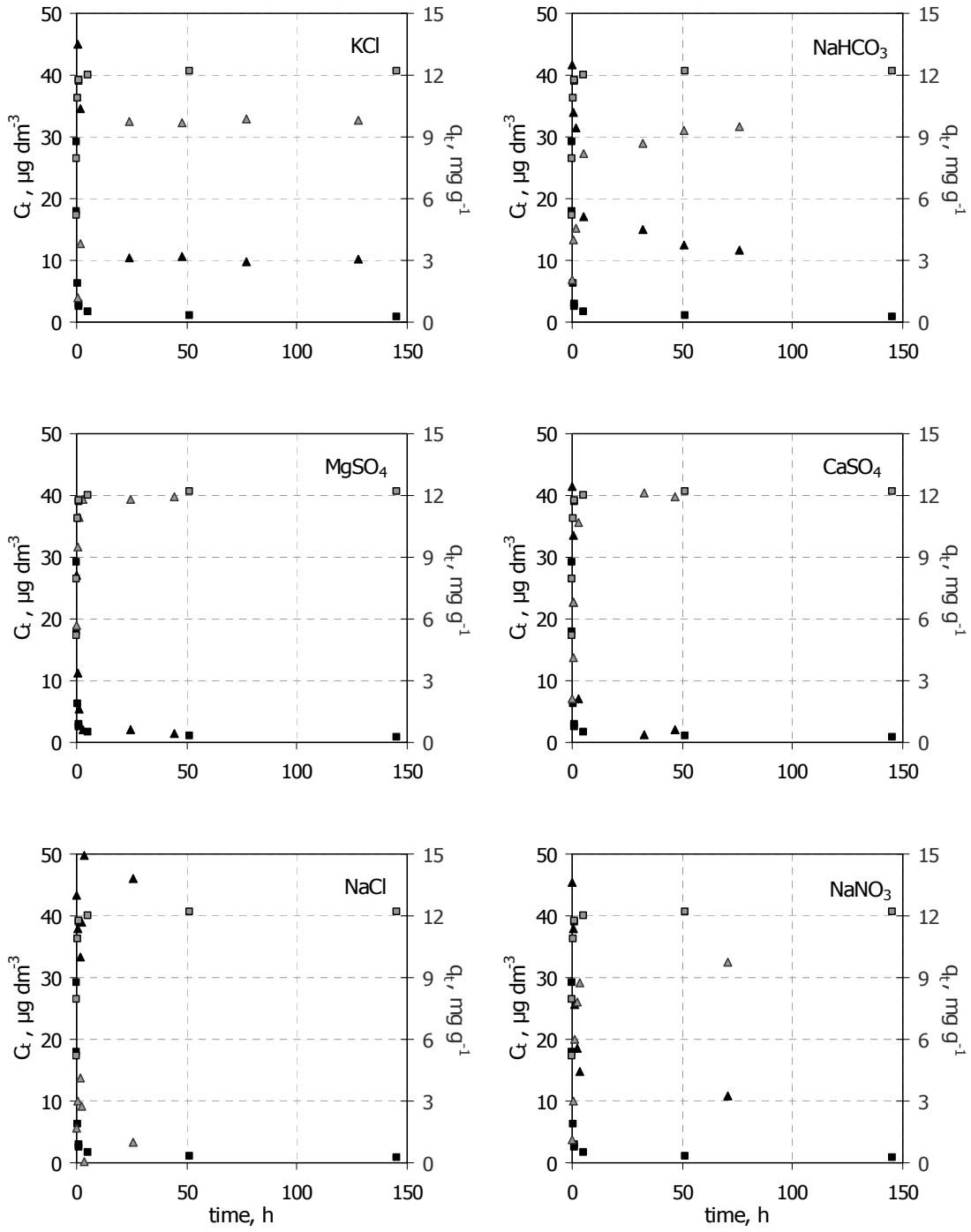

Figure 3.6 – Hg^{2+} concentrations in the liquid phase (C_t) and/or sorbed on ETS-4 (q_t) as a function of time, in the presence of competitive ions in solution. Error bars for Hg^{2+} measurements are omitted for clarity. Black symbols – Hg^{2+} in solution; Grey symbols – Hg^{2+} sorbed; Square symbols – without competition; Triangular symbols – with competition.

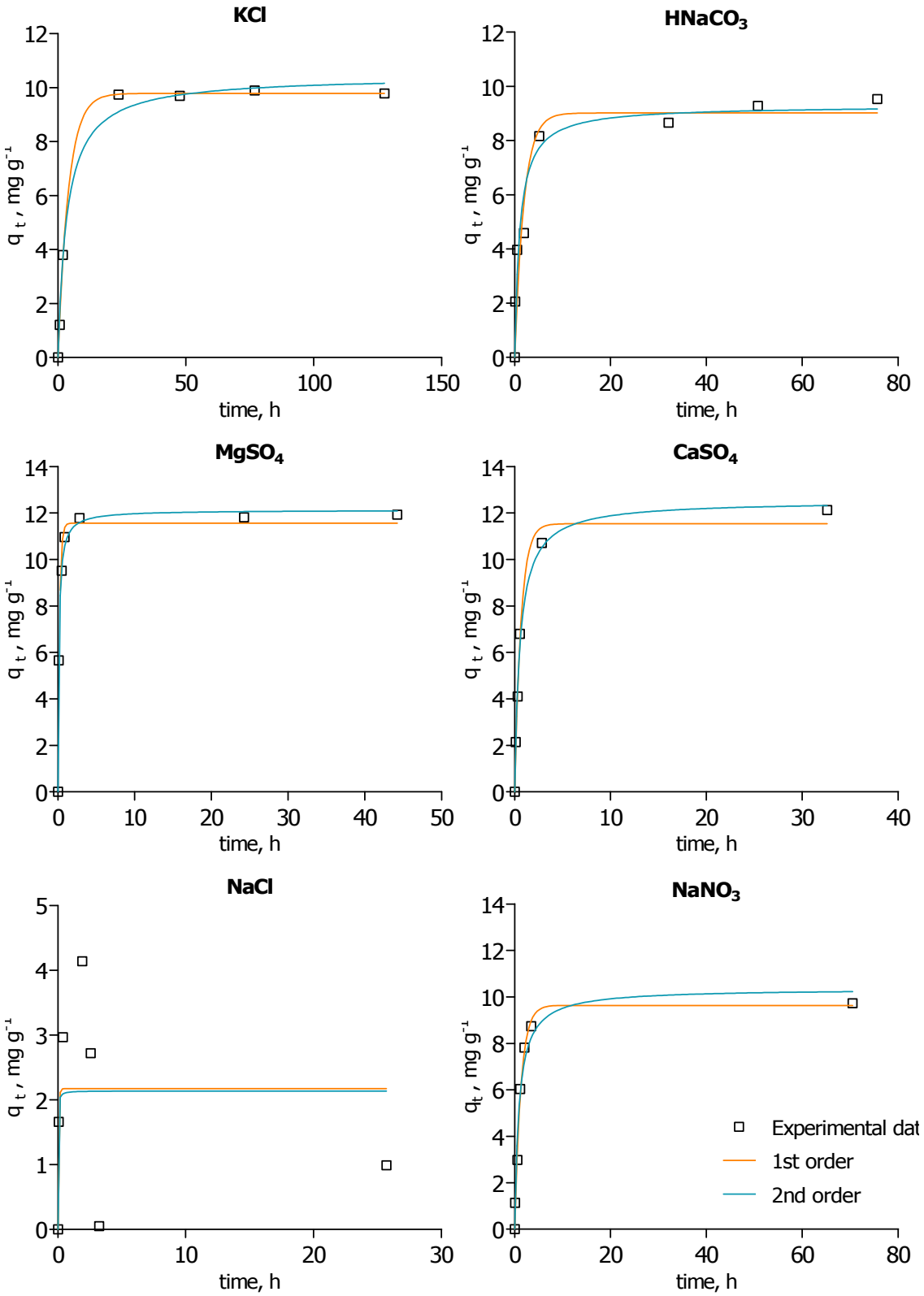

Figure 3.7 – Experimental and modelled kinetic results using pseudo-first- and pseudo-second-order equations for the removal of Hg^{2+} from solution by ETS-4 under the competition by different salts also present in solution.

Table 3.6 – First- and second-order sorption rate constants obtained for the removal of Hg^{2+} from liquid phase by ETS-4, in the presence of competing ions. For comparison, the experimental q_e is shown together with that obtained from the fitting corresponding to first- and second-order kinetics.

		First-order kinetics			**Second-order kinetics**		
Salts	q_e ($mg \cdot g^{-1}$)	k_1 (h^{-1})	R^2	q_e - *fitted* ($mg \cdot g^{-1}$)	k_2 ($g \cdot mg^{-1} \cdot h^{-1}$)	R^2	q_e - *fitted* ($mg \cdot g^{-1}$)
None	12.2	5.062	0.994	11.86	14984	0.989	12.5
KCl	9.78	0.2446	0.999	9.79	329	0.993	10.4
$NaHCO_3$	9.53	0.5241	0.9240	9.02	775	0.953	9.29
$MgSO_4$	11.9	4.680	0.987	11.6	13786	0.998	12.1
$CaSO_4$	12.0	1.514	0.991	11.5	3628	0.995	12.5
NaCl	0.99	20.82	0.270	2.173	1146	0.258	2.14
$NaNO_3$	9.73	0.7768	0.9913	9.64	1249	0.976	10.4

3.6. Conclusions

The potential of titanosilicate materials ETS-10, ETS-4 and AM-2 for being used in the purification of water contaminated with Hg^{2+} levels typical of natural systems has been evaluated. All the materials are able to remove Hg^{2+} from solution, even at low initial concentrations, although they display different uptake capacity. They are, thus, promising materials for Hg^{2+} decontamination of natural freshwaters.

ETS-4 is the most efficient titanosilicate investigated, able to uptake more than 98% of Hg^{2+} ions, starting from an initial Hg^{2+} concentration of 50 $\mu g \cdot dm^{-3}$ and attaining more than 12 $\mu g \cdot mg^{-1}$ of sorbed Hg^{2+} in about five hours.

Even at relatively high concentrations, the major freshwater cations, Ca^{2+}, Na^{+} and Mg^{2+}, do not significantly reduce the affinity of ETS-4 for Hg^{2+}. The effect of pH increase on the Hg^{2+} removal efficiency seems to be more important than the cationic competition, probably because of change in the mercury speciation. The most important reduction of the ETS-4 Hg^{2+} removal ability is caused by Cl^{-} ions, due to the formation of metal chloro-complexes. Thus, the titanosilicates reported here are not useful for the remediation of salty or sea waters.

It seems that in the sorption of Hg^{2+} two mechanisms are in operation: fast ion exchange and slow chemisorption. The sorption of Hg^{2+}, in the presence or absence of competing cations, is described by both pseudo first and second-order kinetic models. Ca^{2+}, Na^{+} and Mg^{2+} competition slows down the kinetics of Hg^{2+} sorption, but does not reduce significantly the uptake capacity of ETS-4.

Chapter 4

Influence of stirring rate, contact time, ETS-4 mass, initial Hg^{2+} concentration, temperature and pH on Hg^{2+} removal efficiency by ETS-4

4.1. Introduction

It is well know that operating conditions such as contact time, initial metal concentration, adsorbent mass, pH and temperature may have a strong effect on heavy metal removal. In the previous chapter, ETS-4 has been shown to have a remarkable capacity to remove Hg^{2+} from aqueous solutions. The following stage of my study consisted in assessing the effect on this process of the above-mentioned experimental parameters.

Since the kinetic performance of ion exchange is in general interpreted by semi-empirical pseudo first- and second-order equations (Lagergren, 1989, Ho and McKay, 1999a; Ho and McKay, 1999b; Reddad et al., 2002; Yardim et al., 2003; Chiron et al., 2003; Aksu, 2005; Zhang et al., 2005; Lopes et al. 2007), these kinetic models will be applied to investigate the Hg^{2+} removal mechanisms and the sorption rate. However, these models are merely correlative, which limits their application and extrapolation. A more reliable approach deals with the application of the Nernst-Planck equations to describe mass transport in ionic systems, in which both concentration and electric potential gradients, induced by the different counter ions motilities, are accounted for (Helfferich, 1995; Rodrígez et al., 1998; Valverde et al., 2004). In this chapter I also present a mathematical model based on the Nernst-Planck approach to describe the ion-exchange process, which was developed by the Chemical Engineering group of University of Aveiro. Additionally, the experimental equilibrium data on Hg^{2+} removal are fitted to Langmuir and Freundlich models and thermodynamic parameters calculated for the Hg^{2+} sorption to explain the process feasibility.

4.2. Experimental conditions

Batch experiments were performed by contacting under agitation 2 dm^3 of Hg^{2+} solution and ETS-4 powders in volumetric flasks. For each experiment stirring was kept until Hg^{2+} concentration in solution remained constant, *i.e.* until solution-solid equilibration was achieved. The effect of each parameter on the ETS-4 sorption capacity was studied individually, by changing a parameter and keeping all the others constant.

Table 4.1 and Table 4.2 depict respectively, the experimental conditions used for the evaluation of the stirring rate, the ETS-4 mass and initial Hg^{2+} concentration effect, and the experimental conditions used for the evaluation of the pH and temperature effect.

Table 4.1 – Experimental conditions (stirring rate, ETS-4 mass and initial Hg^{2+} concentration) used in the stirring rate, ETS-4 mass and initial Hg^{2+} concentration effect experiments.

	Stirring (rpm)	**Mass** (mg ± 0.001* mg)	**C_0** (μg·dm^{-3})	**pH_0** (±0.1*)
Stirring rate effect	**60**	8.030	50.00 ± 0.12	4.9
	500	8.085		
	900	8.094		
	1400	8.024		
ETS-4 mass effect	1400	**0.573**	50.00 ± 0.12	---
		0.851		---
		1.639		---
		2.223		---
		3.450		---
		5.055		4.7
		8.024		4.9
		12.201		5.3
		16.233		7.3
Initial [Hg^{2+}] effect	1400	8.024	**50.00 ± 0.12**	4.9
		8.053	**150.00 ± 0.25**	4.0
		8.059	**170.00 ± 0.35**	3.9
		8.034	**250.00 ± 0.44**	3.7

* tolerance; value ± standard deviation

The stirring rate effect on Hg^{2+} removal by ETS-4 was studied at room temperature (294 K) for four different values (60, 500, 900 and 1400 rpm). For the three highest rates (500, 900 and 1400 rpm) the Hg^{2+} solution/ETS-4 powder was completely homogeneous suspension, while for the lowest velocity (60 rpm) the ETS-4 powder settled down in the volumetric flask bottom.

The effect of ETS-4 mass was evaluated at room temperature (294 K) for nine different masses ranging from 0.573 to 16.233 mg, while the effect of initial Hg^{2+} concentration was assessed for four different concentrations (50, 150, 170 and 250 μg·dm^{-3}). The pH values of these solutions were not adjusted. In the case of initial Hg^{2+} concentration effect study the solution pH depends directly on the amount of Hg^{2+} standard solution (1×10^{3} mg·dm^{-3})

that is necessary to obtain the desired Hg^{2+} concentration, since the pH of the Hg^{2+} standard solution is well below 7, in order to keep Hg^{2+} ion stabilized in solution. In the case of ETS-4 mass effect study, the solution pH increases with increasing ETS-4 mass due to ion exchange between alkali cation in framework and hydrogen ion through hydrolysis (Pitcher et al., 2004; Choi et al., 2006a).

Table 4.2 – Experimental conditions (ETS-4 mass, initial pH and temperature) used in the pH and temperature effect experiments.

	Mass (mg ± 0.001* mg)	**pH_0** (±0.1*)
pH effect	8.004	**2.0** (HNO_3)
	8.078	
	8.180	**2.9** (HNO_3)
	8.154	
	8.048	
	8.180	**3.8** (HNO_3)
	8.107	
	8.184	
	8.024	**4.9** (None)
	8.094	
	8.109	
	8.050	**6.2** (NaOH)
	8.102	
	8.114	**6.9** (NaOH)
	8.103	
	8.127	**8.0** (NaOH)
	8.127	
	8.098	**9.3** (NaOH)
	8.114	
	8.069	**10.0** (NaOH)
	8.037	

Cont.	**Mass** (mg ± 0.001* mg)	**pH_0** (±0.1*)
pH effect	8.088	**6.2** (KOH)
	8.067	
	8.118	**6.9** (KOH)
	8.108	
	8.066	**8.0** (KOH)
	8.025	
	8.096	**9.3** (KOH)
	8.134	
	8.095	**10.0** (KOH)
	8.046	
	Mass (mg ± 0.001* mg)	**Temperature** (K ± 1K)
temperature effect	8.008	**277**
	8.095	
	8.020	
	8.024	**294**
	8.094	
	8.085	
	8.083	**313**
	8.066	
	8.080	

* tolerance; (HNO_3) - solution pH adjusted by acidification with HNO_3 conc.; (NaOH) - solution pH adjusted by alkalisation with NaOH 0.1M; (KOH) - solution pH adjusted by alkalisation with KOH 0.1M.

The pH effect on Hg^{2+} removal by ETS-4 was studied at room temperature (294 K) for different pH levels ranging from 2 to 10, using an initial Hg^{2+} concentration of 50 $\mu g \cdot dm^{-3}$ and a stirring rate of 1400 rpm. For pH values lower than 4.9 (*ca*. 2, 3 and 4) the solution pH was adjusted with HNO_3 concentrated, while for pH values higher than 4.9 (*ca*. 6, 7, 8, 9 and 10) the solution pH was initially adjusted with NaOH 0.1M. In order to investigate the effect of the alkalisation with NaOH, a second set of experiments were done for the

same pH values using KOH 0.1M as alkalisation solution. The effect of temperature on Hg^{2+} removal by ETS-4 was studied for three different temperatures: 277, 294 and 313 K, for an initial Hg^{2+} concentration of 50 μg·dm^{-3}, pH 4.9 and a stirring rate of 1400 rpm.

4.3. Stirring rate

The results obtained from the stirring rate study indicated that, except for the lowest rate (60 rpm), the quantity of Hg^{2+} removed by ETS-4 at the equilibrium (12.1±0.1 mg·g^{-1}) and the Hg^{2+} uptake (98±1%) are not dependent of the stirring velocity (Figure 4.1). However, it must be highlighted that the sorption was relatively slow for the lowest stirring velocity (60 rpm) here considered. At 60 rpm, the equilibrium time was *ca*. 150 hours while for the other stirring rates the equilibrium time was 24 hours. These results indicate that the diffusion of Hg^{2+} ions into the ETS-4 may be the limiting step for the sorption of Hg^{2+} and thus stirring used in batch studies must be high enough to break the diffusion resistance.

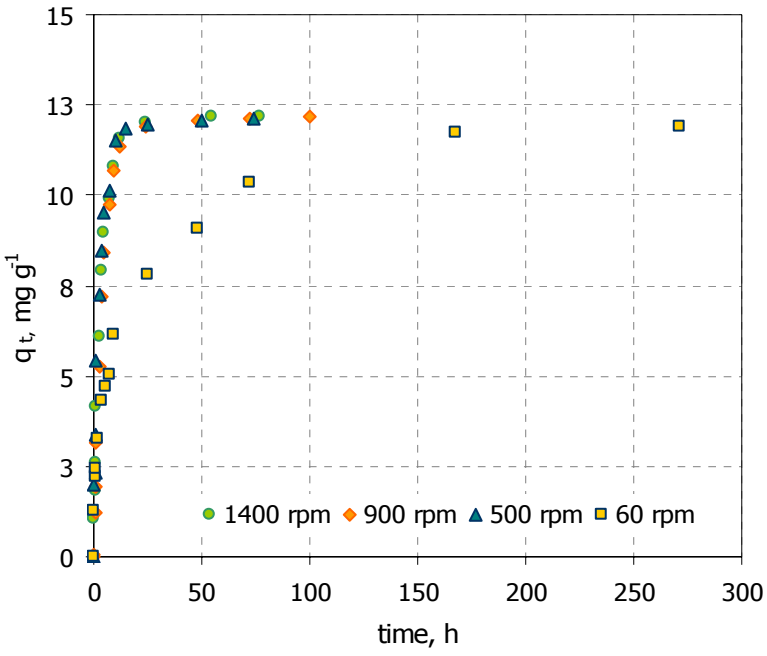

Figure 4.1 – Variation of q_t as function of time for different stirring rates, at 294 K.

4.4. Contact time

The experimental Hg^{2+} concentrations in solution as a function of time and the corresponding amounts of Hg^{2+} sorbed onto ETS-4, are shown respectively in Figure 4.2 and Figure 4.3 for (**a**) nine different masses of ETS-4 and the same initial Hg^{2+} concentration (50 $\mu g \cdot dm^{-3}$) and for (**b**) the same ETS-4 mass (8 mg) and four different Hg^{2+} concentrations. For all ETS-4 masses and Hg^{2+} concentrations used, a decrease with time of the Hg^{2+} concentration in the liquid phase was observed, even when starting from a higher concentration ($[Hg^{2+}]$ = 250 $\mu g \cdot dm^{-3}$) (Figure 4.2). According with Figure 4.2 and Figure 4.3 equilibrium is attained in 24 h for all Hg^{2+} concentrations used and for ETS-4 masses $\geq$ 3.45 mg. However, as long as ETS-4 mass decreases, the time necessary to attain the equilibrium increases. This fact is particularly notorious when comparing the equilibrium time for the lowest and the highest ETS-4 mass: 216 h for the lowest (0.573 mg) and 24 h for the highest one (16.2 mg). This fact suggests that equilibrium time can be drastically affected by small variations in ETS-4 mass and not so much by Hg^{2+} concentration variations. Moreover, the profile of the curves on the insets of Figure 4.3-a and Figure 4.3-b reveal that during the first 10 h or so, the Hg^{2+} removal increased abruptly and then caught up approaching equilibrium.

4.5. Mass of ETS-4

The ETS-4 mass is an important parameter to obtain quantitative Hg^{2+} removal, since it influences the contact time necessary to reach equilibrium and the sorption capacity.

Although the Hg^{2+} concentration in the liquid phase decreases with time for all ETS-4 masses used, (Figure 4.2-a) achieving clean water, of drinking quality ($[Hg^{2+}] \leq 2$ $\mu g \cdot dm^{-3}$) (http://www.inspect-ny.com/water/levels.htm) was only possible with the employment of ETS-4 masses higher or equal to 3.45 mg (Table 4.3). Moreover, with the utilization of about 16 mg of ETS-4 the residual Hg^{2+} concentration in the liquid phase was lower than 0.3 $\mu g \cdot dm^{-3}$, which corresponds to more than 99% of Hg^{2+} removal.

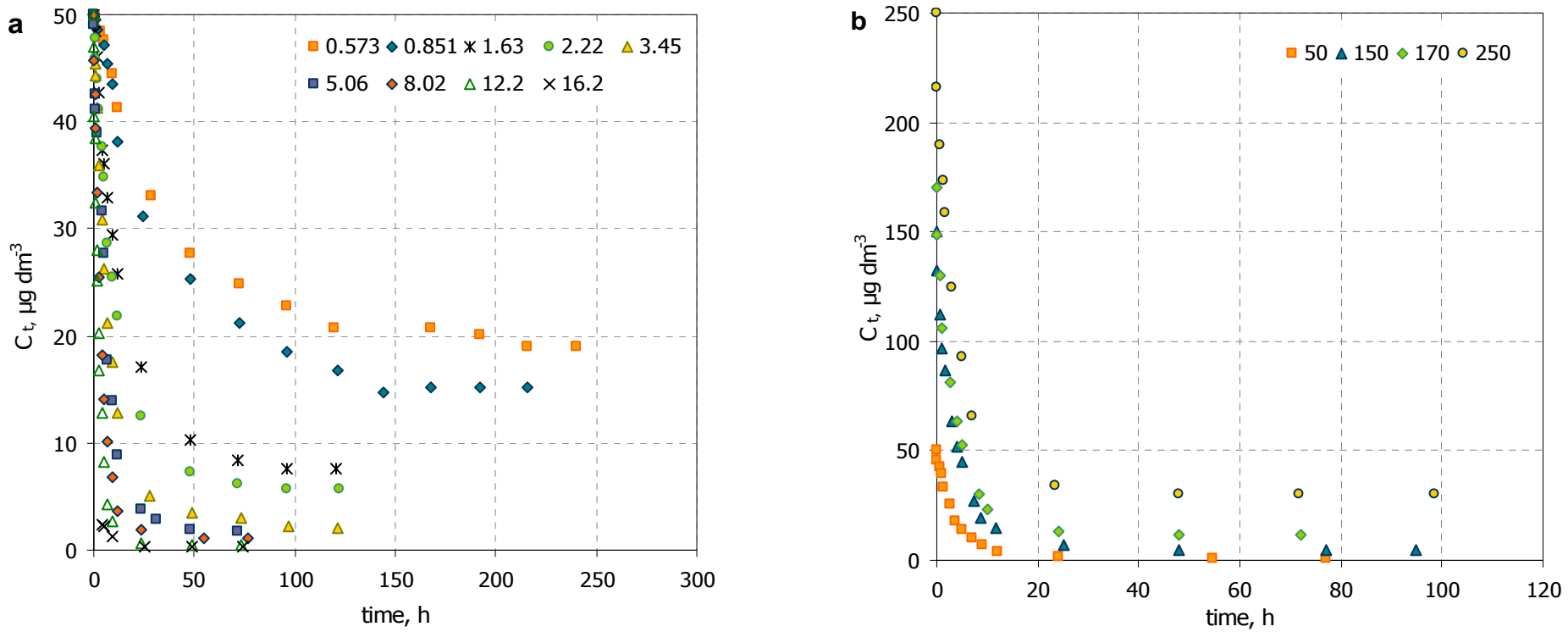

Figure 4.2 – Variation of C_t as function of time, at 294 K. Conditions: **a** – initial Hg^{2+}concentration of 50 µg·dm^{-3} and different ETS-4 masses; **b** – 8 mg of ETS-4 and different initial Hg^{2+} concentrations.

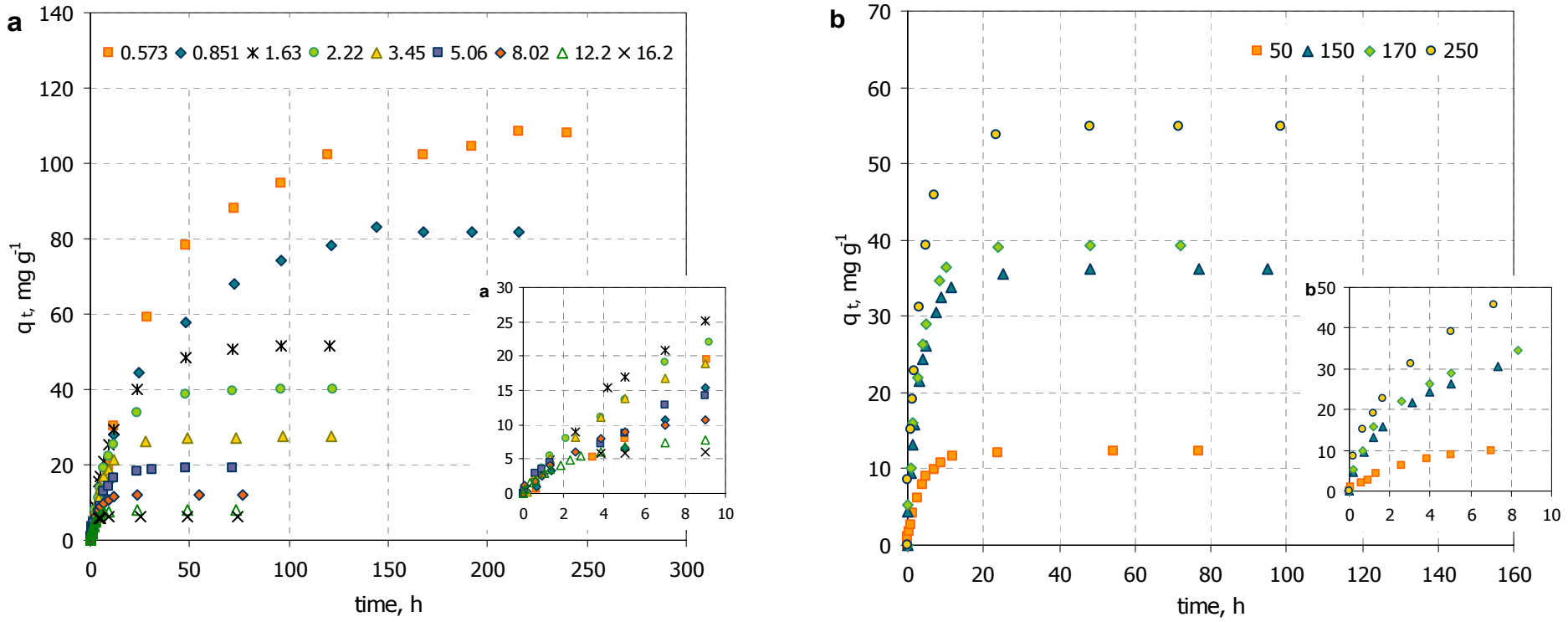

Figure 4.3 – Variation of q_t as function of time, at 294 K. Conditions: **a** – initial Hg^{2+}concentration of 50 μg·dm^{-3} and different ETS-4 masses; **b** – 8 mg of ETS-4 and different initial Hg^{2+} concentrations.

Table 4.3 – Experimental Hg^{2+} uptake, q_e, C_e and contact time, for each ETS-4 mass studied.

	Experimental parameters			
Mass (mg ± 0.001* mg)	Hg^{2+} uptake (%)	q_e ($mg \cdot g^{-1}$)	C_e ($\mu g \cdot dm^{-3}$)	Time (h ± 0.02* h)
0.573	61.9 ± 0.3	108.09 ± 0.56	19.03 ± 0.09	240.00
0.851	69.7 ± 0.5	81.90 ± 0.60	15.15 ± 0.22	216.08
1.639	84.7 ± 0.5	51.68 ± 0.27	7.65 ± 0.18	120.12
2.223	88.7 ± 0.6	39.89 ± 0.24	5.66 ± 0.24	121.80
3.450	95.8 ± 0.4	27.77 ± 0.10	2.09 ± 0.13	121.12
5.055	96.4 ± 0.4	19.07 ± 0.06	1.81 ±0.09	72.00
8.024	97.8 ± 0.3	12.19 ± 0.03	1.10 ± 0.02	77.00
12.201	99.0 ± 0.3	8.11 ± 0.02	0.50 ± 0.00	73.00
16.233	99.5 ± 0.3	6.13 ± 0.01	0.27 ± 0.00	102.00

* tolerance; value ± standard deviation

As shown in Figure 4.4, a remarkable increase in the equilibrium adsorbed concentration is observed when the ETS-4 mass decreases. At equilibrium, q_e values range from 6.13 (for 16.2 mg of ETS-4) to 108 $mg \cdot g^{-1}$ (for 0.573 mg of ETS-4) (Table 4.3).

Furthermore it must be highlighted that in absolute terms, the Hg^{2+} uptake (%) decreases with decreasing ETS-4 mass (Figure 4.4) but it is remarkable that only half microgram of ETS-4 is able to remove more than 60% of the Hg^{2+} present in solution. This is because for a certain initial Hg^{2+} concentration, increasing ETS-4 mass provides greater surface area and increases the number of available sorption sites (Rengaraj et al., 2001). Anyway, the increase of q_e with the increase of ETS-4 mass will only occur as long as the maximum ETS-4 capacity is not fulfilled.

Other reports on the effect of the adsorbent concentration on heavy metals removal have also concluded that increasing the adsorbent concentration results in an increase in the removal percentage of metal ion. Some examples are the work of Kocaoba (2007), on

Pb^{2+} and Cd^{2+} removal by Amberlite IR 120 resin and dolomite, the work of Tüzün et al. (2005) on biosorption of Hg^{2+}, Cd^{2+} and Pb^{2+} ions onto microalgae *Chlamydomonas reinhardtii* and the work of Dakiky et al. (2002) on Cr^{6+} removal using low-cost adsorbents (*e.g.* wool, olive cake, sawdust, pine needles, cactus leaves).

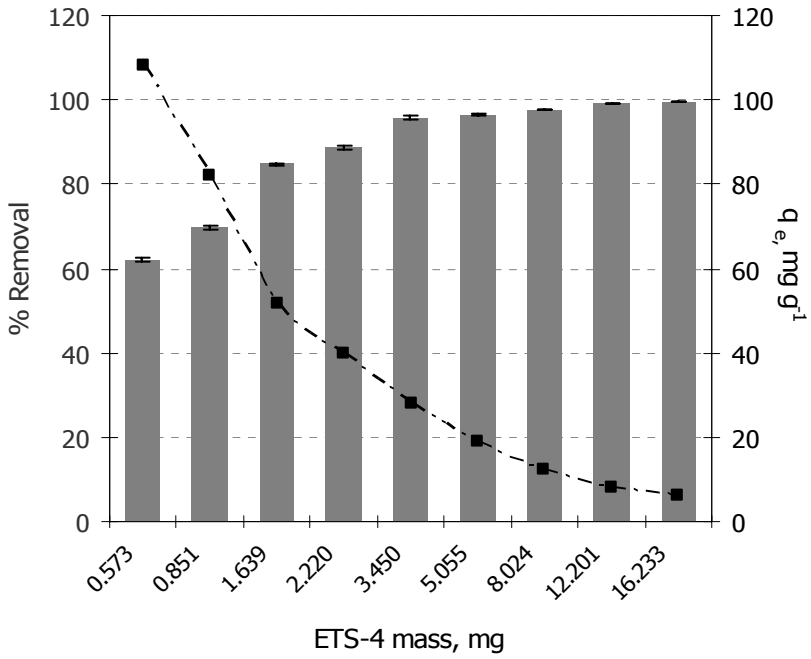

Figure 4.4 – Effect of ETS-4 mass on Hg^{2+}removal (columns) and on adsorbed concentration (line).

The kinetics of Hg^{2+} removal by different masses of ETS-4 was studied. To assess the effect of the mass of ETS-4 used on the sorption kinetic rates, the Hg^{2+} removal with time was described by the pseudo-first and pseudo-second order kinetic models. The rate constants (k_1 and k_2) and the q_e values in equations (1.10) and (1.15) are presented in Table 4.4 for the different masses of ETS-4 employed and were obtained using GraphPad Prism 5 program using the least squares as fitting method and the Marquardt and Levenberg algorithm for minimizing the function.

The experimental kinetic data are shown in Figure 4.5 together with the modelled curves obtained from pseudo-first- and pseudo-second-order equations. As shown in Table 4.4, the regression coefficients for both kinetic models are good (>0.95).

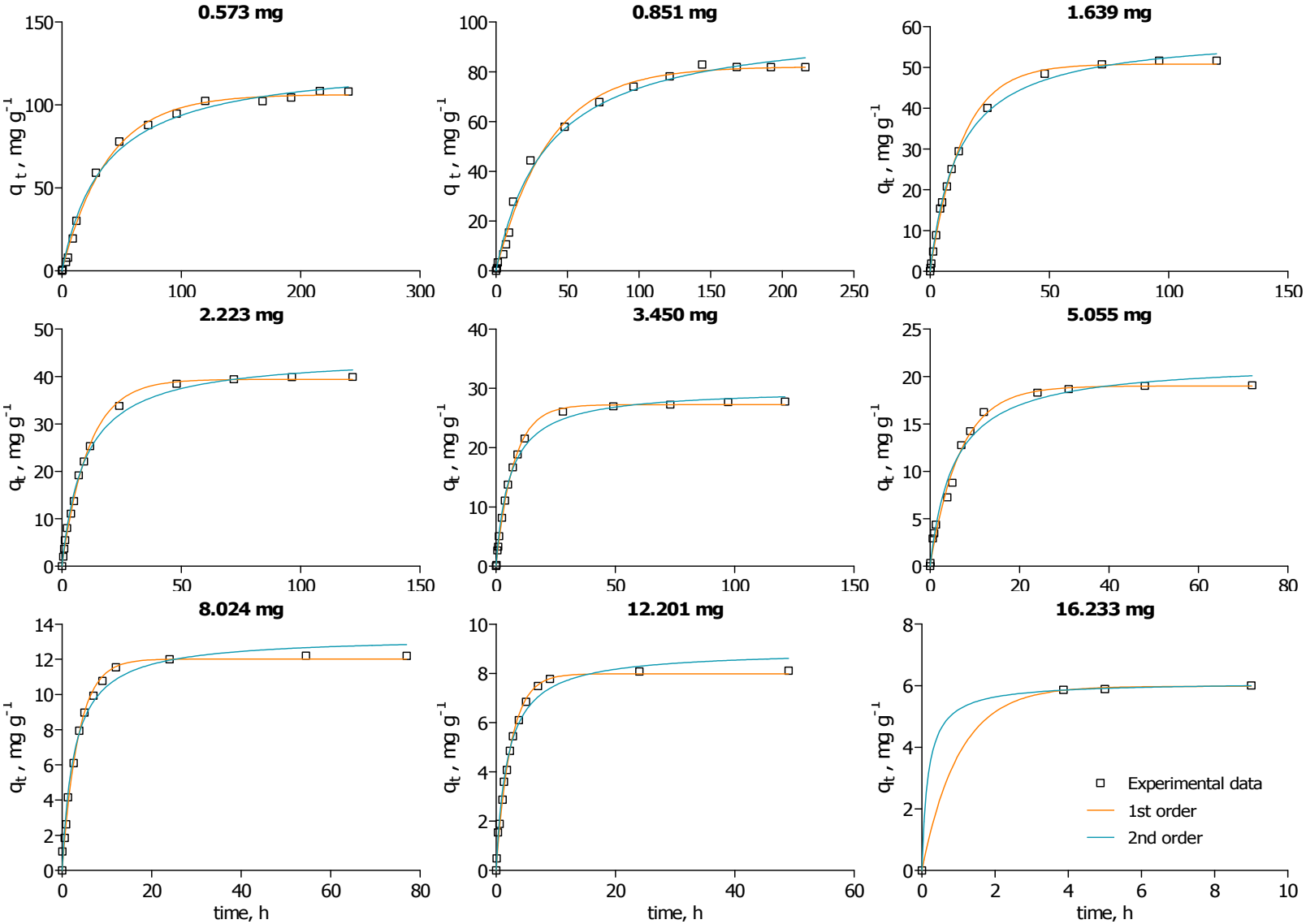

Figure 4.5 – Experimental and modelled kinetic results using pseudo-first- and pseudo-second-order equations.

Table 4.4 – Kinetic sorption rate constants k_1 (pseudo first-order Lagergren) and k_2 (pseudo second-order), experimental and calculated q_e, and the corresponding correlation coefficients (R^2) of the fittings, for different masses of ETS-4.

		First-order kinetics			**Second-order kinetics**		
Mass (mg)	q_e (mg·g^{-1})	k_1 (h^{-1})	R^2	q_e - *fitted* (mg·g^{-1})	k_2 (g·mg^{-1}·h^{-1})	R^2	q_e - *fitted* (mg·g^{-1})
0.573	108.09	0.026	0.996	106.30	57556	0.992	127.60
0.851	81.90	0.027	0.994	82.07	27741	0.992	99.84
1.63	51.68	0.074	0.988	50.84	16731	0.998	58.74
2.22	39.89	0.089	0.998	39.41	9263	0.996	44.65
3.45	27.77	0.136	0.999	27.24	4617	0.995	29.96
5.06	19.07	0.149	0.990	18.99	1858	0.985	21.59
8.02	12.19	0.276	0.996	12.01	869	0.998	13.29
12.2	8.115	0.410	0.995	7.983	378	0.989	8.938
16.2	6.127	0.985	1.000	5.982	1333	1.000	6.116

For the experimental conditions used in this work, a good agreement between the experimental data and the curves derived from both first and second kinetic models was obtained, indicating that they are able to predict the kinetic behaviour of Hg^{2+} removal. Furthermore, by comparing the experimental and fitted q_e values, it is perceptible that the second-order kinetic model slightly overestimates the equilibrium value while the first-order kinetic model slightly underestimates it.

4.6. Initial Hg^{2+}concentration

The initial Hg^{2+} concentration is also an important parameter to attain quantitative Hg^{2+} removal because influences the metal uptake mechanism (Sharaf et al., 2007) since at low concentrations the metal is sorbed by specific sites, while increasing metal concentrations the specific sites saturate and the exchange sites are filled. Furthermore, the initial Hg^{2+} concentration may also influence the contact time necessary to reach equilibrium and the sorption capacity (Reddad et al., 2002).

For all initial Hg^{2+} concentrations employed the Hg^{2+} concentration in the liquid phase decreases with time (Figure 4.2-b), but the variation of initial metal concentration does not influence the contact time necessary to reach equilibrium as reported by Reddad et al. (2002) on their work on Pb^{2+} and Cu^{2+} adsorption onto sugar beet pulp. However, only for the lowest concentration it was possible to obtain clean water of drinking quality. It is obvious that by increasing the ETS-4 mass it would be possible to achieve a better water quality for the highest concentrations, but although the residual Hg^{2+} concentration for the highest concentrations is higher than 2 $\mu g \cdot dm^{-3}$ (Table 4.5) it is significantly lower than the maximum value admissible by the Portuguese legislation for discharges of effluents by industries into water bodies (50 $\mu g \cdot dm^{-3}$).

In the range of concentrations studied, a noticeable increase on the Hg^{2+} sorption on ETS-4 occurred with the increase of the initial Hg^{2+} concentration (Figure 4.6). The equilibrium q_e values ranged from 12.2 to 54.8 $mg \cdot g^{-1}$ (Table 4.5), corresponding to initial Hg^{2+} concentrations of 50 and 250 $\mu g \cdot dm^{-3}$, respectively. Green-Ruiz (2006) reported the same pattern on mercury (II) removal by *Bacillus* sp. and suggested that a higher ionic strength of Hg^{2+} provokes more mercury (II) sorption. In contrast, the Hg^{2+} uptake (%) increases with decreasing initial Hg^{2+} concentration (Figure 4.6), though the uptake percentage is higher than 88% for all initial concentrations studied. This is explicable by the fact that more active sites are available for relatively fewer number of heavy metals ions (Mishra et al., 2007).

Table 4.5 – Experimental Hg^{2+} uptake, q_e, C_e and contact time, for each initial Hg^{2+} concentration studied.

	Experimental parameters			
Hg^{2+} concentration ($\mu g \cdot dm^{-3}$)	Hg^{2+} uptake (%)	q_e ($mg \cdot g^{-1}$)	C_e ($\mu g \cdot dm^{-3}$)	Time (h ± 0.02* h)
50	97.8 ± 0.3	12.19 ± 0.03	1.10 ± 0.02	77.00
150	96.9 ± 0.2	36.13 ± 0.06	4.69 ± 0.02	95.00
170	93.3 ± 0.3	39.38 ± 0.09	11.33 ± 0.08	72.00
250	88.0 ± 0.6	54.77 ± 0.37	29.99 ± 1.42	98.57

* tolerance; value ± standard deviation

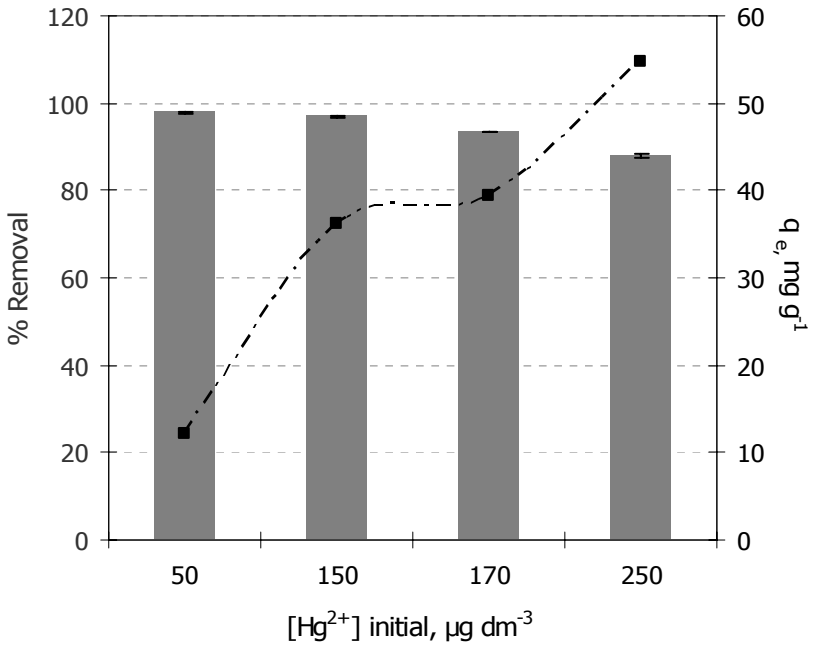

Figure 4.6 – Effect of initial Hg^{2+} concentration on Hg^{2+} removal (columns) and on adsorbed concentration (line).

Some authors (Tüzün et al., 2005; Yavuz et al., 2006 and Sharaf et al., 2007) have reported for other metals and other adsorbents that adsorbed concentration starts to increase when increasing the initial metal concentration until it reaches a plateau value, which is an indication of adsorbent saturation. In this case, the adsorbed concentration has not reached yet a plateau value. Indeed it seems that it is still growing with increasing the initial Hg^{2+} concentration, although the removal percentage decreased with increasing initial Hg^{2+} concentration (Figure 4.6). These results suggest that an increase in solution

pH due to higher amounts of standard solution used to prepare the desired Hg^{2+} solutions led to a competition between H^+ and Hg^{2+} ions for the ion exchange with the Na^+ present in the ETS-4 framework.

Analogously to the previous section, both pseudo first- and pseudo second-order kinetic models were fitted to the experimental data in order to assess the differences in the kinetic rates. The experimental quantity of Hg^{2+} removed per gram of ETS-4, together with the modelled curves obtained from pseudo-first- and pseudo-second-order equations are shown in Figure 4.7. The kinetic parameters of both models and the correlation coefficient (R^2) of the fittings, are present in Table 4.6.

As confirmed by the correlation coefficients of the fittings, both kinetic models well describe the sorption of Hg^{2+} ions (Figure 4.7).

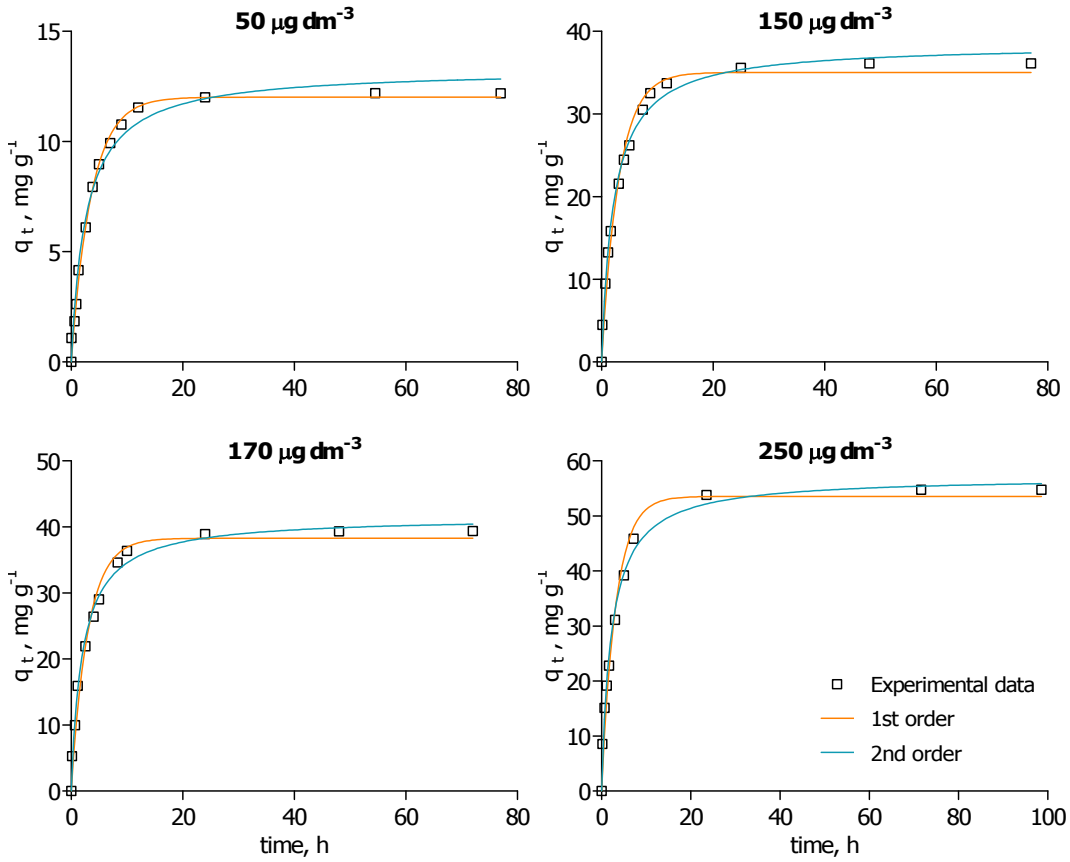

Figure 4.7 – Experimental and modelled kinetic results using pseudo-first- and pseudo-second-order equations.

Table 4.6 – Kinetic sorption rate constants, k_1 (pseudo first-order Lagergren) and k_2 (pseudo second-order), experimental and calculated q_e, and the corresponding correlation coefficients (R^2)of the fittings, for different initial Hg^{2+} concentrations.

		First-order kinetics			**Second-order kinetics**		
Hg^{2+} concentration ($\mu g \cdot dm^{-3}$)	q_e ($mg \cdot g^{-1}$)	k_1 (h^{-1})	R^2	q_e - *fitted* ($mg \cdot g^{-1}$)	k_2 ($g \cdot mg^{-1} \cdot h^{-1}$)	R^2	q_e - *fitted* ($mg \cdot g^{-1}$)
50	12.19	0.276	0.996	12.01	870	0.988	13.29
150	36.13	0.323	0.986	35.02	26055	0.994	38.44
170	39.38	0.332	0.982	38.30	35375	0.993	41.57
250	54.77	0.312	0.978	53.55	83619	0.990	57.14

4.7. pH

The pH of the solution is largely recognised as a crucial parameter on the removal of heavy metals (*e.g.* Mohan et al., 2001; Yardim et al., 2003; Álvarez-Ayuso et al., 2003; Walcarius et al., 2004; Lv et al., 2005; Machida et al., 2005; Zhang et al., 2005; Yavuz et al., 2006; Kocaoba, 2007; Romera et al., 2007). It determines the surface charge of the adsorbent and the degree of ionisation and speciation of the species to be removed (Reddad et al., 2002; Sharaf et al., 2007).

Depending on the pH and chloride concentrations ranges the most important species existing in natural waters are Hg^{2+}, $HgCl_2$ at low pH (<4), $Hg(OH)^+$, Hg(OH)Cl at moderate pH (4-7), and hydroxo species $Hg(OH)_2$, $Hg(OH)_3^-$ at high pH (>7) (Walcarius et al., 2004; Mishra et al., 2007). The existence of such species and their uptake by the adsorbents are expected to influence the overall removal process.

In dilute solutions, heavy metals are mainly present in the form of mononuclear hydrolysis products, but their species distributions are related to many factors such as pH, ionic strength, anions and metal ion concentration (Lv et al., 2005). The Hg^{2+} solutions used in this study were prepared from $Hg(NO_3)_2$ standard solution and according to Lv et al. (2005) the speciation diagrams of metal ion species in the presence of NO_3^- and OH^- are different. The Hg^{2+} concentrations used in this study are considerably low (50 $\mu g \cdot dm^{-3}$ which is equivalent to 2.49×10^{-6} M) and consequently Hg(II) species like $Hg(NO_3)^+$ or $Hg(NO_3)_2$ are irrelevant.

Figure 4.8 depicts the speciation diagram of Hg(II) species in aqueous solution at 298.15 K. Hg^{2+} ions are soft Lewis acids and through the K_a values (Aylett, 1973) of the Hg^{2+} hydrolysis:

$$Hg^{2+}_{(aq.)} + 2\,H_2O_{(aq.)} \rightleftharpoons Hg(OH)^+_{(aq.)} + H_3O^+_{(aq.)} \qquad K_{a1} = 10^{-3.5}$$

$$Hg(OH)^+_{(aq.)} + 2\,H_2O_{(aq.)} \rightleftharpoons Hg(OH)_{2\,(aq.)} + H_3O^+_{(aq.)} \qquad K_{a2} = 10^{-2.7}$$

it was possible to calculate the ionisation fractions (α_0; α_1 and α_2) (Cavaleiro, 1997) which were used to built the speciation diagram for the most important Hg(II) species, Hg^{2+}; $Hg(OH)^+$ and $Hg(OH)_2$.

$$\alpha_0 = \frac{\left[Hg^{2+}\right]}{\left[Hg^{2+}\right]+\left[Hg(OH)^+\right]+\left[Hg(OH)_2\right]} = \frac{\left[H_3O^+\right]^2}{\left[H_3O^+\right]^2 + K_{a1}\left[H_3O^+\right] + K_{a1}K_{a2}}$$

$$\alpha_1 = \frac{[Hg(OH)^+]}{[Hg^{2+}]+[Hg(OH)^+]+[Hg(OH)_2]} = \frac{K_{a1}[H_3O^+]}{[H_3O^+]^2 + K_{a1}[H_3O^+]+K_{a1}K_{a2}}$$

$$\alpha_2 = \frac{[Hg(OH)_2]}{[Hg^{2+}]+[Hg(OH)^+]+[Hg(OH)_2]} = \frac{K_{a1}K_{a2}}{[H_3O^+]^2 + K_{a1}[H_3O^+]+K_{a1}K_{a2}}$$

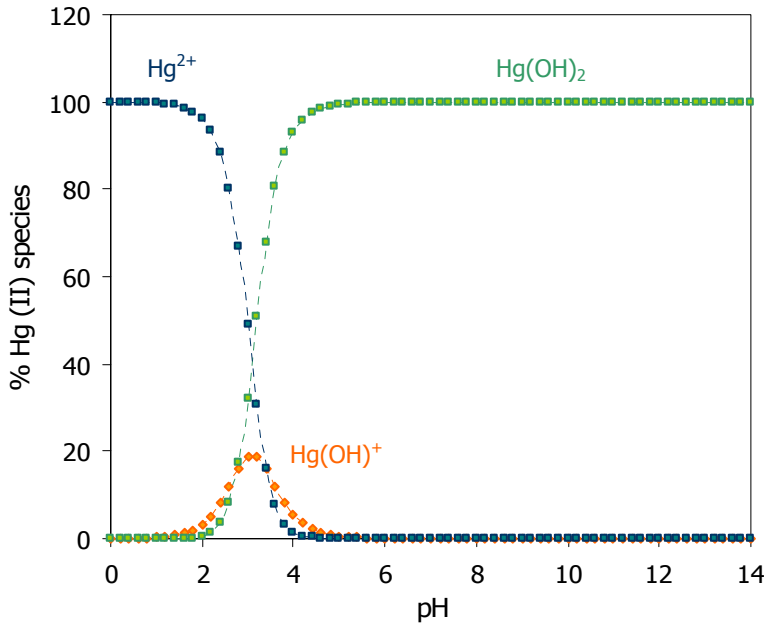

Figure 4.8 – Speciation diagram for Hg(II) in aqueous solution.

The effect of pH on Hg^{2+} removal by ETS-4 was studied in the pH range of 2 to 10 (Table 4.7). Figure 4.9 depicts the Hg^{2+} concentrations in the liquid phase (C_t) and sorbed on ETS-4 (q_t) as a function of time, in the pH range studied. For the pH values 6, 7, 8 and 9, only the solutions that were adjusted with NaOH 0.1 M are represented.

For all pH values studied, there is a decrease of the Hg^{2+} concentration in the liquid phase and consequently an increase of the amount of Hg^{2+} sorbed on ETS-4 with time, but the equilibrium times remain unchanged (Figure 4.9). However, the removal extent depends strongly on the solution pH. Both q_e and removal percentage, increase sharply with increasing pH until they reach a maximum value pH *ca*. 4-6.

Table 4.7 – Experimental Hg^{2+} uptake, q_e, C_e and contact time, for each pH studied.

		Experimental parameters			
pH (± 0.1)		Hg^{2+} uptake (%)	q_e ($mg \cdot g^{-1}$)	C_e ($\mu g \cdot dm^{-3}$)	Time (h ± 0.02* h)
2.0 (n=2)	HNO_3	20.3 ± 4.0	2.52 ± 0.52	39.87 ± 2.01	50.52
2.9 (n=3)	HNO_3	66.4 ± 5.6	8.19 ± 0.64	16.81 ± 2.80	48.13
3.8 (n=3)	HNO_3	95.6 ± 0.9	11.73 ± 0.18	2.22 ± 0.43	48.14
4.9 (n=3)	None	97.2 ± 0.4	12.00 ± 0.06	1.38 ± 0.19	48.00
6.2 (n=2)	NaOH	97.2 ± 0.4	12.03 ± 0.08	1.39 ± 0.22	48.00
	KOH	97.7 ± 0.5	12.09 ± 0.09	1.16 ± 0.26	48.02
6.9 (n=2)	NaOH	80.9 ± 2.7	9.98 ± 0.32	9.53 ± 1.34	48.01
	KOH	88.8 ± 0.9	10.94 ± 0.10	5.61 ± 0.45	48.00
8.0 (n=2)	NaOH	74.2 ± 0.3	9.13 ± 0.04	12.91 ± 0.17	48.12
	KOH	86.3 ± 0.0	10.73 ± 0.04	6.83 ± 0.01	48.02
9.3 (n=2)	NaOH	59.5 ± 1.5	7.34 ± 0.19	20.24 ± 0.73	48.06
	KOH	78.8 ± 1.1	9.72 ± 0.17	10.58 ± 0.56	48.08
10.0 (n=2)	NaOH	51.0 ± 2.1	6.34 ± 0.27	24.48 ± 1.03	48.01
	KOH	68.5 ± 1.7	8.50 ± 0.19	15.77 ± 0.83	48.03

* tolerance; mean ± standard deviation

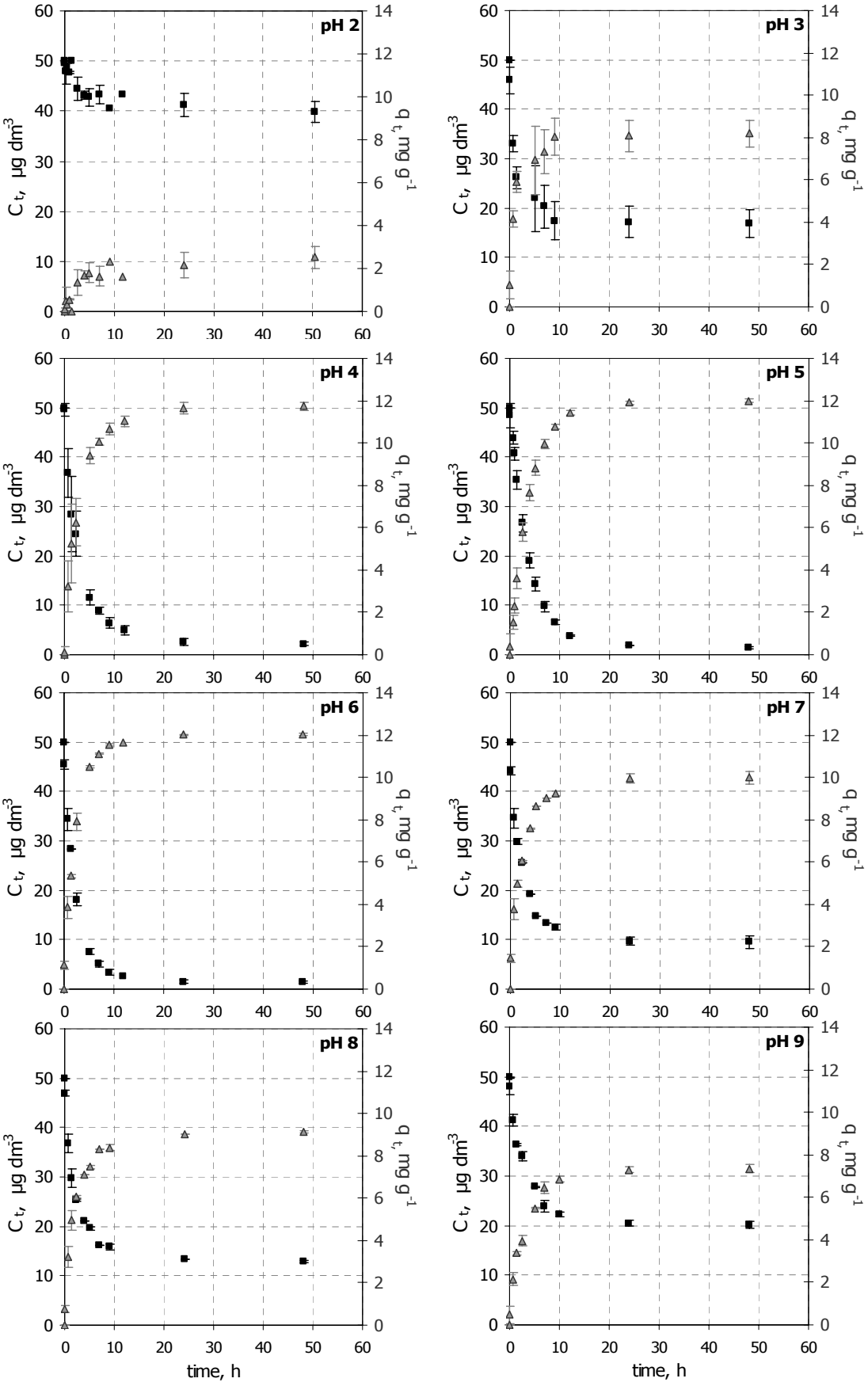

Figure 4.9 –Hg^{2+} concentrations in the liquid phase (C_t) and sorbed on ETS-4 (q_t) as a function of time, for different pH values. Black symbols – Hg^{2+} in solution; Grey symbols – Hg^{2+} sorbed.

The adsorbed concentration at equilibrium and the Hg^{2+} removal percentage increase, respectively, from 2.52 to 12.0 $mg \cdot g^{-1}$ and from 20.3 to 97.2% with an increase in solution pH from 2 to 6. Moreover, the sorption capacity and the Hg^{2+} removal percentage begin to decrease with increasing solution pH for pH values higher than 6, and reach almost half of the maximum values at pH 10 (6.34 $mg \cdot g^{-1}$ and 51.0%, respectively).

It was expected that the Hg^{2+} removal efficiency of ETS-4 decreases at low pH values due to competition between H^+ protons and free Hg^{2+} ions for the exchange with cations (Álvarez-Ayuso et al., 2003; Green-Ruiz et al., 2006; Kocaoba, 2007), namely sodium, initially present in ETS-4. However, the worst results on Hg^{2+} removal by ETS-4, which were observed for the lowest pH value studied (2.0), may also be a consequence of the partial collapse of the material's structure. Increasing pH leads to a decrease in H^+ concentration and consequently the exchange of Hg^{2+} with the cations in the ETS-4 structure is favoured. However, at higher pH values non-charged hydroxo species (*e.g.* $Hg(OH)_2$) form and are not removed by cation exchange, thus decreasing the removal efficiency.

The main mechanism of Hg^{2+} uptake onto ETS-4 is ion exchange at an optimal pH range from 4 - 6. However, the speciation diagram (Figure 4.8) indicates that the dominant Hg(II) species at pH>4 is $Hg(OH)_2$. Nevertheless, Machida et al., 2005 pointed out that the mononuclear metal ions (M^{2+}) are converted into other species more easily at higher M(II) rather than lower concentrations. Other authors (Yavuz et al., 2006; Green-Ruiz, 2006) refered that precipitation of mercury ions becomes significant at pH higher than 7, but it also depends on the concentration of Hg^{2+} in the medium. Moreover, Zhang et al. (2005) presented the solubility of Hg(II) *vs.* solution pH in the absence of adsorbent and asserted that for initial Hg(II) concentration <120 $mg \cdot dm^{-3}$ $Hg(OH)_2$ dissolves in the solution and accordingly, it is impossible to precipitate mercury only by adjusting the solution pH when the Hg(II) concentration is less than this value. Thus, in my study, where the Hg(II) concentration used was only 50 $\mu g \cdot dm^{-3}$ (<120 $mg \cdot dm^{-3}$), $Hg(OH)_2$ probably transforms into other species and the cation exchange process may proceed.

In order to investigate if the decrease of removal efficiency at higher pH is also determined by the type of solution used to adjust the solution pH, another set of experiments were performed using 0.1 M KOH, instead of 0.1 M NaOH. The results obtained are shown on Figure 4.10 and allow the following conclusions. The Hg^{2+} removal is influenced by the solution pH, however the extent to which it occurs depends on the type of solution used to adjust the solution pH. For values equal or higher than 7 the Hg^{2+} removal percentage is dramatically affected by the type of base used and it becomes even more significant with increasing pH since that implies the addition of higher quantities of base. These results confirm that the removal mechanism is based on the ion exchange

between the metal cations (Hg^{2+} and perhaps $Hg(OH)^{+}$) and the cations (Na^{+}) present in ETS-4. The increase of Na^{+} concentration in the liquid phase does not favour the Hg^{2+} ion exchange because liquid-solid phase Na^{+} concentration gradient is reduced.

In the case of solution pH adjustment with 0.1 M KOH, a decrease in Hg^{2+} removal percentage is also observed but to a lesser extent than with 0.1 M NaOH. The decrease of Hg^{2+} removal percentage with increasing solution pH may be related with Hg (II) speciation or with competition between Hg^{2+} and K^{+} ions or a combination of both. Further studies should be done to confirm these hypotheses.

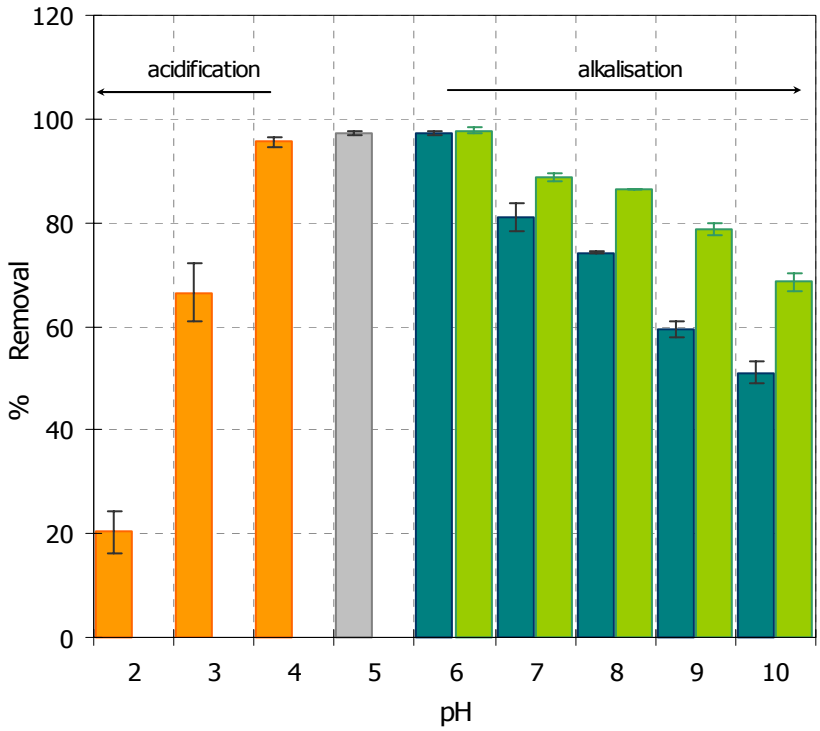

Figure 4.10 – Effect of pH on Hg^{2+} removal. Orange columns – pH adjusted with HNO_3 conc.; Grey column – without pH adjustment; Blue columns – pH adjusted with NaOH 0.1 M; Green columns – pH adjusted with KOH 0.1 M.

4.8. Temperature

In certain cases temperature is an important parameter in heavy metal removal. The effect of temperature on the Hg^{2+} removal by ETS-4 was investigated at 277.15 (4ºC), 294.15 (21ºC) and 313.15 K (40ºC) (Table 4.8).

Table 4.8 – Experimental Hg^{2+} uptake, q_e, C_e and contact time, for each temperature studied.

	Experimental parameters			
Temperature (K ±1 K)	Hg^{2+} uptake (%)	q_e ($mg \cdot g^{-1}$)	C_e ($\mu g \cdot dm^{-3}$)	Time (h ± 0.02* h)
277.15 (n=3)	97.9 ± 0.8	12.13 ± 0.09	1.07 ± 0.38	48.00
294.15 (n=3)	97.2 ± 0.4	12.00 ± 0.06	1.38 ± 0.19	48.00
313.15 (n=3)	91.2 ± 1.2	11.29 ± 0.16	4.42 ± 0.62	48.22

* tolerance; value ± standard deviation

An increase in q_e and Hg^{2+} removal is observed by decreasing the temperature of the system (Figure 4.11). The results also show that the decrease of q_e and Hg^{2+} removal is more pronounced at the highest temperature. Rising the temperature leads to a decrease of the adsorbed concentration at equilibrium from 12.13 to 11.29 $mg \cdot g^{-1}$.

Under the experimental conditions used, temperature changes do not affect the time necessary to reach equilibrium and, although the Hg^{2+} concentration in the liquid phase decreases with time for all temperatures (Figure 4.12), clean water of drinking quality was not obtained for the highest temperature (313.15 K).

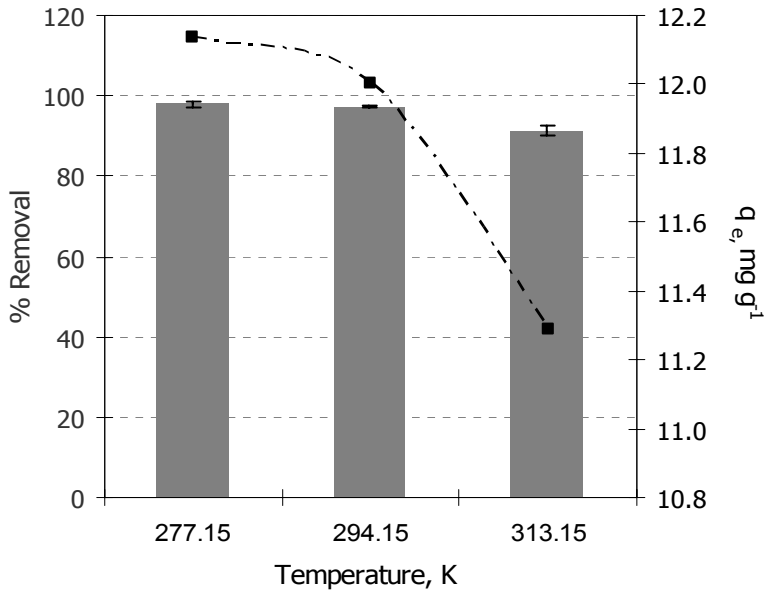

Figure 4.11 – Effect of temperature on Hg^{2+} removal (columns) and on adsorbed cocentration (line).

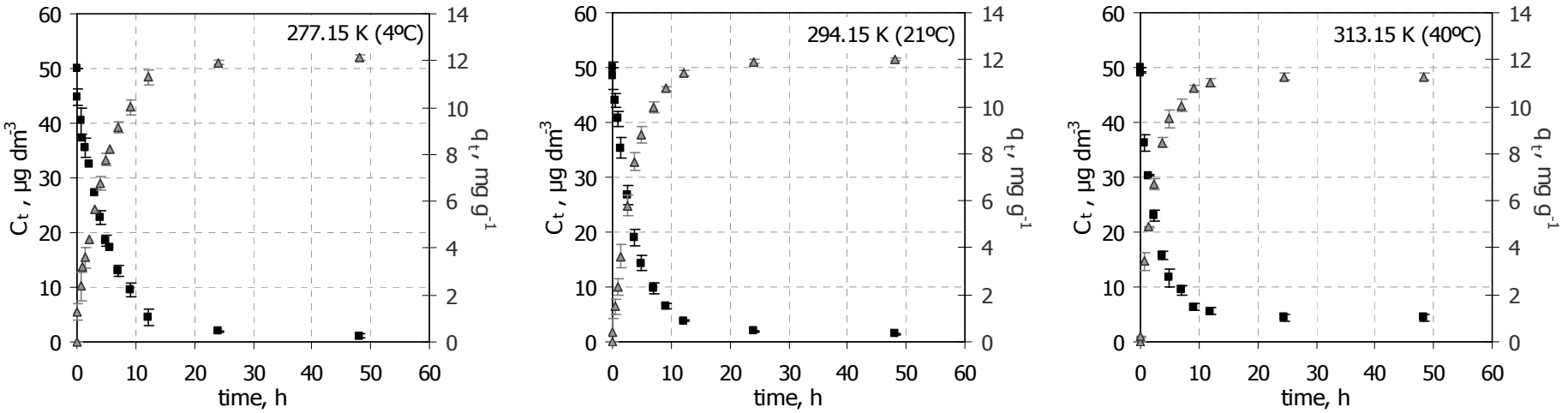

Figure 4.12 – Hg^{2+} concentrations in the liquid phase (C_t) and sorbed on ETS-4 (q_t) as a function of time, for different temperatures. Black symbols – Hg^{2+} in solution; Grey symbols – Hg^{2+} sorbed.

Thermodynamic parameters, Gibbs free energy (ΔG°), enthalpy (ΔH°) and entropy (ΔS°) change for the system Hg^{2+}/ETS-4 were calculated with the following equations (Pavel et al., 2003; Choi et al., 2006b; Yavuz et al., 2006; Kocaoba, 2007; Sharaf et al., 2007):

$$\Delta G^\circ = -\Re T \ln K_d \quad (4.1)$$

$$\Delta G^\circ = \Delta H^\circ - T\Delta S^\circ \quad (4.2)$$

combining equations 4.1 and 4.2:

$$\ln K_d = \left(\frac{\Delta S^\circ}{\Re}\right) - \left(\frac{\Delta H^\circ}{\Re T}\right) \quad (4.3)$$

where $\Re$ is the gas constant (8.314 $J \cdot mol^{-1} \cdot K^{-1}$), T is the temperature (K) and K_d is the distribution coefficient ($dm^3 \cdot g^{-1}$):

$$K_d = \frac{q_e}{C_e} \quad (4.4)$$

ΔH° ($kJ \cdot mol^{-1}$) and ΔS° ($kJ \cdot mol^{-1} \cdot K^{-1}$) may be obtained from the slope and intercept of $\ln K_d$ versus $1/T$ plot, while the free energy ΔG° ($kJ \cdot mol^{-1}$) are, subsequently, calculated with equation 4.2. ΔH°, ΔS° and ΔG° are collected in Table 4.9.

Table 4.9 – Thermodynamic parameters for Hg^{2+} uptake on ETS-4

ΔH°	ΔS°	ΔG° ($kJ \cdot mol^{-1}$)		
($kJ \cdot mol^{-1}$)	($kJ \cdot mol^{-1} \cdot K^{-1}$)	277.15 K	294.15 K	313.15 K
-29.94	-0.029	-21.89	-21.40	-20.85

The negative values of ΔG° indicate the spontaneous nature of the Hg^{2+} sorption on ETS-4 for all temperatures studied and the increase of their absolute values with decreasing temperature shows that lower temperatures favour Hg^{2+} removal. The negative values of enthalpy changes (ΔH°), show that Hg^{2+} sorption on ETS-4 is exothermic. A negative ΔS° suggests that Hg^{2+} is stable on the "adsorption" sites of ETS-4 resulting in less migration along the framework (Choi et al., 2006b).

4.9. Sorption equilibrium

The distribution of the adsorbate between between the liquid and the solid phase at equilibrium is given by the corresponding adsorption isotherm , which represents the ratio

between the quantity adsorbed and remaining in solution at a given temperature, at equilibrium (Igwe and Abia, 2007). The Langmuir (equation 1.32) and Freundlich (equation 1.35) isotherms were the models chosen to fit the experimental data. The experimental results are shown in Figure 4.13, together with fittings of the referred models.

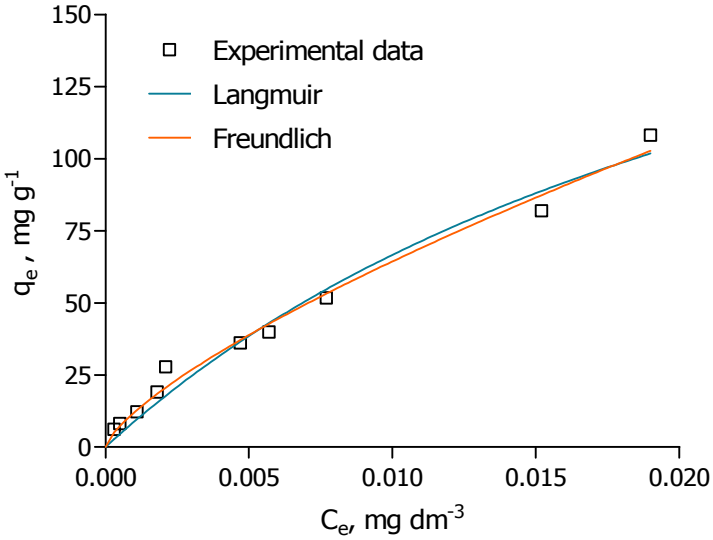

Figure 4.13 – Experimental equilibrium data and modelled results using Langmuir and Freundlich equations at 294 ± 1K

The isotherms are positive and concave to the concentration axis. In the range of experimental conditions used, there is a good agreement between experimental data and Freundlich isotherm (R^2=0.988). The equilibrium data is also well describe by the Langmuir isotherm (R^2=0.975). Similar results were obtained by Green-Ruiz (2006) on mercury (II) removal by *Bacillus* sp. The Freundlich and Langmuir parameters and the corresponding correlation coefficients are presented in Table 4.10 and were obtained by nonlinear regression analysis using GraphPad Prism 5 program, using the least-squares as fitting method and the Marquardt and Levenberg algorithm for minimizing the function.

Table 4.10 – Freundlich and Langmuir isotherm constants for Hg^{2+} sorption on ETS-4 at 294K

Model	q_{max}	K_L	n	K_f	R^2
	(mg·g^{-1})	(dm^3·mg^{-1})		(mg$^{1-1/n}$·(dm^3)$^{1/n}$·g^{-1})	
Langmuir	246.3	37.08	---	---	0.975
Freundlich	---	---	1.37	1848	0.988

Both K_f and n are empirical constants, related to adsorption capacity of the adsorbent and adsorption intensity, respectively (Zhang et al., 2005). A higher K_f value indicates higher capacity for adsorption and $1/n$ shows the variation of adsorption with concentration. $1/n$ is also a measure of the surface heterogeneity ranging between 0 and 1, becoming more heterogeneous as its value gets closer to zero (Zhang et al., 2005; Yavuz, et al., 2006). The magnitudes of K_f and n indicate easy separation of Hg^{2+} from liquid phase and favourable sorption ($1 < n < 10$).

According to the Langmuir isotherm, the Langmuir constant K_L is 37.08 $dm^3 \cdot mg^{-1}$ and the monolayer capacity q_{max} of ETS-4 is 246.3 $mg \cdot g^{-1}$. The maximum ETS-4 sorption capacity estimated by the Langmuir isotherm is higher than that of other adsorbents in literature, namely a few types of activated carbon (Krishnan and Aniudhan, 2002; Yardim et al., 2003) and it is considerable higher than q_{max} values found for materials such as biosorbents (*e.g.* bacteria, wood, alga), and even other zeolitic minerals (Table 4.11). However, the estimated ETS-4 sorption capacity for Hg^{2+} ions is considerably lower than that of commercial ACF-1603-15 activated carbon fibre, with values 290-710 $mg \cdot g^{-1}$ (Nabais et al., 2006).

Table 4.11 – Langmuir isotherm constants for Hg^{2+} sorption on other adsorbents.

Adsorbent	q_{max} ($mg \cdot g^{-1}$)	K_L ($dm^3 \cdot mg^{-1}$)	Temperature (K)	Reference
Rice husk ash	6.72	0.016	303	Feng et al., 2004
Bacillus sp.	7.94	1.120	298	Green-Ruiz, 2006
Zeolitic mineral	10.1	0.238	---	Gebremedhin-Haile et al., 2003
Fly ash	13.4	0.083	---	Banerjee et al., 2004
Activated carbon	25.8	0.450	---	Rao et al., 2009
Eucalyptus bark	33.1	13.9×10^3	---	Ghodbane & Hamdaoui, 2008
Carbon aerogel	34.9	0.483	---	Goel et al., 2005
Activated carbon	43.8	0.239	303	Ranganathan, 2003
Seaweed biomass	84.7	1.044	298	Zeroual et al., 2003
Yeast cells	93.4	0.158	298	Yavuz et al. 2006
Algal biomass	122.4	---	298	Tüzün et al., 2005
Papaya wood	155.6	0.004	303	Basha et al., 2008
Furfural carbon	174.0	---	---	Yardin et al., 2003
Activated carbon	188.7	0.028	303	Krishnan & Aniudhan, 2002

The separation factor R_L (equation 1.34), which points out the nature of sorption was 0.6 indicating that Hg^{2+} has a higher affinity for the solid phase (ETS-4) than for the liquid phase.

4.10. Nernst-Planck based model results

As described in chapter 1, a mathematical model based on the Nernst-Planck approach was developed to describe the ion-exchange process. The Nernst-Planck model results for three different experimental conditions will be presented and compared with the results obtained previously for the second order kinetic model.

However, before proceeding further, I need to point out that q values presented in this section will be expressed as moles of solute per unit of volume of the solid phase ($mol \cdot m^{-3}$), and not mass of solute per unit of mass of the solid phase ($mg \cdot g^{-1}$), as done until now. This transformation is necessary in equations where both q values and C values appear, as in equation 1.26. The reason for this is that C values are always expressed as moles (or mass) per unit of volume, and, thus for the units to be the same in each term of the equation, the units of the q values must also be on a volume basis. To be consistent the q values presented in Table 4.12 for the second-order model are expressed as moles per unit of volume of the solid phase ($mol \cdot m^{-3}$). Moreover, since the ion-exchange may be represented by conventional chemical equilibrium (Helfferich, 1995) between two counter ions (A and B), hereafter two subscripts will be introduced: A - counter ion initially present in the bulk solution (Hg^{2+}) and B - counter ion initially present in the particle (Na^{+}).

In Figure 4.14 and Figure 4.15, the experimental data are plotted together with model results for three different experimental conditions investigated (Table 4.1: 1.369, 2.223 and 3.450 mg of ETS-4). Figure 4.14 displays the normalized Hg^{2+} concentration in the fluid along time, whereas Figure 4.15 shows the evolution of the average particle concentration with time.

The experimental data follows expected trends: (i) Hg^{2+} removal is initially faster, slowing down until equilibrium is attained. Such fact is due to the large mass transport driving forces observed at the beginning, since ETS-4 particles are initially free of Hg^{2+}. (ii) The amount of Hg^{2+} removed increases with increasing mass of ETS-4, because the extensive ion exchange capacity is proportional to solid mass (remember the initial solution

concentration is fixed and equal to 50 μg·dm^{-3}). (iii) Equilibrium is reached faster for higher ETS-4 masses.

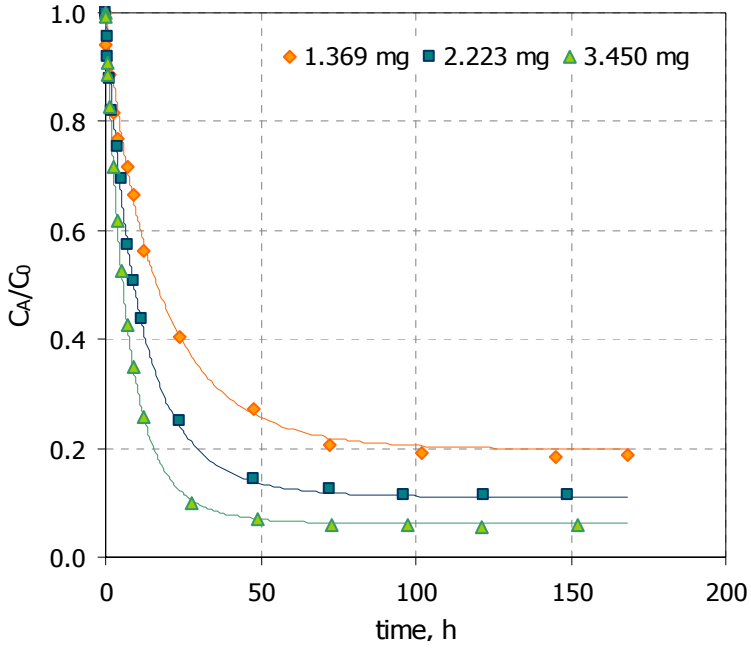

Figure 4.14 – Normalized Hg^{2+} concentration in solution with time: modelling (lines) and experimental data (points).

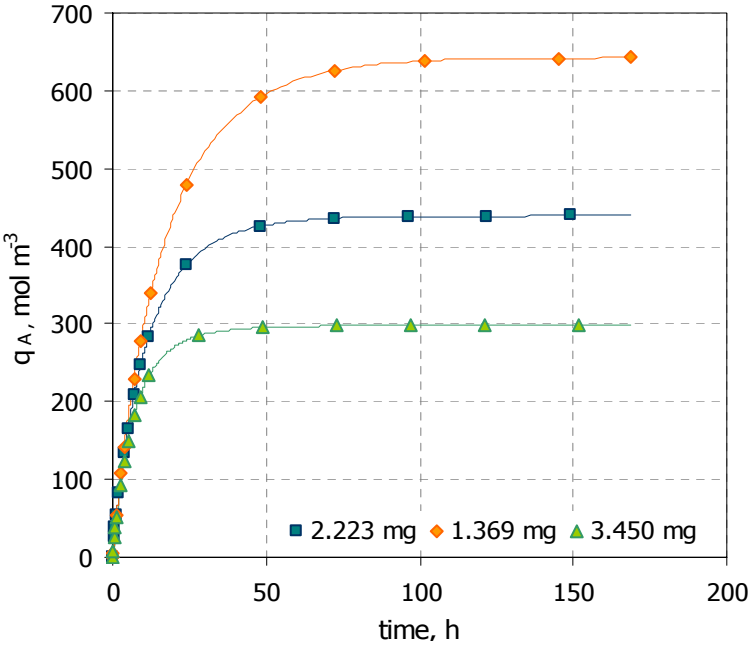

Figure 4.15 – Average Hg^{2+} concentration in the particle with time: modelling (lines) and experimental data (points).

Figure 4.14 and Figure 4.15 show the good representation achieved with the Nernst-Planck (NP) based model. Fine agreement is observed in the steep descendent part of each curve and its transition to the horizontal branch (i.e. its elbows), where kinetic is frequently

difficult to fit or simulate. The average absolute deviation found is very small, $AAD = 2.69\%$ (47 data points), which is within experimental accuracy (5-8%). Table 4.12 depicts the modelling results, namely: the optimised parameters of the NP based model D_A and D_B, which are respectively the self-diffusion coefficients of species A (Hg^{2+}) and B (Na^+), and k_f, which is the convective mass transfer coefficient and the $AADs$ corresponding to this and to the pseudo second-order model adopted for comparison (Equation 1.15).

The NP self-diffusivities are $D_A = 1.108\times10^{-19}$ $m^2 \cdot s^{-1}$ and $D_B = 7.873\times10^{-19}$ $m^2 \cdot s^{-1}$, which indicate larger Na^+ (species B) mobility inside particles. Their orders of magnitude are consistent with both the small pore diameters of microporous titanosilicate ETS-4 (3-4 Å) and the strong and long range nature of the electrostatic interactions. Similar and even smaller values (10^{-17} – 10^{-26} $m^2 \cdot s^{-1}$) are reported in literature for several ion-exchange systems involving other microporous materials, such as Analcite, Shabazite, semi-crystalline Zeolite-NaA, and beryllophosphate-G (Brooke and Rees, 1969; Slater, 1991; Coker and Rees, 1992; Coker and Rees, 2005).

Table 4.12 – Calculated results obtained with the Nernst-Planck based model and the pseudo second-order equation: parameters fitted and average absolute deviations.

	Nernst-Planck model				**Pseudo second-order model**		
Mass (mg)	D_A ($m^2 \cdot s^{-1}$)	D_B ($m^2 \cdot s^{-1}$)	k_f ($m \cdot s^{-1}$)	AAD (%)	q_A ($mol \cdot m^{-3}$)	k_2 ($m^3 \cdot mol^{-1} s^{-1}$)	AAD (%)
	1.108×10^{-19}	7.873×10^{-19}	5.82×10^{-6}				
1.369				3.71	651.26	4.54×10^{-8}	12.21
2.223				2.03	437.58	7.55×10^{-8}	22.31
3.450				2.49	299.50	1.43×10^{-7}	45.90
Global				**2.69**			**27.83**

In Figure 4.16-a and Figure 4.16-b the calculated versus experimental Hg^{2+} solution concentrations are graphed in normalized form, respectively for the NP based model and for the pseudo second-order equation. These figures show the excellent performance of the proposed NP based model and the poor representations achieved by the pseudo second-order equation, illustrating the deviations listed in Table 4.12: $AAD_{NP} = 2.69\%$ and

$AAD_{2nd-order}$ =27.83%. It should be mentioned that the number of data points is the same in both cases (47). Furthermore, the pseudo second-order model almost always overestimates results, in contrast with NP model which scatters deviations around zero.

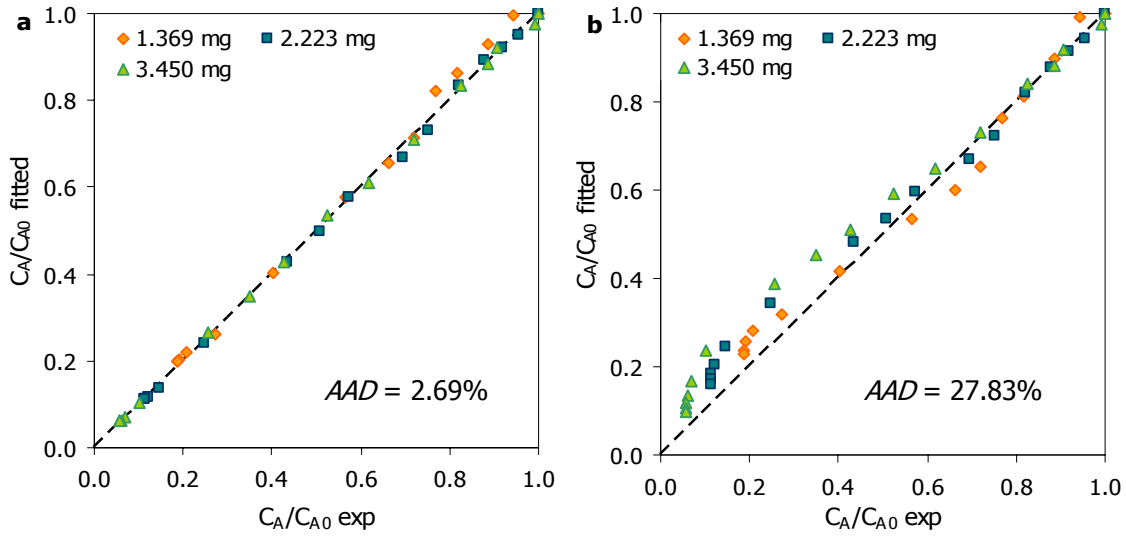

Figure 4.16 – Calculated versus experimental normalized Hg^{2+} concentrations in bulk solution: (a) Nernst-Planck based model of this work; (b) pseudo second-order model.

Finally, the predictive capability of the proposed NP based model was also evaluated by taking three additional sets of data from the study of ETS-4 mass effect presented in section 4.5. These set of data were simulated using only the parameters correlated previously and listed in Table 4.12. The resulting curves are shown in Figure 4.17 together with the experimental data and the corresponding average absolute deviation. We may conclude the NP based model provides reliable (AAD =6.78%) well inside experimental accuracy (5-8%), even for distinct operating conditions.

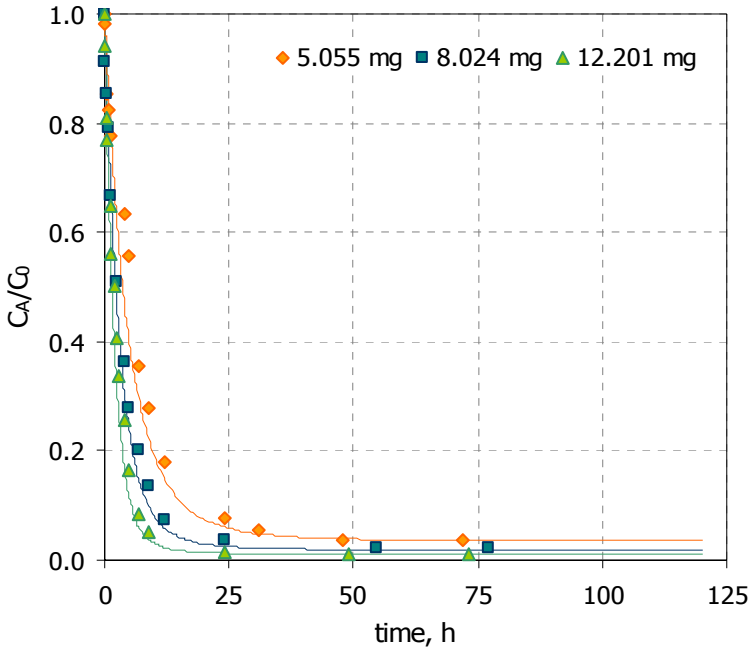

Figure 4.17 – Analysis of the predictive capability of the Nernst-Planck based model proposed in this work: Experimental and calculated normalised Hg^{2+} concentration in solution versus time.

4.11. Conclusions

The sorption capacity of microporous titanosilicate ETS-4 was investigated under different experimental conditions in order to evaluate the effect of the stirring rate, contact time, amount of ETS-4, initial Hg^{2+} concentration, pH and temperature on Hg^{2+} ions removal from aqueous solution.

The batch experiments performed revealed that the ETS-4 sorption capacity for Hg^{2+} ions is strongly dependent on the contact time, ETS-4 mass, initial Hg^{2+} concentration and solution pH and, to a lesser extent, temperature. If the ETS-4/Hg^{2+} system is perfectly homogenous the ETS-4 sorption capacity does not dependent on stirring rate.

The removal of Hg^{2+} ions from aqueous solutions increases with increasing contact time, ETS-4 mass, solution pH until it attains a maximum value at 4-6, and with decreasing initial Hg^{2+} concentration and temperature. The optimum conditions for effective (>95%) Hg^{2+} removal are pH 4-6, 277 -294 K, contact time 24 hours, 2.5 - 8 $mg \cdot dm^{-3}$ of ETS-4 and an initial Hg^{2+} concentration ≤150 $\mu g \cdot dm^{-3}$. These operating conditions are very attractive from the industrial point of view because the application of ETS-4 in the treatment of wastewater and/or industrial effluents will not require large amounts of adsorbent, neither energy supply for temperature adjustments. These conditions become even more interesting in the case of medical institutions liquid effluents (pH 6.6, Tolosana and Ehrlich, 2000), nickel electroplating process (pH 6.0, Álvarez-Ayuso et al., 2003), copper smelter

(pH 6.3, Chojnacki et al., 2004), gold ore tailings (pH 6.0, Benavente et al., 2008) and chlor-alkali effluents (pH 7.6, Sobral et al., 2004), since no significant pH adjustments to the effluent are necessary.

In the range of Hg^{2+} concentrations studied ($0< C_e <20$ μg·dm^{-3}), the equilibrium data is well fitted by both Langmuir and Freundlich isotherms. According with the Langmuir isotherm, the maximum ETS-4 sorption capacity for Hg^{2+} ions is 246 mg·g^{-1} at 294 K and the separation factor indicates favourable Hg^{2+} sorption. The negative values of the Gibbs free energy and enthalpy changes indicate that the Hg^{2+} sorption process is spontaneous and exothermic.

The ion exchange kinetics of Hg^{2+} uptake is described by the Nernst-Planck based model, which combines both intra-particle and film diffusion resistances. The deviations found are small, AAD =2.69% and lower than those obtained for the pseudo-second order kinetic model (AAD =27.83%). The model performs accurately even in the transition from the steep descent to the horizontal branch of the C_A / C_{A0} versus time curve, where data are commonly most difficult to fit. Furthermore, the Nernst-Planck based model exhibits fine predictive capability, since it was able to simulate four sets of data taken from section 4.5 with only AAD =6.78%.

On the whole, these results confirm that ETS-4 has a large potential to be used as a cleaning material for *e.g.* wastewater Hg^{2+}.

Chapter

5

Comparison of Hg^{2+} removal capacity of zeolites A and X with ETS-4 titanosilicate

5.1. Introduction

Among all treatment processes (*e.g.* chemical reduction, precipitation, ion exchange, reverse osmosis, adsorption and coagulation) available for mercury removal from water and wastewater, adsorption is the most attractive one due to its simplicity and effectiveness (Ranganathan, 2003; Zhang et al., 2005; Lopes et al., 2007). The typical adsorbents for Hg^{2+} ions removal are activated carbons and zeolites, but in the past few years a wide range of materials have been emerging as alternative low-cost adsorbents (Di Natale, et al., 2006).

Among the different materials which can be used as heavy-metal adsorbents, zeolites appear as one of the most promising (Álvarez-Ayuso et al., 2003). Zeolites occur naturally but can be produced synthetically. Structural imperfections, a variety of particle sizes, degree of hydration and the presence of clays and other slime particles may lead to differences in properties between natural zeolites (Chojnacki et al., 2004). In contrast, synthetic zeolites have well-defined structures (Lopes et al., 2007) and higher sorption capacities (Álvarez-Ayuso et al., 2003). Several studies have reported the successful application of natural zeolites (Singh et al., 2000; Panayotova, 2001; Álvarez-Ayuso et al., 2003; Gebremedhin-Haile et al., 2003; Chojnacki et al., 2004; Payne and Abdel-Fattah, 2004) as well synthetic zeolites (Kim and Keane, 2000; Singh et al., 2000; Álvarez-Ayuso et al., 2003; Gebremedhin-Haile et al., 2003; Payne and Abdel-Fattah, 2004) to remove heavy metal ions from waters and wastewaters.

In the previous chapters, the ETS-4 sorption capacity for Hg^{2+} ions has been comprehensively investigated and this material confirmed to have potential for removing Hg^{2+} from aqueous solutions (q_{max} =246 $mg \cdot g^{-1}$). However, is ETS-4 good enough to replace the adsorbents used at present in water treatment processes, especially zeolites? This chapter assesses and compares the capacity of zeolites A (ZA) and X (ZX), and titanosilicate ETS-4, to remove low levels of aqueous Hg^{2+}.

5.2. Experimental conditions

ETS-4 was synthesised using the procedure described in chapter 1, while zeolites A and X were prepared using a synthesis procedure modified from Robson, 1998. Metasilicate (BDH), sodium silicate solution (Merck, 8 % Na_2O, 27 % SiO_2, 65 % H_2O) and sodium aluminate (Riedel-de-Haen, Na_2O, 41%; Al_2O_3, 54%) were used as the Si and Al sources.

The synthesis of Zeolite A was performed as follows: solution 1 was made by dissolving 30.96 g Metasilicate into 42 g of H_2O. Solution 2 was made by dissolving 13.78 g sodium aluminate into 50 g of H_2O. After being completely dissolved the two solutions were mixed and stirred for 30 minutes. This gel, with a molar composition $3.24Na_2O:Al_2O_3:2.0SiO_2:80H_2O$, was transferred to a Teflon-lined autoclave and treated at 373 K (100 ºC) for 4.25 hours under autogenous pressure without agitation. The product was removed from heat source, cooled to below 30 ºC, filtered off, washed with distilled water and dried at 353 -383 K (80-110 ºC) overnight.

Zeolite X was synthesized as follows: an alkaline solution was made by dissolving 12.32 g NaOH, 8.97 g KOH and 7.87 g of sodium aluminate into 41.72 g of H_2O. A second solution was made by mixing 20.38 g of sodium silicate solution with 29.87 g of H_2O. Afterwards, the second solution was added into the first one and stirred for 30 minutes. The gel, with a molar composition $5.57Na_2O:1.63K_2O:Al_2O_3:2.20SiO_2:113H_2O$, was transferred to a Teflon-lined autoclave and treated at 343 K (70 ºC) for 3 hours and then at 370 K (97 ºC) for 2 hours under autogenous pressure without agitation. The product was filtered off, washed with distilled water and dried at 373 K (100 ºC), equilibrated over saturated aqueous NaCl. The reagents used in the synthesis of microporous materials were of analytical reagent grade, obtained from chemical commercial suppliers and used without further purification.

Table 5.1 depicts the principal features of the adsorbents. The ETS-4, zeolite A and X particle sizes were estimated from SEM images (Hitachi S-4100) and the density and pore size were calculated from crystallographic data and cation exchange capacity (CEC) was calculated from molecular weight and exchangeable cations.

Table 5.1 – Features of titanosilicate ETS-4, zeolite A and zeolite X

	ETS-4	**ZA**	**ZX**
Formula	$Na_9Ti_5Si_{12}O_{38}(OH)\cdot 12H_2O$	$Na_{12}Al_{12}Si_{12}O_{48}\cdot 27H_2O$	$Na_{73}K_{22}Al_{95}Si_{97}O_{384}\cdot 260H_2O$
Theoretical CEC ($meq\cdot g^{-1}$)	5.54	5.48	5.09
Density ($g\cdot cm^{-3}$)	2.2	2.01	1.95
Particle diameter (μm)	0.5-0.9	<1	3-5
Pore size (nm)	0.4	0.41 × 0.41	0.74 × 0.74

The sorption capacity of each adsorbent was evaluated in batch conditions for three different masses, at room temperature (294±1 K). In each experiment, a corresponding amount of adsorbent and 2000 cm^3 of 50 $\mu g \cdot dm^{-3}$ Hg^{2+} solution were kept in contact, with stirring (1400 rpm), until the Hg^{2+} concentration in solution remained constant. Table 5.2 depicts the experimental conditions used in the sorption experiments.

At the end each sorption experiment, ETS-4 was recovered by filtration in order to perform FT-IR and X-ray diffraction (XRD) analyses. However in some cases the amount of ETS-4 was too small to be recovered.

The FT-IR spectra of pristine ETS-4 and Hg^{2+} loaded ETS-4 (ETS4-Hg) were recorded on a Mattson 7000 Fourier transform infrared spectrometer in the transmission mode using KBr diluted samples, in the range 280-4000 cm^{-1}, resolution of 2 cm^{-1}. Powder XRD patterns were recorded on a Philips X'Pert diffractometer using Cu-K_α radiation (λ=1.5406 Å), in the range 7-58º 2θ.

In order to check the regeneration and reusability of ETS-4, zeolite A and zeolite X, desorption studies were performed using Hg^{2+} loaded adsorbents. After sorption experiments the different materials were collected by filtration, and after being dried at 310 K (37 ºC) the recovered mass was used in the respective desorption study. Desorption studies were performed at 294±1 K by contacting under agitation (1400 rpm) the recovered mass and 2 dm^3 of desorption solution, until Hg^{2+} concentration in liquid phase remained constant. Two desorption media were tested: Milli-Q water (acidified with 25 µL of HNO_3) and $NaNO_3$ solution (1×10^{-3} M). In the sorption part, some adjustments in adsorbent mass and initial Hg^{2+} concentration were done, relatively to the previous experiments, to guarantee that the mass of adsorbent recovered had enough Hg^{2+} loaded for desorption studies. Therefore, *ca.* 20 mg of adsorbent were used and the initial Hg^{2+} concentration increased from 50 to 125 $\mu g \cdot dm^{-3}$.

Table 5.3 depicts the experimental conditions used in the sorption and desorption experiments.

To verify the sorption effectiveness of ETS-4 using a real Hg^{2+} wastewater, this material was used to decontaminate 2 dm^3 of solution deriving from our Analytical Chemistry laboratory's mercury liquid wastes. The real Hg^{2+} wastewater was characterized in terms of Hg^{2+} concentration and pH (Table 5.4).

Table 5.2 – Experimental conditions (mass and pH) used in the experiments.

Adsorbent	**Mass (mg)** (±0.001 mg[†] or ±0.1 mg[‡])	**pH** (±0.1)
ETS-4	8.024[†]	4.9
	8.094[†]	
	8.095[†]	
	50.063[†]	6.6
	50.599[†]*	
	302.9[‡]*	9.7
	303.1[‡]	
Zeolite A	8.097[†]	---
	8.637[†]	
	50.232[†]	7.7
	50.341[†]	
	303.0[‡]	8.6
	309.3[‡]	
Zeolite X	8.147[†]	5.3
	8.294[†]	
	8.458[†]	
	50.094[†]	7.6
	50.281[†]	
	50.269[†]	
	306.5[‡]	8.6
	318.0[‡]	

* samples used for FTIR ad RXD analyses

Table 5.3 – Experimental conditions (mass and pH) used in the sorption and desorption experiments.

	Sorption		**Desorption**		
	Mass (mg ± 0.001 mg)	pH (± 0.1)	Desorption medium	Mass recovered (mg ± 0.001 mg)	pH (± 0.1)
ETS-4	20.378	4.6	Milli-Q	10.945	4.0
	20.526	5.5	$NaNO_3$	9.266	5.5
ZA	20.441	5.6	Milli-Q	9.918	4.0
	20.730	5.5	$NaNO_3$	11.328	5.5
ZX	20.323	5.5	Milli-Q	6.901	4.0
	20.356	5.5	$NaNO_3$	7.407	5.6

Table 5.4 – Experimental conditions (mass, pH, volume and initial Hg^{2+} concentration) used in real Hg^{2+} wastewater treatment process.

	Dilution factor	**Mass** (mg ± 0.001* mg)	**pH** (± 0.1*)	**C_0** ($\mu g \cdot dm^{-3}$)
Wastewater	---	---	1.2	2 066 ± 34
Wastewater-10	10	25.429	4.4†	160 ± 2
Wastewater-20	20	25.316	5.6†	78.2 ± 1.6

*tolerance; †after adjustment with KOH; value ± standard deviation

5.3. Adsorbents sorption capacity

The evaluation of ETS-4, zeolite A (ZA) and zeolite X (ZX) sorption capacity for Hg^{2+} ions was performed for three different masses of adsorbent: *ca.* 8 mg (Figure 5.1), *ca.* 50 mg (Figure 5.2) and *ca.* 300 mg (Figure 5.3).

Except for zeolite A, 8 mg of adsorbent were enough to decrease considerably the Hg^{2+} concentration in the liquid phase (Figure 5.1). Clearly, Hg^{2+} has very distinct affinity for the various adsorbents. ETS-4 is by far the best material, followed by zeolite X, removing respectively, 96% and 87% Hg^{2+} in 24 hours (Table 5.5). Surprisingly, zeolite A performed poorly removing only 10% Hg^{2+} in the same time (Table 5.5).

Increasing the mass of adsorbent from 8 to 50 mg slightly improved the removal efficiency of zeolite A (from 10 to 11%), did not change the performance of ETS-4 (96%), and deteriorated the removal efficiency of zeolite X (down to 5%) (Table 5.5). The increase of the removal percentage with increasing adsorbent mass is expected because increasing the amount of adsorbent provides larger surface area and number of available sorption sites (Rengaraj et al., 2001). A slight increase on Hg^{2+} removal percentage was observed for zeolite A. In contrast, the removal efficiency of zeolite X decreased dramatically with increasing mass. This unusual behaviour can only be explained by a change in the solution pH. Increasing the zeolite X mass from 8 to 50 mg increased the solution pH from 5.3 to 7.6 due to ion exchange between alkali cation in framework and hydrogen ion (Pitcher et al., 2004; Choi et al., 2006a).

In order to check the hypothesis, at the end of the sorption experiment the solution pH was adjusted with HNO_3 to a pH value *ca.* 5, followed by determination of Hg^{2+} concentration. After the adjustment of the solution pH to a value *ca.* 5, a significant decrease on Hg^{2+} concentration in the liquid phase (Figure 5.2 – points beyond the orange dotted line) and an enormous increase on Hg^{2+} removal percentage by zeolite X occurred (Table 5.5), confirming the hypothesis. Since the pH of the zeolite A solution (50 mg) was also high (7.7) the same procedure was applied to test if the removal efficiency of this material improved with the decrease of the solution pH. A slightly decrease on Hg^{2+} concentration in the liquid phase (Figure 5.2–points beyond the orange dotted line) and a slightly increase on Hg^{2+} removal percentage by zeolite A was observed with the decreasing of solution pH. Moreover, the fact that the removal efficiency of ETS-4 did not increase with the increasing of its mass from 8 to 50 mg may also be a consequence of the increasing of solution pH from 4.9 to 6.6.

The sorption capacity of ETS-4, zeolite A and zeolite X for Hg^{2+} ions when 50 mg of adsorbent are used is ETS-4>>ZA>ZX, with no solution pH adjustment, and ZX≈ETS-4>>ZA if the pH of zeolite A and X solutions is adjusted to *ca.* 5.

A second increase on adsorbent mass from 50 to 300 mg improved considerably the removal efficiency of zeolite A (from 11 to 41%) and zeolite X (from 5 to 30%), (Table 5.5). Again, no effect was observed on the removal efficiency of ETS-4, which remained high (96%).

Table 5.5 – Experimental Hg^{2+} uptake, q_e, C_e and contact time, for each adsorbent studied.

		Experimental parameters			
Adsorbent		Hg^{2+} uptake (%)	q_e ($mg \cdot g^{-1}$)	C_e ($\mu g \cdot dm^{-3}$)	Time (h ± 0.02* h)
ETS-4	*ca.* 8 mg	96.4 ± 0.2	11.95 ± 0.05	1.79 ± 0.11	24.33
	ca. 50 mg	96.1 ± 0.5	1.91 ± 0.03	1.95 ± 0.27	24.00
	ca. 300 mg	96.1 ± 0.3	0.32 ± 0.00	1.96 ± 0.16	24.21
Zeolite A (ZA)	*ca.* 8 mg	9.9 ± 0.0	1.18 ± 0.05	45.07 ± 0.02	24.44
	ca. 50 mg	10.5 ± 6.1	0.21 ± 0.12	44.66 ± 3.05	24.00
		16.9 ± 1.4	*0.34 ± 0.03*	*41.54 ± 3.05*	
	ca. 300 mg	40.5 ± 9.6	0.13 ± 0.03	29.76 ± 4.79	24.00
		45.4 ± 0.8	*0.15 ± 0.00*	*27.30 ± 0.40*	
Zeolite X (ZX)	*ca.* 8 mg	86.7 ± 1.6	10.45 ± 0.14	6.65 ± 0.78	24.00
	ca. 50 mg	4.7 ± 3.2	0.09 ± 0.06	47.65 ± 1.58	24.05
		97.7 ± 0.3	*1.95 ± 0.01*	*1.14 ± 0.04*	
	ca. 300 mg	29.9 ± 5.1	0.10 ± 0.01	35.07 ± 2.56	24.00
		95.4 ± 0.7	*0.31 ± 0.00*	*2.30 ± 0.29*	

*tolerance; mean ± standard deviation; grey italic values are after solution acidification with HNO_3

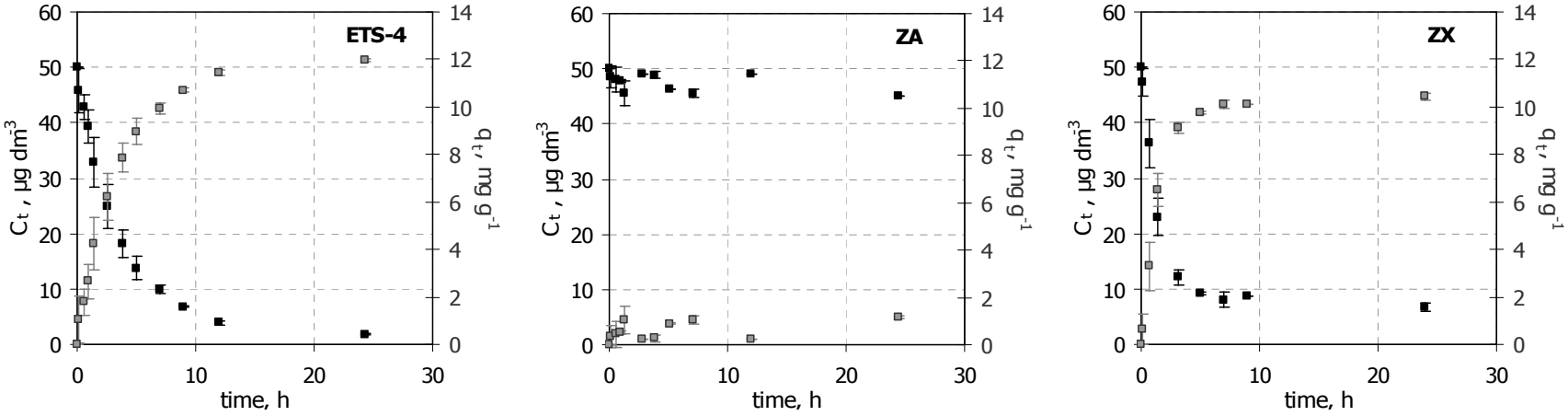

Figure 5.1 – Hg^{2+} concentrations in the liquid phase (C_t) and sorbed (q_t) on ETS-4, zeolite A and zeolite X as a function of time, using *ca.* 8 mg of adsorbent. Black symbols – Hg^{2+} in solution; Grey symbols – Hg^{2+} sorbed.

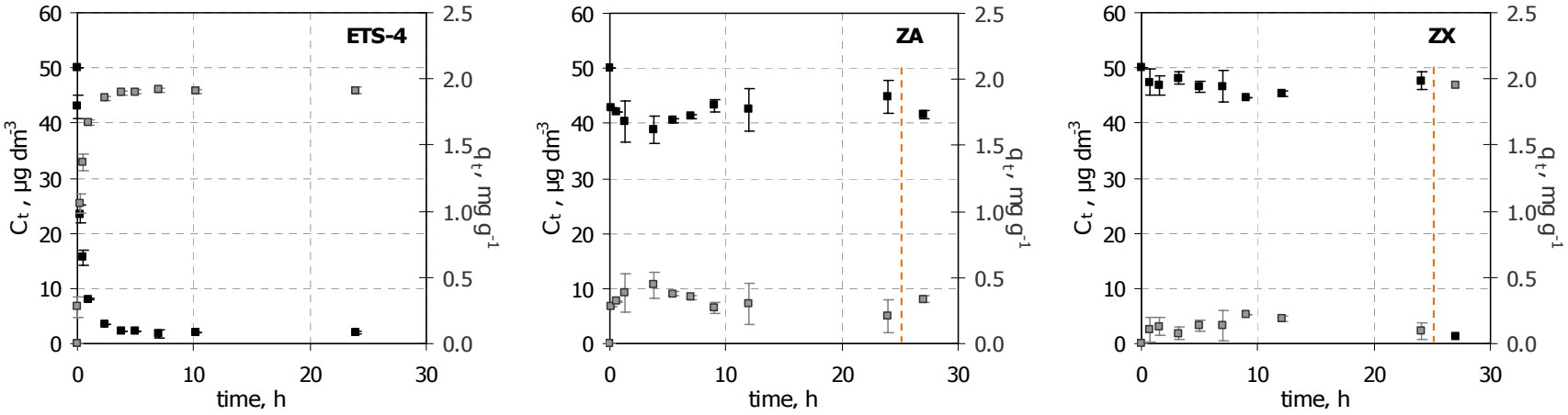

Figure 5.2 – Hg^{2+} concentrations in the liquid phase (C_t) and sorbed (q_t) on ETS-4, zeolite A and zeolite X as a function of time, using *ca.* 50 mg of adsorbent. Black symbols – Hg^{2+} in solution; Grey symbols – Hg^{2+} sorbed. The orange dotted line indicates the adjustment of solution pH to *ca.* 5.

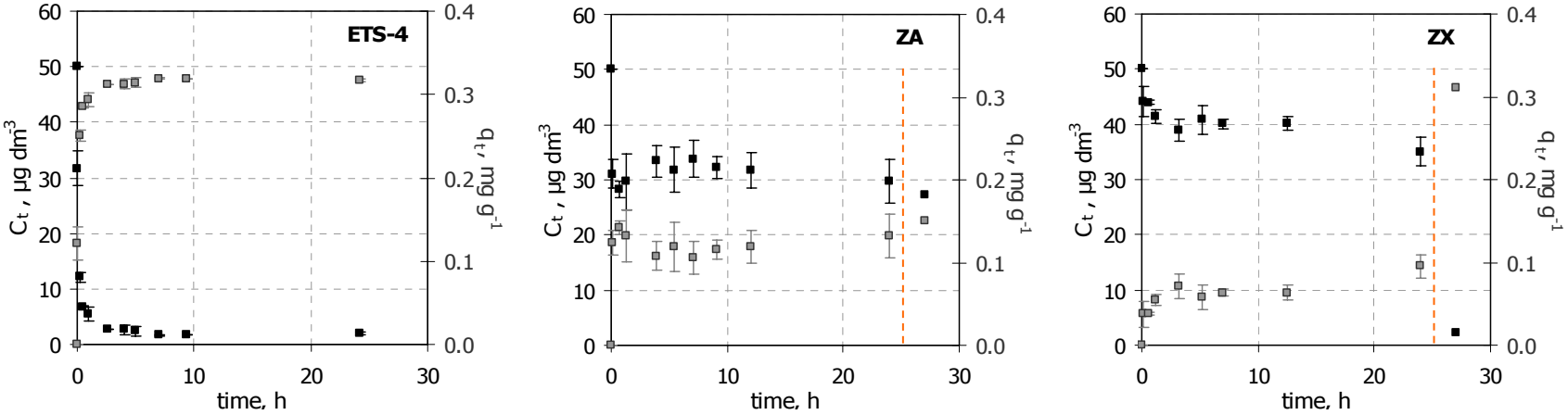

Figure 5.3 – Hg^{2+} concentrations in the liquid phase (C_t) and sorbed (q_t) on ETS-4, zeolite A (ZA) and zeolite X (ZX) as a function of time, using *ca.* 300 mg of adsorbent. Black symbols – Hg^{2+} in solution; Grey symbols – Hg^{2+} sorbed. The orange dotted line indicates the adjustment of solution pH to *ca.* 5.

Once more, an increasing on solution pH was observed for all materials when the adsorbent mass increased from 50 to 300 mg. The solution pH increased from 6.6 to 9.7 for ETS-4, from 7.7 to 8.6 for zeolite A and from 7.6 to 8.6 for zeolite X. Since the removal efficiency of zeolite X strongly depends on solution pH, at the end of the sorption experiment the solution pH was adjusted to *ca.* 5, analogously to the previous experiment when 50 mg of adsorbent was used. As expected, a considerable decrease on Hg^{2+} concentration in the liquid phase (Figure 5.3–points beyond the orange dotted line) and an increase from 30 to 95% on Hg^{2+} removal percentage by zeolite X was observed (Table 5.5). The same procedure was performed on zeolite A experiment and, once again, only a slight decrease on Hg^{2+} concentration in the liquid phase (Figure 5.3–points beyond the orange dotted line) and a slight increase on the Hg^{2+} removal percentage (from 41 to 45%) was observed with the decreasing of the solution pH. Once more, the fact that removal efficiency of ETS-4 did not increase with the increasing of its mass from 50 to 300 mg may also be a consequence of the increasing of solution pH from 6.6 to 9.7.

The sorption capacity of ETS-4, zeolite A and zeolite X for Hg^{2+} ions when 300 mg of adsorbent are used was found to be ETS-4>ZA>ZX, with no adjustment in the solution pH, and ETS-4≈ZX>ZA if the pH of zeolite A and X solutions was adjusted to *ca.* 5. In general, the sorption capacity of the adsorbents decreased while their removal efficiency increased, with increasing the adsorbents masses.

5.4. Desorption study

Desorption of pre-uptake Hg^{2+} ions on ETS-4, zeolite A and zeolite X was studied at room temperature (294 K) in two desorption media, Milli-Q water acidified with HNO_3 and $NaNO_3$ solution (1×10^{-3}). Desorption percentage for all adsorbents is shown in Figure 5.4.

The high values of desorption percentage obtained for zeolite A and zeolite X (Table 5.5), suggest that Hg^{2+} ions are weakly sorbed on these two adsorbents, and both can be regenerated. In the case of zeolite A this fact is not particularly important since only zeolite X exhibited some ability to remove Hg^{2+} from aqueous solutions, under the operating conditions employed. The very low values of desorption percentage found for ETS-4 (2 and 3%, respectively in Milli-Q and $NaNO_3$ desorption media) suggest that Hg^{2+} ions are strongly sorbed on ETS-4 and that this material can be used to immobilize Hg^{2+} ions.

Table 5.6 – Experimental sorption and desorption parameters, for each adsorbent studied.

	Sorption – Experimental parameters			**Desorption – Experimental parameters**				
	q_e (mg·g^{-1})	C_e (µg·dm^{-3})	Time (h ± 0.02* h)	Desorption medium	C_{max} (µg·dm^{-3})	C_e (µg·dm^{-3})	Desorption (%)	Time (h ± 0.02* h)
ETS-4	10.63 ± 0.12	16.66 ± 1.15	48.17	Milli-Q	58.19 ± 0.66	1.06 ± 0.03	1.8 ± 0.1	72.33
	11.13 ± 0.03	10.73 ± 0.13	71.17	$NaNO_3$	51.58 ± 0.14	1.48 ± 0.05	2.9 ± 0.1	72.00
Zeolite A	0.14 ± 0.25	123.6 ± 2.5	49.00	Milli-Q	0.67 ± 1.20	0.66 ± 0.06	98.5 ± 176	72.00
	0.15 ± 0.14	123.4 ± 1.5	48.58	$NaNO_3$	0.88 ± 0.82	0.86 ± 0.01	98.2 ± 91.7	71.58
Zeolite X	9.45 ± 0.08	28.95 ± 0.79	48.00	Milli-Q	32.61 ± 0.28	32.38 ± 0.18	99.3 ± 1.0	72.33
	11.09 ± 0.02	12.16 ± 0.05	48.00	$NaNO_3$	41.06 ± 0.08	28.00 ± 0.50	68.2 ± 3.2	72.25

*tolerance; value ± standard deviation

In the experimental conditions used it was not possible to regenerate ETS-4, however the increasing of the desorption percentage when the desorption medium changed from Milli-Q water to $NaNO_3$ solution suggests that cation exchange occurred between the Hg^{2+} ions in the ETS-4 structure and the Na^+ in solution. It is possible that increasing the Na^+ concentration a higher desorption percentage will be achieve.

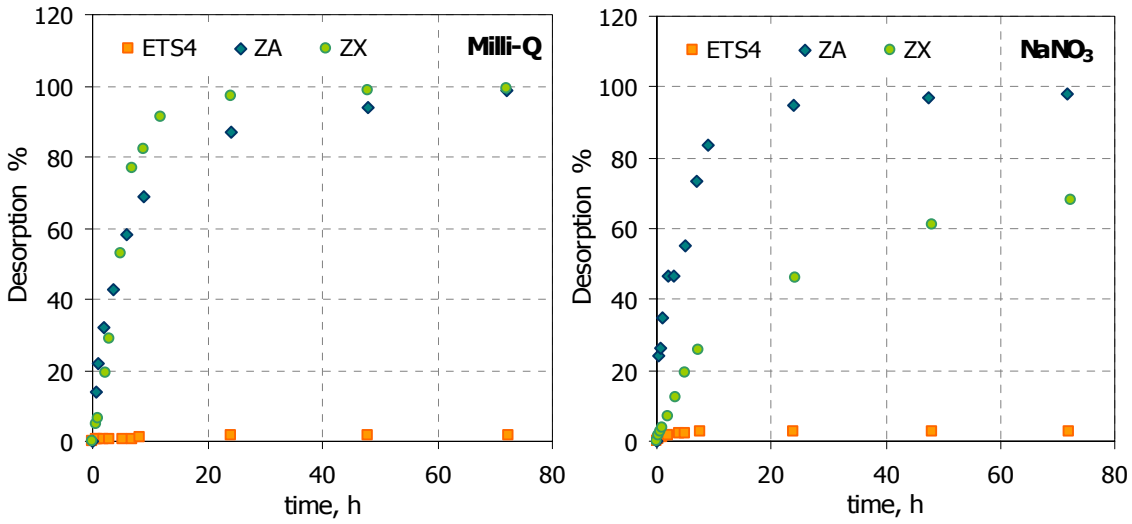

Figure 5.4 – Hg^{2+} desorption from ETS-4, zeolite A (ZA) and zeolite X (ZX) as a function of time, in two desorption media.

5.5. Treatment of real Hg^{2+} wastewater

The Analytical Chemistry laboratory from the Chemistry Department of the University of Aveiro performs frequently mercury analyses in environmental matrices, which originates daily Hg^{2+} residues due to the preparation of Hg^{2+} standards.

2 dm^3 of solution deriving from Analytical Chemistry laboratory's mercury liquid wastes were treated at room temperature (294 K) with ETS-4 in order to verify the effectiveness of this material on real Hg^{2+} wastewater. The results obtained for the real Hg^{2+} wastewater diluted 20 times (Hg^{2+} waste DF-20) and 10 times (Hg^{2+} waste DF-10) are shown in Table 5.7.

The high values of Hg^{2+} removal percentage (>77%) confirm the effectiveness of ETS-4 for uptaking Hg^{2+} ions, even in real wastewaters. As expected, the ETS-4 performance is slightly lower in the real Hg^{2+} samples than in the synthetic Hg^{2+} solutions prepared for all ETS-4 sorption studies. The difference observed between ETS-4 performance (uptake

percentage, sorption capacity and residual Hg^{2+} concentration) in real and synthetic Hg^{2+} samples is attributed to the presence of other ions.

Table 5.7 – Experimental Hg^{2+} uptake, q_e, C_e and contact time, for the real Hg^{2+} wastewater.

	Experimental parameters			
Hg^{2+} waste	Hg^{2+} uptake (%)	q_e (mg·g^{-1})	C_e (μg·dm^{-3})	Time (h ± 0.02* h)
Hg^{2+} waste DF-20	79.7 ± 2.6	4.92 ± 0.13	15.9 ± 0.2	70.00
Hg^{2+} waste DF-10	77.9 ± 1.6	9.79 ± 0.16	35.3 ± 0.4	70.00

*tolerance; value ± standard deviation

5.6. Hg^{2+} influence on ETS-4 structure

5.6.1. FT-IR

According with Karge (1998) vibrations of the framework of zeolites give rise to typical bands in the mid- and far-IR. The FT-IR spectra of pristine and Hg^{2+} loaded ETS-4 samples are shown in Figure 5.5. No significant differences were observed between pristine and Hg^{2+} load samples.

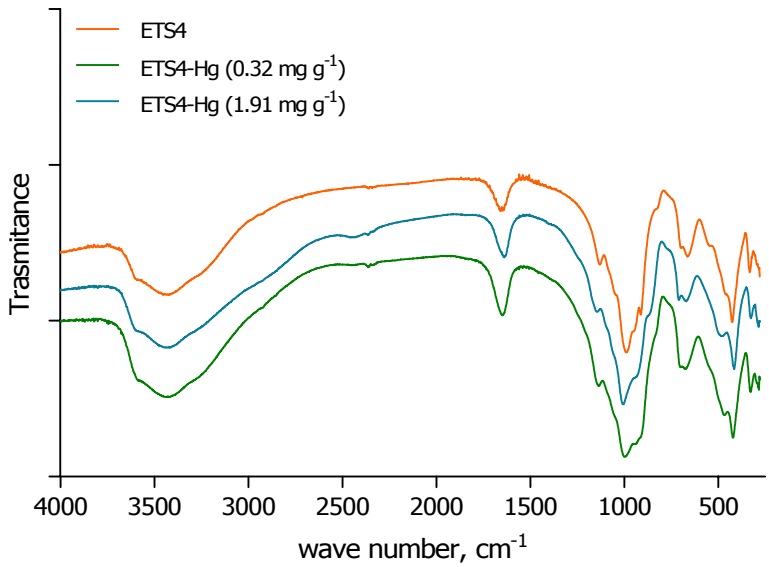

Figure 5.5 – FT-IR spectra of pristine and Hg^{2+} loaded ETS-4 samples.

The main adsorption bands observed in ETS-4 FT-IR spectra are: a broad band at 3450 cm^{-1}; a strong band at 1650 cm^{-1}; a weak peak at 1145 cm^{-1}; a strong band at 1000 cm^{-1}; three weak peaks at 700, 670 and 470 cm^{-1}, a strong peak at 420 cm^{-1} and a weak peak at 330 cm^{-1}. The broad band at 3450 cm^{-1} could be assigned to –OH groups associated with a Brønsted site, known as "bridging" hydroxyls (Dyer, 1988; Karge, 1998). The strongly intense band at 1000 cm^{-1} is dominated by Si-O stretching (Pavel et al., 2003), and in the mid-frequency range of FT-IR spectra (400-800 cm^{-1}) both Ti-O and Si-O modes contribute to the peaks (Pavel et al., 2003).

5.6.2. X-Ray powder diffraction

The powder X-ray diffraction is a technique for the determination of the bulk structure of crystalline solids (Bowker, 1998). In this method, X-ray irradiation of the powders produces a scattering pattern from the regular arrays of atoms (or ions) within the structure (Dyer, 1988). It reflects the framework and non-framework symmetry of the constituents of each solid to produce a diagnostic fingerprint of 2θ (or d) spacings according to the Bragg equation: $n\lambda = 2dSin\theta$ (5.1)

where n is an integer, λ is the wavelength of the incident X-rays, d is the value of the interlayer spacings of the component atoms and ions and θ is the scattering angle (Dyer, 1988).

The powder XRD pattern of pristine and Hg^{2+} loaded ETS-4 samples are shown in Figure 5.6.

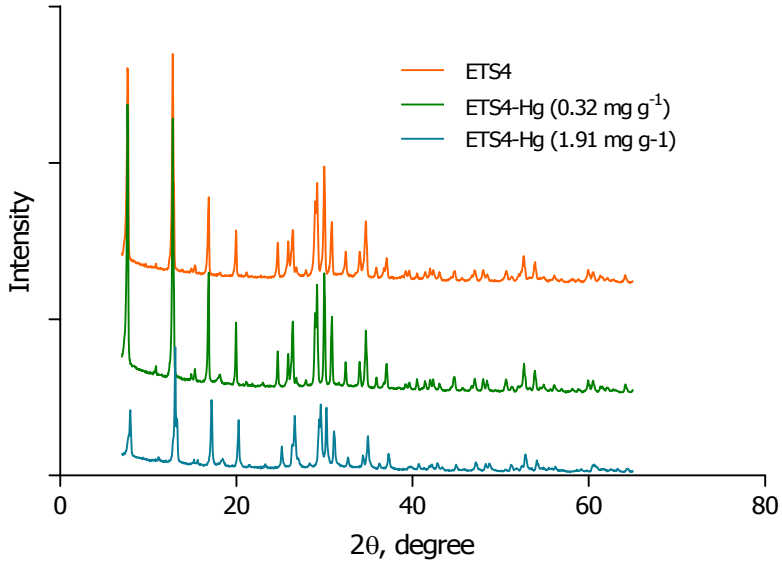

Figure 5.6 – Powder XRD pattern of pristine and Hg^{2+} loaded ETS-4 samples.

No noteworthy differences were observed between the pristine and the Hg^{2+} loaded samples, suggesting that ETS-4 structure did not change noticeably with the incorporation of Hg^{2+} in its extra-framework.

5.7. Conclusions

The sorption capacity and Hg^{2+} removal efficiency of ETS-4, zeolite A and zeolite X were evaluated at 294±1 K using three different masses of adsorbent. In general, the adsorbed concentration of Hg^{2+} on ETS-4, zeolite A and zeolite X decrease with increasing the solid mass while, in parallel, the removal percentage increases. Moreover, the sorption Hg^{2+} on zeolite X is drastically affected by the solution pH.

Under the experimental conditions used, ETS-4 performed better than both zeolites. The highest adsorbed concentration of Hg^{2+} on ETS-4 was 11.95 $mg \cdot g^{-1}$, which is higher than the one found for zeolite X (10.45 $mg \cdot g^{-1}$), which is much higher than the one found for zeolite A (1.18 $mg \cdot g^{-1}$). Although the performance of zeolites A and X was relatively poor, especially that of zeolite A, the optimal experimental conditions for using these materials were not investigated and, thus, there is room for much optimisation and improvement. The desorption capacity of zeolite A is higher than the one of zeolite X, which is much higher than the desorption capacity of ETS-4. It is interesting to note that Hg^{2+} ions are weakly sorbed on zeolite A and X and strongly sorbed on ETS-4, which represents a disadvantage for ETS-4 in terms of adsorbent regeneration but an advantage in terms of Hg^{2+} immobilization.

ETS-4 is also a good material to remove Hg^{2+} from real Hg^{2+} wastewaters, removing more than 77% of total Hg^{2+} However the very acid character of the real wastewater is a hindrance to its removal performance. Overall ETS-4 may be a good alternative to zeolites A and X.

Chapter

6

ETS-4 fixed-bed ion exchange system for Hg^{2+} removal

6.1. Introduction

In the previous chapters, all studies have focused on the Hg^{2+} removal by microporous materials, in particular ETS-4, in a batch mode. However, for industrial water treatment, operation in a fixed-bed mode is preferable and consequently experimental and theoretical data obtained in these conditions are desirable from the industrial point of view (Lv et al., 2007).

The fixed-bed mode consists in feeding continuously an influent containing a contaminant (*e.g.* heavy metal ions), into a column packed with a particular adsorbent. Gradually, the adsorbent is getting exhausted (*i.e.*, its capacity to remove the contaminant is over), from the inlet end toward the outlet end, until at some point it ceases to perform (Cooney, 1998). It is then common to send the feed to a second column, while the adsorbent in the first one is replaced or regenerated, and so forth (Cooney, 1998).

In this chapter I evaluate the efficiency of ETS-4 for Hg^{2+} ions removal from aqueous solutions using a fixed-bed mode system. The main goals of the work are to assemble an ETS-4 fixed-bed column and investigate its efficiency to remove Hg^{2+} ions from aqueous solutions under certain operating conditions.

6.2. Column design assemble

The first step in the preparation of the ETS-4 fixed-bed ion exchange was the filling up of the column. ETS-4 is a powder and packing a column with it would probably originate problems such as the formation of a pulp and, moreover, the ETS-4 powder probably would be dragged by the feed stream. A more appropriate choice would be to use pellets. However, the synthesis of ETS-4 pellets has never been done in our laboratory and its successful production will require time. One alternative to the ETS-4 pellets is the synthesis of ETS-4 inside the column using a stainless steel material as support. A common stainless steel dish-cloth was found to be a low-cost alternative to the commercial support pieces.

The following prototype design (Figure 6.1) was considered for the column manufacture. Column dimensions were restricted by the size of autoclave used in the ETS-4 synthesis.

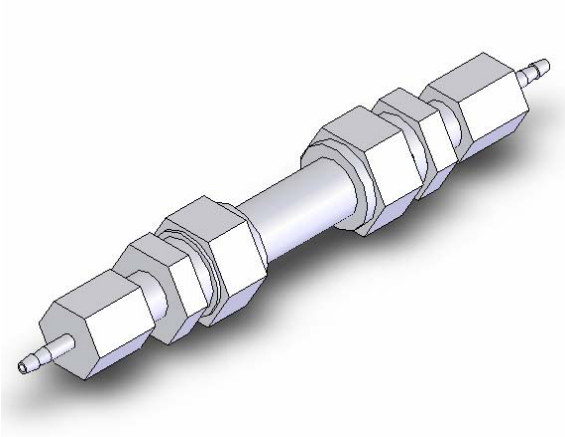

Figure 6.1 – Prototype design for ETS-4 fixed-bed column. (This sketch was made using SolidWorks program)

The column consists of: (a) two tube adapters made in the workshop of the Physics Department of University of Aveiro, (b) two male fittings (internal Ø 16 mm) purchased from Swagelock; (c) two stainless steel nets; (d) a stainless steel tube and (e) an ordinary stainless steel dish-cloth (Figure 6.2).

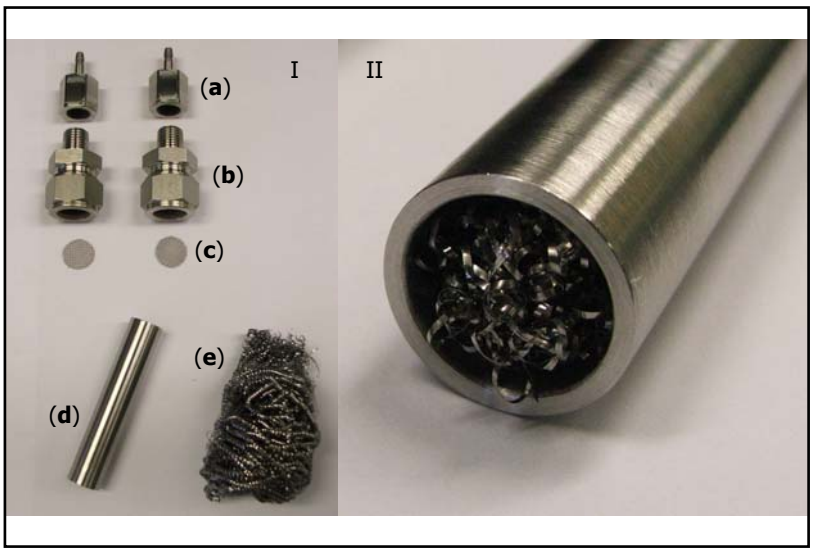

Figure 6.2 – Stainless steel column: I. constituent elements; II. tube detail after filling up with the stainless steel dish-cloth.

The synthesis of ETS-4 was performed on the surface of the stainless steel dish-cloth after filling up the stainless steel tube with it: the tube was washed with a 10% ETS-4 solution, for the deposition of seeds to promote ETS-4 growth, dried and placed inside a Teflon-lined autoclave. Meanwhile, an alkaline solution was made using the procedure described in section 1.3.2.2. The resultant gel was transferred to a Teflon-lined autoclave and treated at 503.15 K (230 ºC) for 24 hours under autogenous pressure. The column

was then inverted and the Teflon-lined autoclave refilled with the gel and treated at 503.15 K (230ºC) for another 24 hours, under autogenous pressure. The final column was washed at room temperature with distilled water and dried at 70 ºC for 3 days. Some steps of the ETS-4 synthesis are shown in Figure 6.3, namely the preparation of the gel and the filling of the autoclave, with the tube inside, with the prepared gel. The synthesis procedure was performed twice because the quantity of gel added should never be more than ¾ of autoclave's capacity. After ETS-4 synthesis, some important parameters of the ETS-4 fixed-bed column were evaluated and are depicted in Table 6.1.

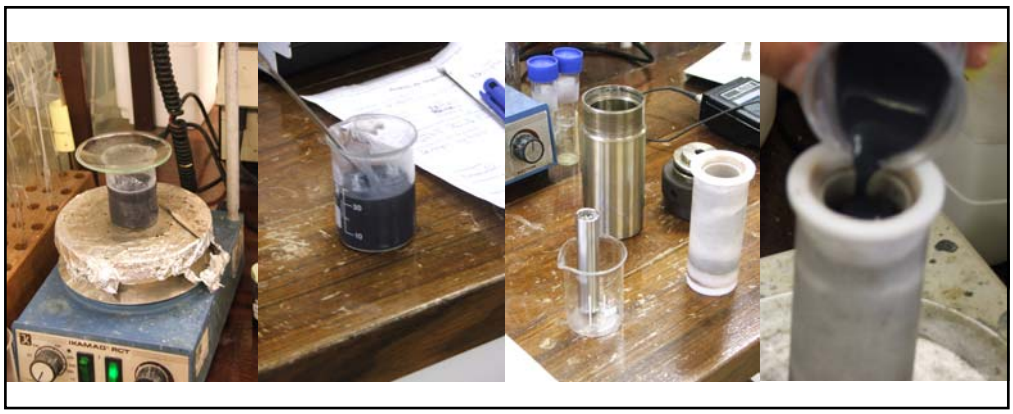

Figure 6.3 – A few steps of the synthesis of ETS-4 inside the tube.

At last, the assembly of the column was performed Figure 6.4.

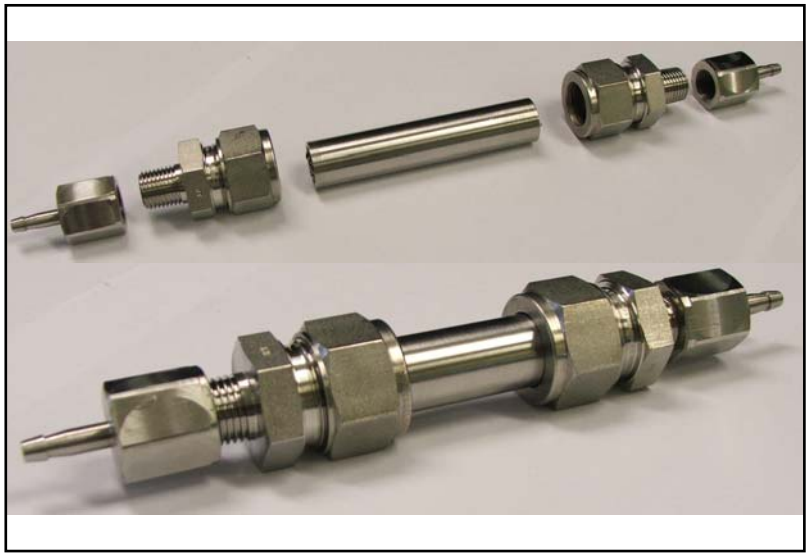

Figure 6.4 – Assembling the column.

Table 6.1 – Principal parameters of the ETS-4 fixed-bed column.

Parameters	
Length	80.0 mm
Internal diameter	13.0 mm
Empty volume	6.54 cm^3
ETS-4 mass	340 mg

6.3. Experimental set-up and procedure

The experimental set-up (Figure 6.5) used in the fixed-bed mode consists of a volumetric flask (2000 cm^3), with the influent solution, a peristaltic pump (Ismatec MS-reglo) and a Tygon® tube (internal Ø 2.79 mm) and the ETS-4 fixed-bed column.

Figure 6.5 – Fixed-bed mode: experimental set-up.

Hg^{2+} solutions were prepared daily by diluting the stock solution ($Hg(NO_3)_2$, 1000 $mg{\cdot}dm^3$) to the desired concentration, in high-purity water. The fixed-bed experiments were performed isothermally (294 K) and started when the feed stream (influent) containing Hg^{2+} ions was continuously fed into the column in an up-flow mode. Aliquots (25 cm^3) were collected at increasing times at the outlet of the column (effluent), adjusted to pH<2 with HNO_3 Hg free and then analysed by cold vapour atomic fluorescence spectrometry (CVAFS). The flow rate was regulated with a variable peristaltic pump

(Ismatec MS-reglo). Two experiments were performed in the continuous mode and the detailed operating conditions used are reported in Table 6.2.

Table 6.2 – Experimental conditions (total volume that passed through the column, flow rate, pH, initial Hg^{2+} concentration and temperature) used in the continuous experiments.

	Experimental conditions			
	Total volume (dm^3)	Flow rate ($cm^3 \cdot min^{-1}$)	pH (± 0.1*)	C_0 ($\mu g \cdot dm^{-3}$)
Experiment 1	4.7	0.65	4.6	50.00 ± 0.12
Experiment 2	50.0	8.45	4.1	125.00 ± 0.23

*tolerance; value ± standard deviation

In the first experiment, I kept the initial Hg^{2+} concentration used in the batch mode and used the slowest rotation speed of the peristaltic pump, in order to get the lowest flow rate possible. I wanted to guarantee that the residence time of Hg^{2+} ions would be long enough for ETS-4 uptake.

Based on the results obtained with the operating parameters used in the first experiment, in the second experiment I increased the initial Hg^{2+} concentration from 50 to 125 $\mu g \cdot dm^{-3}$ and increased the rotation speed of the peristaltic pump, in order to get a higher flow rate. The removal process was interrupted at the end of a working day and restarted in the following morning. The time counter was interrupted simultaneously with the turn off of the peristaltic pump.

Between experiments 1 and 2 occurred regeneration phase of the column:

- 2 dm^3 of hot acidified Milli-Q water (318 K; 45ºC), followed by
- a few cm^3 of NaOH solution (~0.1 M), followed by 2 dm^3 Milli-Q water
- 2 dm^3 of $NaNO_3$ 0.001 M

6.4. Hg^{2+} removal by ETS-4 in a fixed-bed column

The amount of Hg^{2+} ions sorbed per unit mass of ETS-4 (q, $mmol \cdot g^{-1}$) in the column was calculated using the following equation:

$$q = \frac{Q_{tot}}{W} = \frac{\sum_{i=1}^{n} v \times (t_i - t_{i-1}) \times \left[1 - \left(C / C_0\right)_i\right] \times C_0}{W} \qquad (6.1)$$

where Q_{tot} (mmol) is the total amount of Hg^{2+} ions sorbed in the ETS-4 column, v ($cm^3 \cdot min^{-1}$) is the flow rate, i is the number of sampling point, t_i (min) is the i time

point, $(C/C_0)_i$ is the ratio of the i effluent concentration over the i influent concentration (mM) and W (g) is the mass of ETS-4 in the column.

The normalized Hg^{2+} concentration and the removal percentage at the column outlet for the experiment 1 and 2 are shown respectively in Figure 6.6-a and Figure 6.6-b.

The results from experiment 1 show that the ETS-4 fixed-bed column efficiently removes the Hg^{2+} ions from the influent solution. After 120 hours of continuous Hg^{2+} removal, the ETS-4 fixed-bed column still removed 96.6 % of the Hg^{2+} ions contained in the influent and the amount of Hg^{2+} ions sorbed per unit mass of ETS-4 in the column 3.31×10^{-3} mmol·g^{-1} (or 0.66 mg·g^{-1}) (Table 6.3). This value is still very far from the ETS-4 maximum capacity (246 mg·g^{-1}) predicted by the Langmuir model in the batch studies. An estimation based on the maximum capacity predicted by the Langmuir model indicates that it will take approximately 4 years and 321 days to completely exhaust the column capacity under the operating conditions used in experiment 1.

In experiment 2, the flow rate was, thus, increased thirteen times and the initial Hg^{2+} concentration 2.5 times. The results from experiment 2 confirm that ETS-4 fixed-bed column removes efficiently the Hg^{2+} ions from the influent solution. During the first 20 hours the removal efficiency at the outlet remained constant (95.0±0.6%) but then it decreases. After 50 dm^3 of influent have passed through the ETS-4 fixed-bed column, the Hg^{2+} concentration in the effluent was 19.46 μg·dm^{-3}, which corresponds to 84.4 % of Hg^{2+} removal. Moreover, the amount of Hg^{2+} ions sorbed per unit mass of ETS-4 in the column was 2.82×10^{-2} mmol·g^{-1} (or 16.58 mg·g^{-1}) (Table 6.3), which is still very far from the ETS-4 maximum capacity (246 mg·g^{-1}) predicted by the Langmuir model. 51 more days would be needed to completely saturate the column.

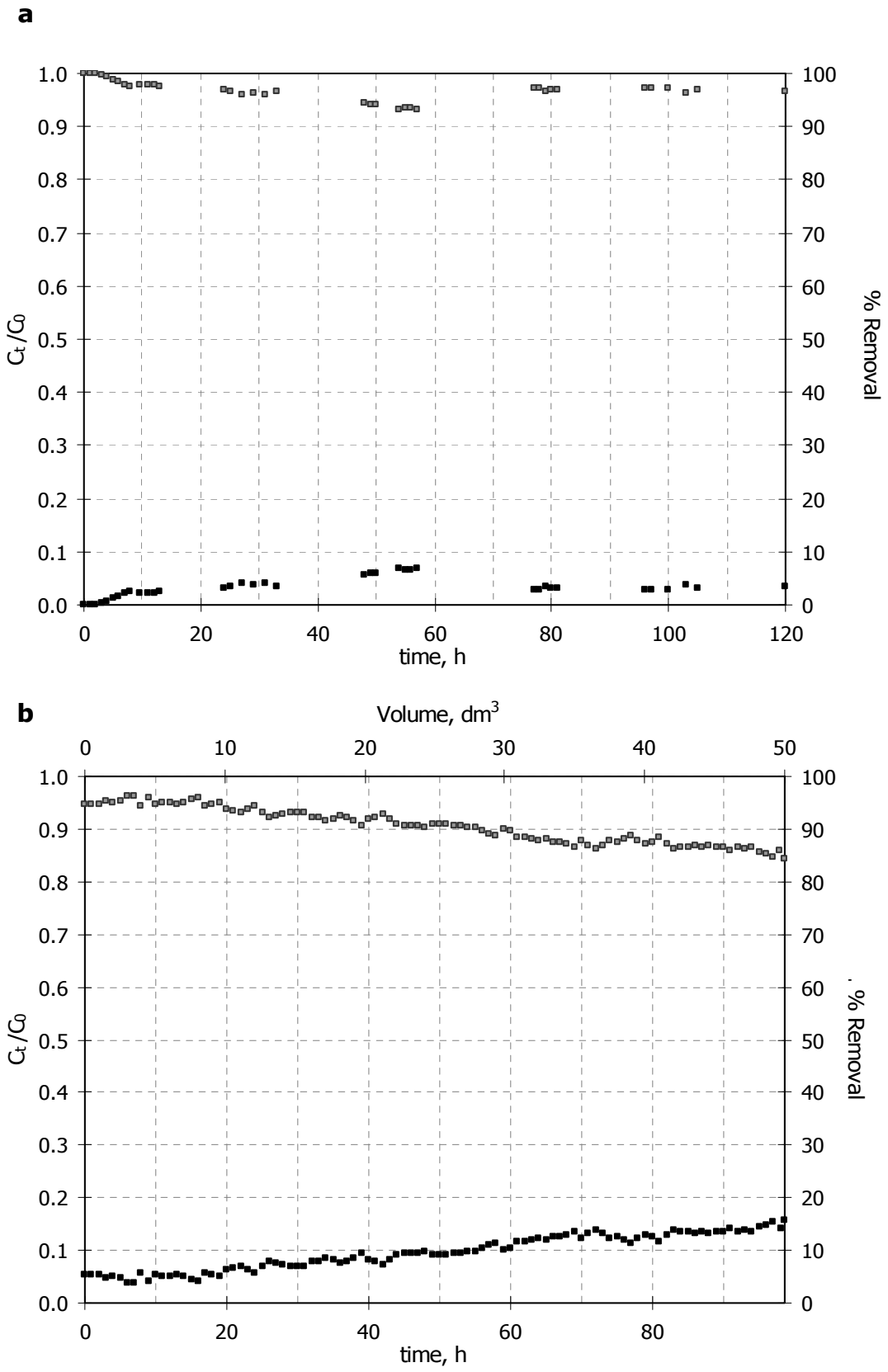

Figure 6.6 – Hg^{2+} removal by ETS-4 in a fixed-bed column as function time for (a) experiment 1 and (b) experiment 2. Black symbols – normalized Hg^{2+} concentration at the column outlet; Grey symbols – removal percentage at the column outlet.

Table 6.3 – Summary of operating conditions for the experiments in fixed-bed column and the corresponding results.

	Operating conditions		**Performance**				
	C_0	v	Time	Removal	C_i	Q_{tot}	q
	(mM)	($cm^3 \cdot min^{-1}$)	(min)	(%)	(mM)	(mmol)	($mmol \cdot g^{-1}$)
Exp. 1	2.49×10^{-7}	0.65	7200	96.6	8.52×10^{-9}	1.13×10^{-3}	3.31×10^{-3}
	($\mu g \cdot dm^{-3}$)				($\mu g \cdot dm^{-3}$)	(μg)	($mg \cdot g^{-1}$)
	50.00				1.71	225.7	0.66
	(mM)	($cm^3 \cdot min^{-1}$)	(min)	(%)	(mM)	(mmol)	($mmol \cdot g^{-1}$)
Exp. 2	6.23×10^{-7}	8.45	5915	84.4	9.70×10^{-8}	2.82×10^{-2}	8.29×10^{-2}
	($\mu g \cdot dm^{-3}$)				($\mu g \cdot dm^{-3}$)	(μg)	($mg \cdot g^{-1}$)
	125.00				19.46	5654	16.58

Table 6.4 depicts an estimation based on the ETS-4 maximum capacity predicted by the Langmuir model in batch mode, of the time necessary to completely exhaust the ETS-4 fixed-bed column, *i.e.* to obtain the breakthrough curves, for different operating conditions.

Table 6.4 – Estimation of the time necessary to exhaust the ETS-4 fixed-bed column for different operating conditions.

	C_0, $\mu g \cdot dm^{-3}$			
v, $cm^3\ min^{-1}$	250	500	750	1000
8.45	660 h/27.5 days	330 h/13.7 days	220 h/9.2 days	165 h/6.9 days
10.0	558 h/23.2 days	279 h/11.6 days	186 h/7.7 days	139 h/5.8 days

6.5. Regeneration of ETS-4 column

The regeneration of ETS-4 fixed-bed column is an important parameter its practical use (Lv et al., 2007). It is known that for low pH values the structure of ETS-4 is unstable and can collapse (chapter 4). Consequently, conventional reagents such as acids cannot be used to regenerate the column. In this study three different solutions were investigated: hot acidified (pH ~4) Milli-Q water (318 K; 45ºC), NaOH solution (~1×10^{-1} M) and $NaNO_3$ 1×10^{-3} M.

The regeneration phase started by passing through the column 2 dm^3 of hot acidified Milli-Q water (v =0.65 $cm^3 \cdot min^{-1}$). Five samples of the effluent were taken at arbitrary

times and the Hg^{2+} concentration in the effluent samples ranged between 0.19 and 0.57 $\mu g \cdot dm^{-3}$, indicating that hot acidified Milli-Q water has low regeneration capacity. Afterwards, a few cm^3 of NaOH solution (~1×10^{-1} M) were fed to the column and a large amount of Hg^{2+} was found in the effluent; unfortunately the CVFAS signal was over ranged and it was not possible to quantify the Hg^{2+} concentration in the effluent. Immediately after 2 dm^3 Milli-Q water was passed through the column to rinse it, since the NaOH solution used previously was excessively concentrated and could destroy ETS-4. After 12h of passing water the Hg^{2+} concentration in the effluent was 0.8 $\mu g \cdot dm^{-3}$.

In order to verify any damage to the ETS-4 fixed-bed column, 25 cm^3 of influent containing Hg^{2+} ions (50 $\mu g \cdot dm^{-3}$) fed the column. The removal percentage at the column outlet was 99%, confirming that the column was in good work conditions. Afterwards, 2 dm^3 of $NaNO_3$ 1×10^{-3} M (v =6.5 $cm^3 \cdot min^{-1}$) were passed through the column, and the effluent was collected every 10 minutes during the first hour and then at 170, 260 and 310 minutes at the column outlet. The Hg^{2+} concentration in the effluent as function time is shown in Figure 6.7.

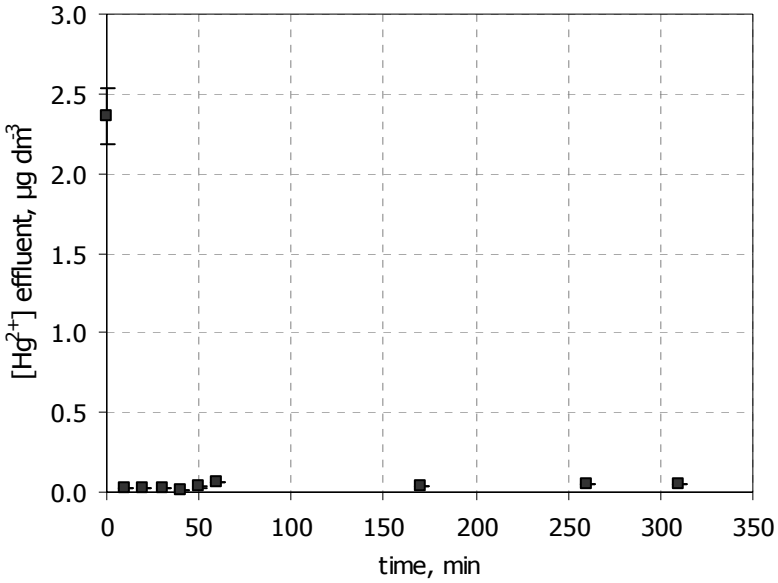

Figure 6.7 – Desorption of Hg^{2+} from ETS-4 fixed-bed column with $NaNO_3$ 1×10^{-3} M (v =6.50 $cm^3 \cdot min^{-1}$).

The results evidence that the regeneration efficiency with $NaNO_3$ (1×10^{-3} M) is greater than with hot acidified Milli-Q water. Furthermore, the highest Hg^{2+} desorption with $NaNO_3$ solution (1×10^{-3} M) seems to occur during the first minutes. Lv et al., (2007) have reported the same profile on the desorption curves of Pb^{2+}-saturated ETS-10 particles in a fixed-bed column with $NaNO_3$ and EDTA-Na_2.

6.6. Conclusions

The removal of Hg^{2+} ions from aqueous solutions in a continuous mode was performed at room temperature, using a home-made ETS-4 fixed-bed ion exchange column. This column produced is distinct from conventional fixed-bed columns, in the filling up method. Usually, in the continuous mode the columns are packed with a granular adsorbent and, in this case the adsorbent (ETS-4) was synthesised inside the column at the surface of an ordinary stainless steel dish-cloth. This system decontaminates 50 dm^3 of an influent containing 125 $\mu g \cdot dm^{-3}$ Hg^{2+} with more than 84% of removal efficiency.

Under the operating conditions used it was not possible to obtain the breakthrough curves in a reasonable time. For this, it will be necessary to increase the Hg^{2+} concentration in the influent, the flow rate or both.

The highest Hg^{2+} desorption from ETS-4 fixed-bed column occurred during the first minutes with $NaNO_3$ solution (1×10^{-3} M), which is a better regenerating medium than hot acidified Milli-Q water.

Chapter 7

Final considerations and future work

Although water is essential for all living organisms and a scarce commodity in several countries around the World, the contamination of surface and ground water by disposal of effluents containing metals and organic pollutants continues until nowadays. The growing environmental pollution requires immediate attention and consequently there is a strong demand to develop efficient technologies for heavy metal removal from natural waters.

The need of cessation or phasing out of discharges, emissions and losses of mercury, which is one of the most toxic metal, during the next decade, combined with true experience and know-how on mercury's environmental chemistry and inorganic materials syntheses and characterization of Analytical Chemistry and Inorganic Chemistry groups of the University of Aveiro, respectively, motivated the development of this work with the aim to test and validate new technologies that allow an effective removal of mercury (II) from aqueous solutions and may be an alternative to conventional water treatment processes.

In this context, microporous materials ETS-10, ETS-4, AM-2, Pharmacosiderite, Petarasite and AV-13 all composed of interconnected octahedral- and tetrahedral-oxide polyhedra, and synthesised in our department by the Inorganic Chemistry group, have been investigating under different operating conditions to assess their potential to be used as mercury (II) decontaminant agents. These materials have, among others, potential novel applications in the fields normally associated with zeolites, such as ion-exchange.

Mercury is very toxic even at trace levels; however the existing studies on the subject usually deal with very high and unrealistic mercury (II) concentrations. On the contrary, this study were performed at mercury (II) concentration levels usually existing in the environment and aimed to reach the desirable zero mercury (II) concentration in the effluents.

Titanosilicate ETS-4 was exhaustively investigated because of its higher removal efficiency, which, like for other adsorbents, is dependent on the operating conditions. In general, the mercury (II) removal capacity increases with increasing contact time, ETS-4 mass and pH and with decreasing temperature and initial Hg^{2+} concentration. The ETS-4 optimal operating conditions are very attractive from the industrial point of view, especially for the treatment of effluents from medical institutions, nickel electroplating process, copper smelter, gold ore tailings and chlor-alkali facilities since does not require larges amount of material, may be performed at room temperature and does not requires significant pH adjustments. Both kinetic and equilibrium data of the ion-exchange process were successfully modelled which is important for industrial applications, since allows to predict the ion exchange process.

Additionally, the higher efficiency of ETS-4 for Hg^{2+} ions is corroborate by the values reported in literature for the sorption capacity of other adsorbents for Hg^{2+} ions and by the higher removal percentage obtained with an ETS-4 fixed-bed ion exchange column,

manufactured in our laboratory. Moreover, all results evidence that ETS-4 has a strong ability for Hg^{2+} uptake and an enormous potential to be use at industrial scale.

Thus, the work was particularly aimed at developing a technology to remove Hg^{2+} ions from wastewater and effluents, based on the ion-exchange properties of ETS-4 titanosilicate, since its high efficiency for uptaking Hg^{2+} ions from solutions, in batch or fixed bed mode, combined with the economic feasibility of the removal process and environmental compatibility make it an excellent Hg^{2+} decontaminant agent to be used in environmental remediation and in water pollution prevention.

This study complements the existing works on the Hg (II) remediation field, filling up the lack of studies on mercury removal from water, especially at low and realistic concentrations found in the environment and introducing new microporous transition metal silicates to be used as substrates for mercury removal, underlining the possible future role that these microporous materials may play in industrial effluents, waste water plants and/or drinking water treatment.

Future work should include obtaining the breakthrough curves of Hg^{2+} for the actual ETS-4 fixed-bed ion exchanger column and the preparation of ETS-4 pellets, for comparison with the present filling of the ETS-4 fixed-bed column. Additionally, its application to real natural water samples should also be contemplate to evaluate the real efficiency of ETS-4 and assess the effect of organic matter and iron and manganese oxides which in Nature are the major sinks for mercury. Another type of experiments and a more ambitious one includes the application of ETS-4 for removal of Hg^{2+} ions at a pilot scale.

Furthermore, the growing development of novel materials makes it crucial to extend the investigation to them in order to find out more efficient materials, especially in application fields where ETS-4 has some limitations such as salty or seawaters. One example of these materials is hybrid materials, which have attracted recently much attention in the scientific community.

Moreover, the know-how acquired in the remediation of contaminated water is an added value for the application of these materials in the development of new technologies for the remediation of heavy metal contaminated soils. Consequently future work should also contemplate the development of experiments aimed at testing and validating technologies that allow a reduction of soils toxicity and an effective improvement of soil function.

Chapter

8

References

A

- Abrams I.M., Aulenbach D.B., Bingham E.C., Bollyky L.J., Brown Jr. T.F., Bruch B., Buchanan R.D., Canter L.W., Caswell C.A., Conway R.A., Crits G.J., Diaper E.W.J., Ferretti J.W.T., Gantz R.G., Gardiner W.C., Gilde Jr. L.C., Kominek E.G., Liu D.H.F., McClure Jr. A.F., Parker F.L., Robertson R.S., Rock D.M., Santhanam C.J., Savage L.S., Smith S.E., Taylor F.B., Walden C.C., Zanitsch R.H., 1997. Removing specific water contaminants. In: Environmental Engineers' handbook. David H.F. Liu and Béla G. Lipták (Eds.), Lewis Publishers, New York, Chapter 8, pp. 964-967.
- Aksu Z., 2005. Application of biosorption for the removal of organic pollutants: a review. Process Biochemistry, 40: 997-1026.
- Al-Attar L., Dyer A., Blackburn R., 2000. Uptake of uranium on ETS-10 microporous titanosilicate. Journal of Radioanalytical and Nuclear Chemistry, 246: 451-455.
- Al-Attar L., Dye A., 2001. Sorption of uranium onto titanosilicate materials. Journal of Radioanalytical and Nuclear Chemistry, 247: 121-128.
- Álvarez-Ayuso E., Garcia-Sanchez A., Querol X., 2003. Purification of metal electroplating waste waters using zeolites. Water Research, 37 (20): 4855-4862.
- Andac M., Asan A., Isildak I., 2003a. Spectrofluorometric determination of mercury(II) with murexide. Journal of Chemical Crystallography, 33: 599-603.
- Andac M., Asan A., Bekdemir Y., Kutuk H., Isildak I., 2003b. Spectrophotometric flow-injection analysis of mercury(II) in pharmaceuticals with p-nitrobenzoxosulfamate. Talanta, 60: 191-197.
- Anderson M.W., Terasaki O., Ohsuna T., Philippou A., Mackay S.P., Ferreira A., Rocha J., Lidin S., 1994. Structure of the Microporous Titanosilicate ETS-10. Nature, 367 (6461): 347-351.
- Andren A.W., Nriagu J.O., 1979. The global cycle of mercury. In: The biogeochemistry of mercury in the environment. J.O. Nriagu (Ed.), Elsevier/North – Holland Biomedical Press, Netherlands, Chapter 1, pp. 1-21.
- Aylett B.J., 1973. Group IIB. In: Comprehensive inorganic Chemistry. J.C. Bailar, H.J. Emeléus, Sir Ronald Nyholm and A.F. Trotman-Dickenson (Eds.), Volume 3, Chapter 30, pp.279.

B

- Babel S., Kurniawan T., 2003. Low-cost adsorbents for heavy metals uptake from contaminated water: a review. Journal of Hazardous Materials, B97: 219-243.

- Banerjee S.S., Joshi M.V., Jayaram R.V., 2004. Removal of Cr(VI) and Hg(II) from aqueous solutions using fly ash and impregnated fly ash. Separation Science and Technology, 39: 1611-1629.
- Basha S., Murthy Z.V.P., Jha B., 2008. Sorption of Hg(II) from aqueous solutions onto Carica papaya: application of isotherms. Industrial & Engineering Chemistry Research, 47: 980-986.
- Batley G.E., Gardner D., 1977. Sampling and storage of natural waters for trace metal analysis. Water Research, 11: 745-756.
- Behrens E.A., Poojary D.M., Clearfield A., 1996. Syntheses, crystal structures, and ion-exchange properties of porous titanosilicates, $HM_3Ti_4O_4(SiO4)_3{\cdot}4H_2O$ ($M=H^+$, K^+, Cs^+), structural analogues of the mineral pharmacosiderite. Chemistry of Materials, 8 (6): 1236-1244.
- Belov N.V., Sandomirsky P.A., 1979. OD-Structure of zorite. Kristallografiya, 24 (6): 1198-1210.
- Benavente M., Álvarez E., Moreno L., Martínez J., 2008. Removal of copper and zinc from gold ore tailings solutions using chitosan. II International workshop on process hydrometallurgy.
- Beneš P., Havlík B., 1979. Speciation of mercury in natural waters. In: The biogeochemistry of mercury in the environment. J.O. Nriagu (Ed.), Elsevier/North – Holland Biomedical Press, Netherlands, Chapter 8, pp. 175-196.
- Beszedits S., 1979. Mercury removal from effluents and wastewaters. In: The biogeochemistry of mercury in the environment. J.O. Nriagu (Ed.), Elsevier/North – Holland Biomedical Press, Netherlands, Chapter 11, pp. 231-269.
- Bortun A.I., Bortun L.N., Clearfield A., 1997. Hydrothermal synthesis of sodium zirconium silicates and characterization of their properties. Chemistry of Materials, 9 (8): 1854-1864.
- Bowker, M. 1998. The basis and application of heterogeneous catalysis. Oxford University press. Oxford, Chapter 6, pp. 58.
- Braun R.D., 1987. Introduction to Instrumental Analysis. McGraw-Hill Book Co., New York, Chapter 8, pp. 233.
- Brooke N.M., Rees L.V.C., 1969. Kinetics of ion-exchange.2. Transactions of the Faraday Society, 65 (562): 2728.

C

- Cavaleiro A.M.V., 1997. Química inorgânica básica. Universidade de Aveiro, Aveiro, Capítulo 4, 122-124.

- Chang L.W., Furst A., Fan A.M., 1999. Metals, toxicity. In: Encyclopedia of Environmental Pollution and Cleanup. Robert A. Meyers and Diane Kender Dittrick (Eds.), John Wiley & Sons, Inc., New York, Volume 2, pp. 985-987.
- Chapman D.M., Roe A.L., 1990. Synthesis, characterization and crystal-chemistry of microporous titanium-silicate materials. Zeolites, 10 (8): 730-737.
- Chiron N., Guilet R., Deydier E., 2003. Adsorption of Cu (II) and Pb(II) onto a grafted silica: isotherms and kinetics models. Water Research, 37: 3079-3086.
- Choi J.H., Kim S.D., Noh S.H., Oh S.J., Kim W.J., 2006a. Adsorption behaviors of nano-sized ETS-10 and Al-substituted ETAS-10 in removing heavy metal ions, Pb^{2+} and Cd^{2+}. Microporous and Mesoporous Materials, 87: 163-169.
- Choi J.H., Kim S.D., Kwon Y.J., Kim W.J., 2006b. Adsorption behaviors of ETS-10 and its variant, ETAS-10 on the removal of heavy metals, Cu^{2+}, Co^{2+}, Mn^{2+} and Zn^{2+} from a waste water. Microporous and Mesoporous Materials 96: 157-167.
- Chojnacki A., Chojnacka K., Hoffmann J., Górecki H., 2004. The application of natural zeolites for mercury removal: from laboratory tests to industrial scale. Minerals Engineering, 17: 933-937.
- Cincotti A., Mameli A., Locci A.M., Orru R., Cão G., 2006. Heavy metals uptake by sardinian natural zeolites: experiment and modelling. Industrial & Engineering Chemistry Research: 45, 1074-1084.
- Clarkson T.W., 1994. The toxicology of mercury and its compounds. In: Mercury pollution: integration and synthesis. Carl J. Watras and John W. Huckabee (Eds.), Lewis Publishers, Section VIII, Chapter 1, pp. 631-641.
- Clearfield A., Bortun A.I., Bortun L.N., Cahill R.A., 1997. Synthesis and characterization of a novel layered sodium titanium silicate $Na_2TiSi_2O_7{\cdot}2H_2O$. Solvent Extraction and Ion Exchange, 15 (2): 285-304.
- Coker E.N., Rees L.V.C. J., 1992. Ion-exchange in beryllophosphate-g. 2. Ion-exchange kinetics. Journal of the Chemical Society-Faraday Transactions, 88 (2): 273-276.
- Coker E.N., Rees L.V.C., 2005. Kinetics of ion exchange in quasi-crystalline aluminosilicate zeolite precursors. Microporous and Mesoporous Materials, 84 (1-3): 171-178.
- Cooney D.O., 1998. Adsorption design for wastewater treatment. Lewis Publishers.

D

- Davis T.A., Volesky B., Vieira H.S.F., 2000. Sargassum seaweed as biosorbent for heavymetals. Water Research, 34: 4270-4278.

- Dakiky M., Khamis M., Manassra A., Mer'eb M., 2002. Selective adsorption of chromium(VI) in industrial wastewater using low-cost abundantly available adsorbents. Advances in Environmental Research, 6 (4): 533-540.
- Di Natale F., Lancia A., Molino A., Di Natale M., Karatza D., Musmarra D., 2006. Capture of mercury ions by natural and industrial materials. Journal of Hazardous Materials, B132: 220–225
- Duarte A.C., Pereira M.E., Oliveira J.P., Hall A., 1991. Mercury desorption from contaminated sediments. Water, Air and Soil Pollution, 56: 77-82.
- Dyer A.; 1988. An Introduction to Zeolite Molecular Sieves. Wiley & Sons Ltd, New York.

E

- El-Kamash A.M., Zaki A.A., El Geleel M.A., 2005. Modelling batch kinetics and thermodynamics of zinc and cadmium ions removal from waste solutions using synthetic zeolite A. Journal of Hazardous Materials, 127 (1-3): 211-220.
- EPA/600/4-91/002, U.S. Environmental Protection Agency, 1994. Environmental Monitoring Systems Laboratory (currently, National Exposure Research Laboratory). Short-term Methods for Estimating the Chronic Toxicity of Effluents and Receiving Waters to Freshwater Organisms, third ed., Cincinnati.

F

- Feng Q., Lin Q., Gong F., Sugita S., Shoya M., 2004. Adsorption of lead and mercury by rice husk ash. Journal of Colloid and Interface Science, 278: 1-8.
- Ferreira A., 1997. Síntese e caracterização de titanossilicatos microporosos. Tese de Doutoramento, Universidade de Aveiro.
- Ferreira A., Lin Z., Soares M.R., Rocha J., 2003. Ab initio structure determination of novel small-pore metal-silicates: knots-and-crosses structures. Inorganica Chimica Acta, 356: 19-26.

G

- Gardner M., Comber S., 1997. Sample filtration as a source of error in the determination of trace metals in marine waters. The Analyst, 122: 1029-1032.
- Gebremedhin-Haile T., Olguin M.T., Solache-Rios M., 2003. Removal of mercury ions from mixed aqueous metal solutions by natural and modified zeolitic minerals. Water Air and Soil Pollution, 148 (1-4): 179-200.

- Ghodbane I., Hamdaoui O., 2008. Removal of mercury(II) from aqueous media using eucalyptus bark: Kinetic and equilibrium studies. Journal of Hazardous Materials, 160: 301-309.
- Gochfeld M., 2003. Cases of mercury exposure, bioavailability, and absorption. Ecotoxicology and Environmental Safety, 56: 174-179.
- Gode F., Pehlivan E., 2003. A comparative study of two chelating ion-exchange resins for the removal of chromium(III) from aqueous solution. Journal of Hazardous Materials, 100 (1-3): 231-243.
- Goel J., Kadirvelu K., Rajagopal C., Garg V.K., 2005. Investigation of adsorption of lead, mercury and nickel from aqueous solutions onto carbon aerogel. Journal of Chemical Technology and Biotechnology, 80: 469-476.
- Green-Ruiz C., 2006. Mercury(II) removal from aqueous solutions by nonviable *Bacillus sp* from a tropical estuary. Bioresource Technology, 97 (15): 1907-1911.
- Grimm A., Zanzi R., Björnbom E., Cukierman A.L., 2008. Comparison of different types of biomasses for copper biosorption. Bioresource Technology, 99: 2559-2565.

H

- Hall A., Duarte A.C., Caldeira M.T.M., Lucas M.F.B., 1987. Sources and sinks of mercury in the coastal lagoon of Aveiro, Portugal. Science of Total Environment, 64 (1-2): 75-87.
- Helfferich F., 1995. Ion Exchange. Courier Dover Publications, New York.
- Ho Y.S., McKay G., 1999a. The sorption of lead (II) ions on peat. Water Research, 33: 578-584.
- Ho Y.S., McKay G., 1999b. Pseudo-second order model for sorption processes. Process Biochemistry, 34: 451-465.
- Ho Y.S., McKay G., 2000. The kinetics of sorption of divalent metal ions onto sphagnum moss flat. Water Research, 34 (3): 735-742.
- Horlick G., 1986. Flame Emission, Atomic Absorption and Atomic Fluorescence Spectrometry. In: Instrumental Analysis. Gary D. Christian and James E. O'Reily (Eds.), Allyn and Bacon, Boston, Chapter 10, pp. 278.
- Hyatt N.C., Hriljac J.A., Choudry A., Malpass L., Sheppard G.P., Maddrell E.R., 2004. Zeolite-salt occlusion: a potential route for the immobilisation of Iodine-129. Scientific Basis for Nuclear Waste Management XXVII, Material Research Society Symposium, Ser. 807, A132.

I

- Igwe J.C., A. Abia A.A., 2007. Equilibrium sorption isotherm studies of Cd(II), Pb(II) and Zn(II) ions detoxification from waste water using unmodified and EDTA-modified maize husk . Electronic Journal of Biotechnology [online], 10 (4). Available from Internet: http://www.ejbiotechnology.info/content/vol10/issue4/full/15/index.html ISSN 0717-3458.
- IPCS (International Programme on Chemical Safety), 1991. Environmental Health Criteria 118 – Inorganic Mercury. United Nations Environment Programme, International Labour Organisation and World Health Organization (Eds.), World Health Organization, pp. 13-147.

J

- Jale S.R., Ojo A., Fitch F.R., 1999. Synthesis of microporous zirconosilicates containing ZrO_6 octahedra and SiO_4 tetrahedra. Chemical Communications, 411-412.

K

- Karge H.G., 1998. Characterization by infrared spectroscopy. Microporous and Mesoporous Materials, 22 (4-6) Special Issue: 547-549.
- Khraisheh M.A.M., Al-degs Y.S., Mcminn W.A.M., 2004. Remediation of wastewater containing heavy metals using raw and modified diatomite. Chemical Engineering Journal, 99: 177-184.
- Kim J.S., Keane M.A., 2000. Ion Exchange of Divalent Cobalt and Iron with Na–Y Zeolite: Binary and Ternary Exchange Equilibria. Journal of Colloid and Interface Science, 232: 126-132.
- Kocaoba S., 2007. Comparison of Amberlite IR 120 and dolomite's performances for removal of heavy metals. Journal of Hazardous Materials, 147 (1-2): 488-496.
- Koudsi Y., Dyer A., 2001. Sorption of ^{60}Co on a synthetic titanosilicate analogue of the mineral penkvilksite-2O and antimonysilicate. Journal of Radioanalytical and Nuclear Chemistry, 247: 209-219.
- Krishnan K.A., Anirudhan T.S., 2002. Removal of mercury(II) from aqueous solutions and chlor-alkali industry effluent by steam activated and sulphurised activated carbons prepared from bagasse pith: kinetics and equilibrium studies. Journal of Hazardous Materials, B92: 161-183.
- Kuznicki S.M., 1989. New crystalline titanium silicate molecular sieve zeolite - with defined X=ray powder diffraction pattern, as adsorbent and catalyst. US Patent 4853202-A.

- Kuznicki S.M., 1990. Mfg. titanium silicate molecular sieve zeolite(s) - by hydrothermally reacting mixts. contg. sources of titanium, silica, alkali, and water. US Patent 4938939-A.
- Kuznicki S.M., Thrush K.A., 1991. Removal of heavy metals from aqueous solutions - using large pore ETS-10 or ETAS-10 molecular sieves, in presence of competing calcium and/or magnesium ions. US Patent 4994191-A.

L

- Lagergren S., 1898. Zur theorie der sogenannten adsorption geldster stoffe. Handlingar, 24: 1-39.
- Lawton W.H., Sylvestre E.A., 1971. Elimination of linear parameters in nonlinear regression. Technometrics, 13 (3): 461.
- Lin L.C., Juang R.S., 2005. Ion-exchange equilibria of Cu(II) and Zn(II) from aqueous solutions with Chelex 100 and Amberlite IRC 748 resins. Chemical Engineering Journal, 112 (1-3): 211-218.
- Lin L.C., Li J.K., Juang R.S., 2008. Removal of Cu(II) and Ni(II) from aqueous solutions using batch and fixed-bed ion exchange processes. Desalination, 225 (1-3): 249-259.
- Lin Z., Rocha J., Brandão P., Ferreira A., Esculcas A.P., Pedrosa J.D., Philippou A., Anderson M.W., 1997. Synthesis and structural characterization of microporous umbite, penkvilksite, and other titanosilicates. Journal of Physical Chemistry B, 101: 7114-7120.
- Lin Z., Rocha J., Ferreira P., Thursfield A., Agger J.R., Anderson M.W., 1999. Synthesis and structural characterization of microporous framework zirconium silicates. Journal of Physical Chemistry B, 103 (6): 957-963.
- Lopes C.B., Otero M., Coimbra J., Pereira E., Rocha J., Lin Z., Duarte A., 2007. Removal of low concentration Hg^{2+} from natural waters by microporous and layered titanosilicates. Microporous and Mesoporous Materials, 103: 325-332.
- Lv L., Tsoi G., Zhao X.S., 2004. Uptake equilibria and mechanisms of heavy metal ions on microporous titanosilicate ETS-10. Industrial Engineering Chemistry Research, 43 (24): 7900-7906.
- Lv L., Hor M.P., Su F., Zhao X.S., 2005. Competitive adsorption of Pb^{2+}, Cu^{2+}, and Cd^{2+} ions on microporous titanosilicate ETS-10. Journal of Colloid and Interface Science, 287: 178-184.
- Lv L., Wang K., Zhao X.S., 2007. Effect of operating conditions on the removal of Pb^{2+} by microporous titanosilicate ETS-10 in a fixed-bed column. Journal of Colloid and Interface Science, 305: 218–225.

M

- Machida M., Yamazaki R., Aikawa M., Tatsumoto H., 2005. Role of minerals in carbonaceous adsorbents for removal of Pb(II) ions from aqueous solution. Separation and Purification Technology, 46: 88-94.
- Miller J.C., Miller J.N., 1993. Statistics for analytical chemistry. Ellis Horwood Limited, Chapter 5, pp. 101-140.
- Misak N.Z., 1995. Adsorption isotherms in ion exchange reactions. Further treatments and remarks on the application of the Langmuir isotherm. Colloids and Surfaces A: Physicochemical and Engineering Aspects, 97: 129-140.
- Mishra S.P., Tiwari D., Prasad S.K., Dubey R.S., Mishra M., 2007. Inorganic particulates in removal of toxic heavy metal ions. Part X: Removal behavior of aluminum hydroxide for Hg(II): A radiotracer study. Journal of Radioanalytical and Nuclear Chemistry, 274 (2): 257-263
- Mohan D., Gupta V.K., Srivastava S.K., Chander S., 2001. Kinetics of mercury adsorption from wastewater using activated carbon derived from fertilizer waste. Colloids and Surfaces A: Physicochemical and Engineering Aspects, 177: 169-181.
- Mukherjee A.B., Zevenhoven R., Brodersen J., Hylander L.D., Bhattacharya P., 2004. Mercury in waste in the European Union: sources, disposal methods and risks. Resources, Conservation and Recycling, 42: 155-182.

N

- Nabais J.V., Carrott P.J.M., Carrott M.M.L.R., Belchior M., Boavida D., Diall T., Gulyurtlu I., 2006. Mercury removal from aqueous solution and flue gas by adsorption on activated carbon fibres. Applied Surface Science, 252 (17): 6046-6052.
- Nam K.H., Tavlarides L.L., 2005. Synthesis of a high-density phosphoric acid functional mesoporous adsorbent: Application to chromium(III) removal. Chemistry of Materials, 17: 1597-1604.
- Namasivayam C., Senthilkumar S., 1998. Removal of Arsenic(V) from aqueous solution using industrial solid waste: Adsorption rates and equilibrium studies. Industrial Engineering Chemistry Research, 37: 4816-4822.
- Nriagu J.O., 1979. Production and uses of mercury. In: The biogeochemistry of mercury in the environment, J.O. Nriagu (Ed.), Elsevier/North – Holland Biomedical Press, Netherlands, Chapter 2, pp. 23-40.

P

- Panayotova M., 2001. Kinetics and thermodynamics of copper ions removal from wastewater by use of zeolite. Waste Management, 21: 671-676.
- Parsons T.R., Maita J., Lalla C.M., 1984. A manual for chemical, biological methods for seawater analysis. Pergamon Press, Toronto.
- Pavel C.C., Popa K., Bilba N., Cecal A., Cozma D., Pui A., 2003. The sorption of some radiocations on microporous titanosilicate ETS-10. Journal of Radioanalytical and Nuclear Chemistry, 258: 243-248.
- Payne K.B., Abdel-Fattah T.M., 2004. Adsorption of divalent lead ions by zeolites and activated carbon: Effects of pH, temperature, and ionic strength. Journal of Environmental Science and Health Part A-Toxic/Hazardous Substances & Environmental Engineering, 39 (9): 2275-2291.
- Pereira M.E., Duarte A.C., Millward G.E., Abreu S.N., Vale C., 1998. An estimation of industrial mercury stored in sediments of a confined Area of the lagoon of Aveiro (Portugal). Water Science and Technology, 37 (6-7): 125-130.
- Pérez-Quintanilla D., Del Hierro I., Fajardo M., Sierra I., 2006. Mesoporous silica functionalized with 2-mercaptopyridine: Synthesis, characterization and employment for Hg(II) adsorption. Microporous and Mesoporous Materials, 89: 58-68.
- Peric J., Trgo M., Medvidovic N.V., 2004. Removal of zinc, copper and lead by natural zeolite - a comparison of adsorption isotherms. Water Research, 38: 1893–1899.
- Petrus R., Warchol J., 2003. Ion exchange equilibria between clinoptilolite and aqueous solutions of Na^{+}/Cu^{2+}, Na^{+}/Cd^{2+} and Na^{+}/Pb^{2+}. Microporous and Mesoporous Materials, 61 (1-3): 137-146.
- Pitcher S.K., Slade R.C.T., Ward N.I., 2004. Heavy metal removal from motorway stormwater using zeolites. Science of the Total Environment, 334 Special Issue: 161-166.
- Popa K., Pavel C.C., Bilba N., Cecal A., 2006. Purification of waste waters containing $^{60}Co^{2+}$, $^{115m}Cd^{2+}$ and $^{203}Hg^{2+}$ radioactive ions by ETS-4 titanosilicate. Journal of Radioanalytical and Nuclear Chemistry, 269(1): 155-160.

R

- Ranganathan K., 2003. Adsorption of Hg(II) ions from aqueous chloride solutions using powdered activated carbons. Carbon, 41: 1087-1092.
- Rao K.S., Sarangi D., Dash P.K., Chaudhury G.R., 2002. Treatment of wastewater containing copper, zinc, nickel and cobalt using Duolite ES-467. Journal of Chemical Technology and Biotechnology, 77 (10): 1107-1113.

- Rao M.M., Reddy D.H.K. K., Venkateswarlu P., Seshaiah K., 2009. Removal of mercury from aqueous solutions using activated carbon prepared from agricultural by-product/waste. Journal of Environmental Management, 90: 634-643.
- Reddad Z., Gerente C., Andres Y., Le Cloirec P., 2002. Adsorption of several metal ions onto low-cost biosorbent: kinetic and equilibrium studies. Environment Science and Technology, 36: 2067-2073.
- Rengaraj S., Yeon K.H., Moon S.H., 2001. Removal of chromium from water and wastewater by ion exchange resins. Journal of Hazardous Materials, 87 (1-3): 273-287.
- Roberts M.A., Sankar G., Thomas J.M., Jones R.H., Du H., Chen J., Pang W., Xu R., 1996. Synthesis and structure of a layered titanosilicate catalyst with five-coordinate titanium. Nature, 381 (6581): 401-404.
- Robson H., 1998. Verified syntheses of zeolite materials. Microporous and Mesoporous Materials, 22 (4-6) Special Issue: 552-663.
- Rocha J., 1996a. Sumário da lição de síntese: Titanossilicatos microporosos e outros sólidos zeolíticos novos.
- Rocha J., Brandão P., Lin Z., Kharlamov A., Anderson M.W., 1996b. Novel microporous titanium-niobium-silicates with the structure of nenadkevichite. Chemical Communications, 669-670.
- Rocha J., Brandão P., Lin Z., Esculcas A.P., Ferreira A., Anderson M.W., 1996c. Synthesis and Structural Studies of Microporous Titanium-Niobium-Silicates with the Structure of Nenadkevichite. Journal of Physical Chemistry, 100 (36): 14978-14983.
- Rocha J., Ferreira A., Lin Z., Anderson M.W., 1998. Synthesis of microporous titanosilicate ETS-10 from $TiCl_3$ and TiO_2: a comprehensive study. Microporous and Mesoporous Materials, 23: 253-263.
- Rocha J., Anderson M.W., 2000. Microporous Titanosilicates and other Novel Mixed Octahedral-Tetrahedral Framework Oxides. European Journal of Inorganic Chemistry, 5: 801-818.
- Rodriguez J.F., Valverde J.L., Rodrigues A.E., 1998. Measurements of effective self-diffusion coefficients in a gel-type cation exchanger by the zero-length-column method. Industrial & Engineering Chemistry Research, 37 (5): 2020-2028.
- Romera E., González F., Ballester A., Blázquez M.L., Muñoz J.A., 2007. Comparative study of biosorption of heavy metal using different types of algae. Bioresource Technology, 98: 3344-3353.
- Rood B.E., Sanford C.L., 1999. Mercury determination in the environment. In: Encyclopedia of Environmental Pollution and Cleanup. Robert A. Meyers and Diane Kender Dittrick (Eds.), John Wiley & Sons, Inc., New York, Volume 2, pp. 984-985.

S

- Schiesser W.E., 1991. The Numerical Method of Lines. Academic Press, USA.
- Shah R., Devi S., 1998. Chelating resin containing s-bonded dithizone for the separation of copper(II), nickel(II) and zinc(II). Talanta, 45: 1089-1096.
- Sharaf M.A., Sayed S.A., Younis A.A., Farag A.B., Arida H.A., 2007. Removal of trace contaminants from water using new chelating resins. Analytical Letters, 40 (16-18): 3443-3456.
- Singh B., Alloway B.J., Bochereau F.J.M., 2000. Cadmium sorption behavior of natural and synthetic zeolites. Communications in Soil Science and Plant Analysis, 31 (17): 2775-2786.
- Skoog D.A., West D.M., Holler F.J., 1996. Fundamentals of Analytical Chemistry. Saunders College Publishing, Fort Worth, Chapter 25, 601 pp.
- Slater M.J., 1991. In: Principles of Ion Exchange Technology. Butterworth-Heinemann. Great Britain, Chapter 3.
- Smart L., Moore E., 1992. Solid state chemistry an introduction. Chapman & Hall London, Chapter 7, pp. 238-268.
- Sobral L.G.S., Fernandes A.L.V., Lima R.B., 2004. Polishing Treatment of Mercury-Bearing Liquid Effluents from the Chlor-Alkali Industry by Using the Biomass *Sargassum Sp.* Proceedings of International Conference on Mercury as a Global Pollutant, Ljubliana, Eslovenia, pdf 346.
- Sprynskyy M., Buszewski B., Terzyk A.P., Namiesnik J., 2006. Study of the selection mechanism of heavy metal (Pb^{2+}, Cu^{2+}, Ni^{2+}, and Cd^{2+}) adsorption on clinoptilolite. Journal of Colloid and Interface Science, 304 (1): 21-28.
- Stumm W., 1992. Chemistry of the Solid-Water Interface: Processes at the Mineral-Water and Particle-Water Interface in Natural Systems. John Wiley & Sons, Inc.

T

- Tolosana S., Ehrlich R., 2000. Composition of liquid effluent discharged by medical institutions in Cape Town. South Africa Journal of Science, 96: 417-420.
- Tüzün I., Bayramoglu G., Yalçın E., Basaran G., Çelik G., Arıca M.Y., 2005. Equilibrium and kinetic studies on biosorption of Hg(II), Cd(II) and Pb(II) ions onto microalgae Chlamydomonas reinhardtii. Journal of Environmental Management, 77: 85-92.

V

- Valverde J.L., De Lucas A., Carmona M., Gonzalez M., Rodriguez J.F., 2004. A generalized model for the measurement of effective diffusion coefficients of

heterovalent ions in ion exchangers by the zero-length column method. Chemical Engineering Science, 59 (1): 71-79.

W

- Walcarius A., Etienne M., Delacote C., 2004. Uptake of inorganic Hg(II) by organically modified silicates: influence of pH and chloride concentration on the binding pathways and electrochemical monitoring of the processes. Analytica Chimica Acta, 508: 87–98.
- Wu F.C., Tseng R.L., Juang R.S., 2001. Kinetic modelling of liquid-phase adsorption of reactive dyes and metal ions on chitosan. Water Research, 35(3): 613-618.

Y

- Yardim M.F., Budinova T., Ekinci E., Petrov N., Razvigorova, M., Minkova V., 2003. Removal of mercury (II) from aqueous solution by activated carbon obtained from furfural. Chemosphere, 52: 835-841.
- Yavuz H., Denizli A., Güngünes H., Safarikova M., Safarik I., 2006. Biosorption of mercury on magnetically modified yeast cells. Separation and Purification Technology, 52: 253-260.

Z

- Zeroual Y., Moutaouakkil A., Dzairi F.Z., Talbi M., Chung P.U., Lee K., Blaghen M., 2003. Biosorption of mercury from aqueous solution by Ulva lactuca biomass. Bioresource Technology, 90 (3): 349-351.
- Zhao G.X.S., Lee J.L., Chia P.A., 2003. Unusual Adsorption Properties of Microporous Titanosilicate ETS-10 toward Heavy Metal Lead. Langmuir, 19: 1977-1979.
- Zhang F.-S., Nriagu J.O., Itoh H., 2005. Mercury removal from water using activated carbons derived from organic sewage sludge. Water Research, 39: 389-395.
- Zhu X., Alexandratos S.D., 2005. Polystyrene-supported amines: Affinity for mercury(II) as a function of the pendant groups and the Hg(II) counterion. Industrial & Engineering Chemistry Research, 44: 8605-8610.
- Zubkova N.V., Pushcharovsky D.Y., 2008. Mixed-Framework Microporous Natural Zirconosilicates. In: Minerals as Advanced Materials I. Sergey V. Krivovichev (Ed.), Springer, pp. 45-47.

Web sites

- EPA (Environment Protection Agency), 2006 – last access on January 2009. Available from: http://www.epa.gov/mercury/roadmap/htm
- Mercury element – last access on January 2009. Available from: http://en.wikipedia.org/wiki/Mercury_(element)
- Chlorine online information resource – last access on January 2009. Available from: http://www.eurochlor.org/makingchlorine
- CERCLA (Comprehensive Environmental Response, Compensation, and Liability Act) Priority List of Hazardous Substances, 2007 – last access on January 2009. Available from: http://www.atsdr.cdc.gov/cercla/07list.html
- Decreto-Lei n.º 236/98. D.R. n.º 176, Série I-A de 1998-08-01 – last access on January 2009. Available from: http://dre.pt/pdf1sdip/1998/08/176A00/36763722.pdf
- Decreto-Lei n.º 52/99. D.R. n.º 43, Série I-A de 1999-02-20 – last access on January 2009. Available from: http://dre.pt/pdf1sdip/1999/02/043A00/09940998.pdf
- Zeolites – last access on February 2009. Available from: http://wikis.lib.ncsu.edu/index.php/Zeolites
- LBC zeolite molecular sieves characteristics – last access on February 2009. Available from: http://www.sinolbc.com
- Table of drinking water contaminant levels - New York state maximum contamination allowed in water – last access on November 2008. Available from: http://www.inspect-ny.com/water/levels.htm

Chapter

9

Supplementary material

Nernst-Planck based model

The development of a mathematical model based on the Nernst-Planck approach to describe the ion exchange process between the Na^+ present in the ETS-4 framework and the Hg^{2+} ions present in the liquid phase, was carried out in collaboration with Chemical Engineering group of the University of Aveiro. The model combines both intra-particle and film resistances to mass transport, and involves three parameters: the self-diffusivities of Hg^{2+} and Na^+, and the convection mass transfer coefficient.

Model equations have been derived assuming the following hypothesis: i) film and intra-particle mass transfer resistances; ii) spherical solid particles; iii) perfectly stirred tank; iv) isothermal and isobaric operation; v) co-ions are excluded from the zeolite particles (Donnan exclusion); and vi) ideal solution behaviour.

Nernst-Planck equations

The ion-exchange may be represented by conventional chemical equilibrium (Helfferich, 1995) between two counter ions. For the case where the ETS-4 is initially in B (Na^+) form and the counter ion in solution is A (Hg^{2+}), the reaction is:

$$z_A \overline{B^{Z_B}} + z_B A^{z_A} \Leftrightarrow z_B \overline{A^{z_A}} + z_A B^{z_B} \tag{1}$$

where z_A and z_B are the electrochemical valences.

The flux of each counter ion in dilute ionic solutions may be described by the Nernst-Planck equations (Helfferich, 1995):

$$J_A = -D_A\left(\frac{\partial q_A}{\partial r}\right) - D_A z_A q_A \frac{F}{\Re T}\left(\frac{\partial \phi}{\partial r}\right) \tag{2}$$

$$J_B = -D_B\left(\frac{\partial q_B}{\partial r}\right) - D_B z_B q_B \frac{F}{\Re T}\left(\frac{\partial \phi}{\partial r}\right) \tag{3}$$

where D_A and D_B are the self-diffusion coefficients of species A and B, q_A and q_B are the molar concentration of counter ions in the particle, F is Faraday constant, $\Re$ is gas constant, T is absolute temperature, ϕ is the electrostatic potential and r is the radial position.

The particle is subjected to the usual restrictions of electroneutrality and nonexistent electric current, mathematically represented by:

$$q_A z_A + q_B z_B = Q \tag{4}$$

$$z_i J_i + z_i J_i = 0 \tag{5}$$

The electrostatic potential term in the transport equations may by eliminated by substituting equations (2) and (3) in equation (5):

$$\frac{F}{\Re T}\frac{\partial \phi}{\partial r} = \frac{z_A\left(D_B - D_A\right)}{z_A q_A (z_A D_A - z_B D_B) + D_B z_B Q}\frac{\partial q_A}{\partial r} \tag{6}$$

After substitution in equation (5), the general expression for the flux of A is obtained:

$$J_A = -\frac{D_A D_B\left(z_B^2 q_B + z_A^2 q_A\right)}{D_A z_A^2 q_A + D_B z_B^2 q_B}\left(\frac{\partial q_A}{\partial r}\right) \tag{7}$$

This equation may be recast as a special form of the Fick's first law, where a coupled inter-diffusion coefficient, D_{AB}, appears:

$$J_A = -D_{AB}\left(\frac{\partial q_A}{\partial r}\right), \text{ and } D_{AB} \equiv \frac{D_A D_B\left(z_A^2 q_A + z_B^2 q_B\right)}{D_A z_A^2 q_A + D_B z_B^2 q_B} \tag{8}$$

D_{AB} depends on D_A, D_B, and the ionic composition of the ETS-4, which varies in the course of ion-exchange.

Material balances and initial and boundary conditions

The material balances to the vessel and over a spherical shell of the ETS-4 particle are, respectively:

$$\frac{\partial C_A}{\partial t} = -\frac{V_s}{V_L}\frac{\partial \bar{q}_A}{\partial t} \tag{9}$$

$$\left(\frac{\partial q_A}{\partial t}\right) = -\frac{1}{r^2}\frac{\partial}{\partial r}\left(r^2 J_A\right) \tag{10}$$

where the average loading per unit particle volume is:

$$\bar{q}_A = \frac{3}{R^3}\int_0^R r^2 q_A dr \tag{11}$$

The above differential equations are subjected to the following initial and boundary conditions.

$$t = 0, \quad q_A = \bar{q}_A = 0 \text{ and } C_A = C_{A0} \tag{12}$$

$$r = R, \quad q_A = q_{As} \tag{13}$$

$$r = 0, \quad \left(\frac{\partial q_A}{\partial r}\right) = 0, \tag{14}$$

The equality of internal and film ionic fluxes must be observed at particle surface, and uniquely determines interface concentrations (hereafter denoted by subscript s):

$$\left(\frac{\partial q_A}{\partial r}\right)_{r=R} = \frac{k_f}{D_{AB}}\left(C_A - C_{As}\right) \tag{15}$$

where k_f is the convective mass transfer coefficient.

Solution approach: numerical methods used

The simultaneous solution of the set of differential and algebraic equations listed above gives the concentration of the Hg^{2+} in water, and its concentration profiles in the solid phase as function of position and time. The model has been solved numerically using the Method of Lines (Schiesser, 1991) and integrated using the Finite-Difference approach. For this purpose, a programme in Matlab has been written, by a Chemical Engineering professor, to solve the resulting Ordinary Differential Equations (ODEs) with 101 grid points and finite-difference approach with central differences of second order. Forward and backward differences formulas were adopted for the first and last nodes, respectively. An odd number of grid points is required when the average loading (Equation 12) is numerically evaluated using the 1/3 Simpson's Rule. Ode 15s has been used to integrate this set of ODEs of the initial-value type.

The self-diffusion coefficients and the convective mass transfer coefficient are the three model parameters to be fitted to the experimental data. Accordingly, a first optimisation step was performed based on the 'elimination of linear parameters in nonlinear regression' technique (Lawton and Sylvestre, 1971). With this procedure, a reduction of the number of parameters that must be estimated by the iterative procedure is achieved, as well as faster convergence attained. Thus, only two initial guesses have to be provided instead of three. Finally, an enhancing optimisation involving all parameters simultaneously was performed, where the results previously obtained from the above mentioned technique were taken as reliable initial guesses.